Cassini Exploration of the Planet Saturn: A Comprehensive Review

Andrew P. Ingersoll[1]

[1]Division of Geological and Planetary Sciences, California Institute of Technology, 1200 East California Blvd, Pasadena, CA 91125, USA

Abstract

Before Cassini, scientists viewed Saturn's unique features only from Earth and from three spacecraft flying by. During more than a decade orbiting the gas giant, Cassini studied the planet from its interior to the top of the atmosphere. It observed the changing seasons, provided up-close observations of Saturn's exotic storms and jet streams, and heard Saturn's lightning, which cannot be detected from Earth. During the Grand Finale orbits, it dove through the gap between the planet and its rings and gathered valuable data on Saturn's interior structure and rotation. Key discoveries and events include: watching the eruption of a planet-encircling storm, which is a 20- or 30-year event, detection of gravity perturbations from winds 9000 km below the tops of the clouds, demonstration that eddies are supplying energy to the zonal jets, which are remarkably steady over the 25-year interval since the Voyager encounters, re-discovery of the north polar hexagon after 25 years, determination of elemental abundance ratios He/H, C/H, N/H, P/H, and As/H, which are clues to planet formation and evolution, characterization of the semiannual oscillation of the equatorial stratosphere, documentation of the mysteriously high temperatures of the thermosphere outside the auroral zone, and seeing the strange intermittency of lightning, which typically ceases to exist on the planet between outbursts every 1–2 years. These results and results from the Jupiter flyby are all discussed in this review.

Keywords

A.P. Ingersoll, api@gps.caltech.edu.

Code availability Not applicable.

Conflict of interest None.

1   Introduction

The planets themselves, Saturn and Jupiter, were an important scientific objective of the Cassini mission, and they are the focus of this review. The review is taken from Volume 1 of the Cassini Final Report (https://pds-rings.seti.org/cassini/). That document contains instrument-specific chapters, other discipline chapters beside the planets themselves, and a science summary with a science assessment for the complete mission. For setting priorities and planning, Cassini had five discipline working groups: Icy satellites, magnetosphere, rings, Saturn, and Titan. The report is taken from the Saturn chapter. The overlap region, where the upper atmosphere of the planet merges with the near-vacuum of space, is covered in the magnetosphere chapter if charged particles are the dominant medium, and in the Saturn chapter if neutral gases are the dominant medium

The focus is on Cassini and the discoveries it made. The report is not a complete review of giant planet atmospheres and interiors. The reference list was compiled from the Cassini instrument reports and from literature searches with keywords Cassini, Saturn OR Jupiter, atmosphere OR interior but NOT magnetosphere, rings, Titan, or other satellites. I was selective with keywords like ionosphere and aurora. I was also selective with models and laboratory work that didn't explicitly use Cassini data. I read abstracts and tried to paraphrase the most important results, but I downloaded and read only about 20% of the papers. The final literature search was done in mid-July of 2020.

Science results are in the first 9 sections of the paper: 1. Introduction. 2. Clouds, composition and chemistry. 3. Heat flux, winds and temperatures. 4. The great storm of 2010–2011. 5. Vortices, mean flow and eddies. 6. Interior structure and rotation. 7. Upper atmosphere physics and chemistry. 8. Jupiter science results. 9. Venus atmosphere. Section 10 gives the open science questions after Cassini. Section 11 gives the Saturn portion of the scientific objectives for the prime and solstice missions. The latter was a mission extension that allowed Cassini to observe all four seasons—summer and fall in the south and winter and spring in the north. The scientific objectives are quite general, but that's as it should be. Cassini was the first Saturn orbiter, and it was an extremely well-equipped spacecraft. It was a flagship sailing into unknown waters, and it was impossible to limit the objectives to a specific list drawn up in advance. Cassini was on a voyage of discovery, and it was wildly successful because there was much to be discovered.

2   Clouds, Composition and Chemistry

2.1   Clouds and Haze

The temperature field, cloud properties, and composition are an interacting system that controls the energy budget of the planet and the clouds and haze that we see in the planet's atmosphere (Fig. 1). Clouds are a tracer of the motion. They form on updrafts, which are part of the energy cycle that controls the zonal winds. Also, clouds interact with the temperature field through condensation and evaporation. Cassini, with its comprehensive array of instruments and unique perspective from different positions in the orbit, has contributed critical data on all of these objectives. In addition, Cassini has spawned exploration of Saturn from Earth-based telescopes.

Timed with the start of Cassini's exploration of the Saturn system, Beebe (2005) presented the case for comparative study of the outer planets. Papers on the Cassini instruments and their ability to measure clouds and haze include: Baines et al. (2005) on the Visual and Infrared Mapping Spectrometer (VIMS), Porco et al. (2005) on the Imaging Science Subsystem (ISS); Flasar et al. (2004, 2005) and Jennings et al. (2017) on the Composite Infrared spectrometer (CIRS); and Janssen et al. (2013) on the Cassini RADAR radiometer. Schinder et al. (2015) give the techniques for probing the electron density and temperature structure with radio occultations.

Banfield et al. (1998) describe the use of near-infrared (IR) spectroscopy from the 5-m Hale telescope at Palomar, California to measure the altitudes and scattering properties of clouds and haze. Similarly, Sanchez-Lavega et al. (2004) described Hubble Space Telescope observations of cloud morphology in Saturn's atmosphere. Temma et al. (2005) used Earth-based telescopic observations to probe the vertical structure of Saturn's cloud layers. Using Hubble Space Telescope (HST) data, Perez-Hoyos et al. (2006) documented short-term variability (weeks to months) associated with cloud reflectivity of the belts and zones. West et al. (2009) gives a comprehensive survey of clouds and haze in Saturn's atmosphere as inferred from Cassini VIMS and ISS, as well as HST and other Earth-based telescopes. Generally cloud particles form by condensation of simple molecules, and haze particles form by condensation of complex molecules that are produced by photochemistry. Ingersoll et al. (2018) present images taken during the last few months of the mission at resolutions down to 0.5 km per pixel. The interesting features include filamentary clouds coherent over 20,000 km and puffy clouds resembling terrestrial cumulus. Spilker (2019) gives the highlights and discoveries obtained during Cassini's final year, including the some of the highest-resolution information about the interior and atmosphere.

Fletcher et al. (2007b) used Cassini CIRS data to probe the vertical and horizontal temperature structure and its relation to the belt and zone cloud structure. Roman et al. (2013) used ISS data to probe the layered cloud structure from the haze layers at 40 mbar to tropospheric clouds at 2.5 bar. Laraia et al. (2013) used Cassini RADAR radiometer data to probe the vertical distribution of NH_3 to depths below its nominal cloud base. Barstow et al. (2016) use Cassini VIMS to document a photochemical origin for the stratospheric haze and either NH_3 or NH_4SH for the deeper tropospheric cloud. Using Cassini ISS data, Dyudina et al. (2016) and Perez-Hoyos et al. (2016) quantified the way the atmosphere scatters light, including the phase function and the spherical and Bond albedos.

Del Genio et al. (2009) give a comprehensive review of Saturn's atmospheric structure and dynamics. The early data come from the Voyager flybys and Earth-based telescopes and then from the remote-sensing instruments on Cassini. The review covers the deep atmosphere, the troposphere, the stratosphere, and dynamical features such as the jets, waves, discrete features. Del Genio and Barbara (2016) provide a classification scheme based on cloud morphology for revealing the underlying dynamics.

2.2 Elemental and Isotopic Abundances

Counted by the number of atoms, the Sun is approximately 99.9% hydrogen/helium and 0.1% everything else. In our solar system, Jupiter comes closest to having the same

abundance ratios relative to H as the Sun and Saturn comes next, with higher heavy-element ratios than Jupiter. Abundance ratios relative to H that are different from the solar ratio provide observational constraints for the formation and evolution of the planet.

The helium to hydrogen ratio in the atmosphere reflects the value in the solar nebula when the planets were forming as well as the degree to which helium has settled toward the core. Settling is thought to happen because helium becomes immiscible in metallic hydrogen, which is the dominant constituent at megabar pressures. The settling releases gravitational potential energy, which affects the cooling history and planetary evolution. In principle, helium is detected by remote sensing through its effect on the molecular weight of the gas. One uses occultation data to get density vs. altitude, and from the hydrostatic equation one gets density vs. pressure. Then one uses infrared data to get temperature vs. pressure, and with the equation of state one can solve for the molecular weight. The method was used for Jupiter and Saturn using Voyager data (Conrath et al. 1984), but the Galileo probe gave a different result for Jupiter and forced a reanalysis for Saturn (Conrath and Gautier 2000). Cassini has collected excellent data using CIRS for the temperature and occultations by several instruments—radio science, VIMS, and the Ultraviolet Imaging Spectrograph (UVIS), but getting a consistent estimate of the helium abundance is difficult. The occultation result depends on the ray path, and that depends on unknown winds and temperatures above the occultation point. The most recent estimate (Koskinen and Guerlet 2018) uses Cassini UVIS for the occultations and CIRS for temperature versus pressure. They get a helium mass fraction Y of 0.16–0.22, which is about 70% of the protosolar mass fraction of 0.27, implying that a certain amount of settling has occurred in Saturn's interior.

Before Cassini reached Saturn, the C/H abundance ratio was known to be higher on Saturn than on Jupiter, which was known to be higher than that on the Sun (Atreya et al. 1999, 2003; Owen and Encrenaz 2003). The C/H ratio is perhaps the most accurately known ratio of all the heavy elements because its molecular form, methane, doesn't condense at Saturn temperatures and isn't readily destroyed in chemical reactions. Cassini CIRS probes the far-infrared rotational lines of the molecule and has determined a volume mixing ratio of $(4.7 \pm 0.2) \times 10^{-3}$, corresponding to a C/H enrichment relative to solar of 10.4 (Fletcher et al. 2009b). This is more than a factor of 2 greater than that for Jupiter but consistent with conventional models of the formation and evolution of the giant planets, which predict increasing ratios to H of the heavy element abundances relative to the Sun from Jupiter to Neptune (Atreya et al. 2019).

Saturn's greater enrichment is also qualitatively consistent with the masses and radii of the two giant planets. These, coupled with the gravitational moments, rotation rate, and an equation of state, give information about the core mass and amount of heavy elements in the molecular envelope (Guillot 1999; Nettelmann et al. 2013). Chemical models preceding the arrival of Galileo and Cassini listed many gases that were potentially observable in the atmospheres of Jupiter and Saturn (Fegley and Lodders 1994). Water is crucial because O is the third most abundant element after H and He, but the vapor pressure is so low at the tops of the clouds that Cassini could not detect it. Methane is much more volatile than water, so it does not condense in Saturn's atmosphere. Thus the C/H ratio derived from methane is likely to be representative of the planet as a whole.

The high C/H ratio is taken as evidence of heavy element enrichment in general and has implications for possible differential sedimentation in the planet's interior over its lifetime (Mousis et al. 2006). Measurements of NH_3, PH_3, C_2H_2, C_2H_6, and CH_4 all are consistent with these gases trapped as clathrate hydrate in the feeding zone of Saturn as the planets were forming (Hersant et al. 2008). Clathrate hydrates require water, and our lack of knowledge of the oxygen abundance allows for a number of interior models with a range of values for the C/O ratio (Lunine 2011). CIRS measurements suggest that Saturn's D/H ratio is less than that for Jupiter, which mostly reminds us that our understanding planetary formation and evolution is incomplete (Pierel et al. 2017).

Although ammonia is the main carrier of nitrogen on Jupiter and Saturn, the isotopic ratio $^{15}N/^{14}N$ can reveal insights into the molecular carrier (N_2 versus NH_3) in the protoplanetary nebula. The Saturnian and Jovian isotopic ratios appear indistinguishable (Abbas et al. 2004; Fletcher et al. 2014; Fouchet et al. 2004a) and distinctly lower in ^{15}N than Titan. That result favors accretion of primordial N_2 on both planets, either in the gas phase from the solar nebula or as ices formed at very low temperature (Fletcher et al. 2014), and a different source reservoir for the ^{15}N-enriched atmosphere of Titan.

2.3   Variability of Trace Gases

The gaseous composition of a giant planet atmosphere varies due to several processes: condensation and precipitation that remove the particles from the gas, updrafts and downdrafts that alter the chemical equilibrium of the various reacting species, and photochemical reactions that lead to dissociation and/or ionization. In addition, the upper atmosphere may receive molecules and solid particles from the rings and satellites.

Fletcher et al. (2011a) review the elements that appear in simple compounds that are detectable in VIMS spectra, including PH_3, NH_3, AsH_3, GeH_3, CO, CH_3D, and $^{13}CH_4$. They use VIMS 4.6–5.1 μm nightside spectra and solve for cloud properties and molecular abundances in the 1–4 bar pressure range. Figure 2 is the result, and there seem to be contradictions in whether there is upwelling or downwelling at the equator. NH_3 is removed from the gas by condensation and precipitation, but only above the 1.5 bar level. PH_3 and AsH_3 are removed from the gas by chemical reactions at pressures 3 bars. The VIMS is seeing variability at different altitudes. Fletcher et al. calculate that the maximum of NH_3 at the equator indicates equatorial upwelling at P < 1.3 bars, and the minima of PH_3 and AsH_3 at the equator indicate equatorial downwelling at P > 2.8 bars. In other words, Fletcher et al. are postulating two stacked, oppositely-directed Hadley cells based on their data. Clouds make the inversion non-unique, and the authors concede that the idea is speculative. The 2-cell idea originated with the Galileo mission to Jupiter (Ingersoll et al. 2000; Gierasch et al. 2000; Showman and de Pater 2005) to explain the preponderance of lightning in the (cyclonic) belts despite strong evidence of upwelling in the upper troposphere of the (anticyclonic) zones (Gierasch et al. 1986).

Fouchet et al. (2009) give a comprehensive review of Saturn composition and chemistry. Howett et al. (2007) and Guerlet et al. (2009) focus on C_2H_2, C_2H_6, and C_3H_8, which are produced above the 1 mbar level by photodissociation of methane. They use Cassini CIRS data to infer a stratospheric circulation from south to north during the southern summer.

Guerlet et al. (2010) added C_3H_8 and CH_3C_2H to the list of tracers and again found evidence of upwelling in the south and downwelling in the north. Fletcher et al. (2007a) also used CIRS data, focusing on phosphine, PH_3. It is in chemical equilibrium below the cloud tops and is destroyed by photolysis in the stratosphere. The altitudes of sources and sinks are opposite to that of C_2H_2 and C_2H_6, but the inferred circulation is similar.

Cassini CIRS data stimulated photochemical modeling in order to quantify the inferred circulations (Dobrijevic et al. 2011; Hue et al. 2015). The data also stimulated laboratory measurements (Auwera et al. 2007; Devi et al. 2014) to refine the infrared absorptions of these gases. Gases like CH_4, C_2H_2, and C_2H_6 absorb and emit in the infrared, and their spatial and temporal variations create temperature variations, which in turn affect the circulation. These interactions are studied with a 2-D photochemical model (Hue et al. 2016). They obtain "moderate" agreement with the observed species distributions, but they say that more sophisticated 2D and 3D representations of transport are needed.

Intensified Earth-based observations are a further desirable result of Cassini's mission to Saturn. Some of the observations immediately preceded the outpouring of Cassini data (Kim and Geballe 2005; Tejfel 2005), both to extend the range of temporal variability and to compare inferences based on different data sets. For instance, microwaves are sensitive to ammonia vapor at deeper levels than those probed by infrared radiation. The Cassini RADAR used in passive mode collects thermal radiation at 2.2 cm wavelength. With laboratory measurements of the ammonia opacity (Hanley et al. 2009), the Cassini 2.2 cm data were used to infer depletion of ammonia below the expected base of the ammonia cloud (Janssen et al. 2013; Laraia et al. 2013). This depletion is observed on Jupiter as well and has not been fully explained. The NH_3 abundance is controlled mostly by condensation and evaporation, which is more tied to the cloud structure, so it reveals different aspects of the circulation (Hurley et al. 2012b) than that of the hydrocarbons.

In giant planet atmospheres, the principal oxygen-bearing molecules are H_2O and CO, with the latter in equilibrium at higher temperatures and pressures than the former. However, water is frozen out at high altitudes, so the presence of CO_2 at the 1 mbar level suggests a source outside the planet. Abbas et al. (2013) argued that the oxygen source is interstellar dust. Cavalie et al. (2019) argued that the plumes of Enceladus are the most likely source. Abbas et al. use Cassini CIRS data and Cavalie et al. use Hershel data, but the latter group base their argument on the fact that stratospheric water peaks at the equator whereas interstellar dust would not.

3 Heat Flux, Winds and Temperatures

3.1 Radiation Budget

The internal heat coming out of the planet is a fundamental quantity relevant to formation and evolution. Because giant planets in our solar system are massive and their surfaces are cold, they cool off slowly. Their interiors are still warm, and they are still releasing some of their heat of formation. To measure the internal power one takes the difference between the emitted infrared power and the absorbed solar power, which is the difference between the incident and reflected sunlight. Using Voyager data, Hanel et al. (1983) estimated the

effective emission temperature as 95.0 ± 0.4 K, corresponding to an average emitted heat flux of 4.62 ± 0.8 Wm^{-2}, and the ratio of emitted power to absorbed power as 1.78 ± 0.09. Thus the internal power divided by the absorbed solar power is 0.78. Using data from Cassini CIRS, Li et al. (2010) estimated the emitted heat flux as 4.952 ± 0.035 Wm^{-2} during 2004–2009, although it decreased by 2% during that time and was 16% higher in the southern hemisphere than in the northern hemisphere. These were likely seasonal changes associated with the approach of vernal equinox in 2009. Li et al. (2015) measured the emitted power vs. latitude from 2004 to 2013 and documented the 2010 great storm's effect, which was to increase the global emitted power by 2% and the power at the latitude of the storm by 9% (Fig. 3). These changes were in addition to a seasonal warming of the north and cooling of the south from 2004 to 2013.

3.2 Seasonal Variations

Two opposing effects control the amplitude of seasonal variations on Saturn (Fig. 4). The obliquity is 26.73°, which is larger than that of Earth, and is tending to produce large seasonal variations in incident sunlight. These variations are augmented by the rings, which block sunlight from reaching large parts of the winter hemisphere. On the other hand, Saturn's troposphere is massive, with clouds of water down to the 20-bar level, assuming the enrichment of water relative to solar composition is the same as that of methane, whose abundance can be measured spectroscopically. Further, the high specific heat of hydrogen gives the troposphere a huge thermal inertia, so the atmosphere tends to average over the seasonal cycle rather than respond to it. Seasonal averaging is reduced in the stratosphere (Fig. 4), because it has less thermal inertia than the troposphere. Seasonal change is reflected in the emitted power as a function of latitude (Li et al. 2015) as the northern hemisphere season changed from winter to late spring over the period 2004–2013 (Fig. 3).

Using Cassini CIRS data Fletcher et al. (2010) showed that the stratosphere has a greater range of temperatures than the troposphere, which is consistent with the greater thermal inertia of the latter. They point out that a photochemical haze develops in the spring/summer hemisphere (Fig. 1). Fletcher et al. (2015) observed polar cooling and depletion of acetylene in the southern hemisphere during fall and winter. Tropospheric temperature variations are small (Fletcher et al. 2016) and show a substantial seasonal lag time, as expected. These seasonal changes are superposed on a general upwelling in the tropics and downwelling at the poles, as revealed by the two states (ortho and para) of the H_2 molecule (Fletcher et al. 2016, 2017). Sinclair et al. (2013) and Sylvestre et al. (2015) compare CIRS observations of C_2H_2, C_2H_6, C_3H_8 and temperature between 2005 and 2010 with a static photochemical model (Moses and Greathouse 2005) and find substantial effects of circulation and transport in addition to variations due to chemistry. Seasonal change of temperature, composition and aerosol is extensively reviewed by Fletcher et al. (2018c).

3.3 Zonal Jets and Temperatures

Winds are motions of the atmosphere relative to the rotating planet, and for Jupiter, Uranus and Neptune the wobble of the planet's tilted magnetic field provides the planetary rotation rate. Saturn's field is tilted less than 0.007° and therefore does not provide a physically-based reference frame (Cao et al. 2020). For locating cloud features, scientists use a period

(10:39:24 s) that was defined following the Voyager encounters, knowing that the computed winds might be systematically too fast or too slow by over 100 ms^{-1}.

Tracking small clouds in sequences of images is the principal way of measuring the winds (Fig. 5). ISS provided the first data at the start of the Cassini mission (Garcia-Melendo et al. 2011b; Porco et al. 2005; Vasavada et al. 2006) and a valuable comparison with Voyager 25 years earlier. VIMS can measure the winds at somewhat deeper levels than ISS. CIRS can measure the gradient of the wind with respect to altitude by measuring the gradient of temperature with respect to latitude and applying the thermal wind equation. Except at the equator, the mean zonal winds—the eastward winds averaged with respect to longitude —are remarkably steady. This conclusion follows, in part, by comparing the mean zonal winds during Voyager times with those measured by Cassini 25–30 years later (Antunano et al. 2015; Choi et al. 2009; Li et al. 2011, 2013; Vasavada et al. 2006). Images taken at wavelengths where methane is a strong absorber tend to sample higher altitudes than those where methane is transparent. Vertical shears show up in the eastward jets (Garcia-Melendo et al. 2009, 2011a, 2011b), which is consistent with the horizontal temperature gradient and the thermal wind equation

At the equator, the speed of the zonal wind in the upper troposphere and stratosphere oscillates with a ~15-year period, which is half the Saturn year (Fouchet et al. 2008) (Fig. 6). In that sense, it is a semiannual oscillation. Since vertical shear in the zonal wind is related to horizontal gradients of temperature through the thermal wind equation, the oscillation reveals itself in the temperatures on either side of the equator. It shows up in the lower panel of Fig. 4 as the tripolar structure spanning the equator. Similar oscillations occur in the stratospheres of Earth and Jupiter. On Jupiter, the period is about four years. On Earth, there are two oscillations: the semi-annual oscillation (SAO), which has a period of six months, and the quasi-biennial oscillation (QBO), which has a period of about 22 months. The QBO is thought to be forced by waves propagating up from the troposphere, with feedback between the wind profile and the altitude where the waves deposit their zonal momentum. Downward propagation of the wind profile and the upward-propagating waves needed to support it have been extracted from CIRS limb observations (Guerlet et al. 2011, 2018).

The SAO period is the time between successive solstices, regardless of sign, and it could be forced by radiation. Sinclair et al. (2014) compare temperatures and gaseous abundances from Cassini with those from Voyager exactly one Saturn year later. They find changes, but most of them could be accounted for by a change in phase of the stratospheric oscillation, suggesting that the oscillation is only "quasi-semiannual". For a review, see Read (2018).

In preparation for the Cassini encounter, Voyager and Hubble Space Telescope observations were used to document the variability of the zonal wind in the equatorial stratosphere (Perez-Hoyos and Sanchez-Lavega 2006; Sanchez-Lavega et al. 2000). Sanchez-Lavega et al. (2007) and Garcia-Melendo et al. (2010) used Cassini ISS images in the methane bands to further document the vertical wind shear and its temporal variability. Li et al. (2008) used Cassini CIRS data, where the oscillation is revealed in stratospheric temperatures, and Li et al. (2011) showed that the temperatures and cloud-tracked winds are consistent with the QBO oscillation mechanism. Schinder et al. (2011) used radio occultations by

the Cassini spacecraft to measure temperature and showed that the zonal wind profile propagates downward as on Earth, consistent with the wave forcing mechanism of the QBO. Downward propagation also shows up in the thermal infrared maps based on CIRS data (Fouchet et al. 2008; Guerlet et al. 2011). Sanchez-Lavega et al. (2016) used ISS data to track individual features in the upper haze and clouds and further demonstrated the intense vertical shears and temporal variability.

A fundamental question dating back to Voyager days (Gierasch et al. 1986), for both Jupiter and Saturn, is why the zonal jets and the flow around the large ovals decay with height above the tops of the clouds. For Saturn this decay is seen, first, by tracking clouds in filters that sample different altitudes, like the winds within ±15° of the equator in Fig. 5 (Garcia-Melendo et al. 2009, 2011b). Second, the decay is inferred from the temperature gradients with respect to latitude—the spiky excursions in Fig. 3 and the little bumps and wiggles at mid latitudes in Fig. 4. These bumps and wiggles are not noise; the peak gradients are located at the latitudes of the zonal jets, and the thermal wind equation integrated upward from the cloud tops indicates that both the eastward jets and the westward jets are losing speed with altitude (Fletcher et al. 2008; Read et al. 2009b). The opposite behavior seems to occur from 2 bars to 300–500 mbar, as seen in Cassini VIMS images (Studwell et al. 2018). The temperature gradients could be forced by differential heating, or the decay of the jets could be forced by wave transport of momentum or both, since the two are linked by the thermal wind equation. Either way, the forcing has not been properly identified and the question remains open.

4   The Great Storm of 2010–2011

4.1   Storm Clouds and Convection

Saturn is prone to large-scale eruptions (Fig. 7). They start with a small cloud that grows rapidly during its first week and expands zonally, until after 2 or 3 months the disturbance has fully encircled the planet within its latitude band. The paper by Sanchez-Lavega (1994) is the definitive pre-Cassini review of these phenomena. He calls them Great White Spots, and he lists five of them before the Cassini era: 1876, 1903, 1933, 1960, and 1990. This gives an average periodicity of 28.5 Earth years, which is close to Saturn's year of 29.46 Earth years. The corresponding latitude bands of these storms are 8±3°, 36±2°, 2±3°, 58±1°, and $12 \pm 1°$, all in the northern hemisphere. Whether the disturbances are in a unique class or just the largest in a continuous distribution of sizes is uncertain. Intermediate-scale storms do exist (Sanchez-Lavega et al. 2020a). And whether the disturbances are locked in phase to Saturn's year is also uncertain, because within each latitude band the period is much longer than a Saturn year. And the great storm of 2010–2011 came 10 years too early to satisfy the annual cycle hypothesis.

Saturn's great storm of 2010–2011 was a singular event in Cassini's 13-year tour of the Saturn system (Sanchez-Lavega et al. 2011, 2018). It began as a small (~1000 km) spot captured in a routine ISS image on December 5, 2010. Cassini Radio and Plasma Wave Spectrometer (RPWS) had been detecting lighting discharges (Fig. 8) from the storm for a few hours when the image was taken (Fischer et al. 2011). The lightning continued for the ~7 month lifetime of the storm as the westward-moving head left behind a tail that

eventually wrapped around the planet. In its mature phase, the storm filled a latitude band 10,000 km wide that was centered at a planetocentric latitude of 35°. Amateur astronomers with Earth-based telescopes were following the storm within days of its appearance, and Cassini began systematic imaging in January 2011.

Visible-light images of clouds in the troposphere (Sanchez-Lavega et al. 2012; Sayanagi et al. 2013) showed that the head spawned large (10,000 km diameter) anticyclones that drifted off to the east and became part of the tail. Amateur astronomers provided nearly continuous coverage. The storm seems to have originated from a feature called the string of pearls, a train of cyclones at the latitude of the great storm (Sayanagi et al. 2014). Garcia-Melendo et al. (2013) are able to reproduce many of the observed morphological features of the storm with a prescribed heat source moving at a prescribed velocity. Li and Ingersoll (2015) present a theory that reproduces the observed drying (low mixing rate of ammonia) of the storm's latitude band (Fig. 9) (Janssen et al. 2013; Laraia et al. 2013) as well as the multi-decadal interval between great storms. The latter is tied to mass loading, i.e., the stabilizing effect of water and ammonia condensation in a low molecular weight (H_2 and He) atmosphere. Above a critical abundance of the condensates, the atmosphere becomes stable after a convective event, and the time needed to destabilize the atmosphere is decades. Based on the C/H ratios for Jupiter and Saturn, assuming the same enrichment factors relative to solar for O/H, Saturn is above the critical value and Jupiter is below it, which could explain why only Saturn has these great storms.

4.2 Chemical Tracers and Vertical Motion

Thermal infrared spectroscopy by Cassini CIRS revealed effects of the storm that penetrated into the stratosphere to the 1 mbar level (Fletcher et al. 2011b). Subsidence of air in the stably-stratified stratosphere produced beacons as much as 16 K warmer than their surroundings (Fig. 10). By May 5, 2011, the beacons had reached temperatures of 226 K, about 80 K warmer than the surrounding stratosphere (Fletcher et al. 2012; Fouchet et al. 2016). The storm produced a 100-fold increase of ethylene in the stratosphere near the beacon (Hesman et al. 2012). Photochemical models cannot explain this increase, so some dynamical mechanism must be at work (Cavalie et al. 2015; Moses et al. 2015). Temperatures in the troposphere at the latitude of the storm increased by 3 K, and the para fraction of H_2 decreased by about 0.4, indicating warm air upwelling from below (Fig. 11) (Achterberg et al. 2014). The speed of the upwelling is uncertain partly because the time constant for approach of para H_2 to equilibrium is uncertain and partly because the existence of a hydrogen dimer complicates the interpretation of the spectrum (Fletcher et al. 2018a).

The 2010–2011 storm seems to have affected clouds and haze, both at the latitude of the storm and farther away. Sromovsky et al. (2013) used VIMS spectra to study the composition of the cloud particles lofted by the storm, and found evidence of ammonia ice, water ice, and ammonium hydrosulfide. This is the first spectroscopic evidence of water ice in Saturn's atmosphere and indicates upwelling from 200 km below the tops of the ammonia clouds. Further study of the aftermath of the storm reveals clearing of the ammonia cloud with some residual particles of other species (Sromovsky et al. 2016). According to an analysis of VIMS data, a residual haze layer persisted in the upper troposphere and

lower stratosphere as well (Oliva et al. 2016). The great storm seems to have caused a 10 K warming of the middle atmosphere (0.5–5 mbar) at the equator, providing evidence of teleconnections between latitudes (Fletcher et al. 2017).

5 Vortices, Mean Flow and Eddies

5.1 North Polar Hexagon

Saturn's hexagon is a six-lobed meandering pattern in an eastward jet centered at 75° north latitude (Fig. 12). The excursions in latitude are approximately ±1°, which gives the structure its polygonal shape. Larger excursions would give it a more sinusoidal, wave-like shape. The hexagon was discovered in Voyager images taken in 1980 and was discovered again by Cassini VIMS, before the spring equinox when the North Pole was still in darkness (Baines et al. 2009b). Its effects extend into the stratosphere to altitudes of 0.5 mbar (Adriani et al. 2015; Fletcher et al. 2018b; Pryor et al. 2019; Sanz-Requena et al. 2018; Sanchez-Lavega et al. 2020a, 2020b). Based on ISS and VIMS imaging, the hexagon is a meandering jet whose 6-lobed pattern moves slowly or not at all relative to the nominal rotation rate for Saturn, which was defined following the Voyager encounter (Desch and Kaiser 1981). Small clouds within the jet move at ~125 ms^{-1} relative to the pattern. Thus the hexagon is like a road fixed in the Voyager reference frame, and the clouds in the jet are cars moving along the road. Based on the hexagon's long-term stability, Sanchez-Lavega et al. (2014) argue that it is a deep-seated feature that could reveal the true rotation of the planet.

Each pole of Saturn is occupied by a single isolated cyclonic vortex with peak winds of 150 ms^{-1} (Dyudina et al. 2008, 2009; Sanchez-Lavega et al. 2006; Antunano et al. 2015; Liu et al. 2019). The latitude of the peak winds is 88.5° (Antunano et al. 2015), which means that the average relative vorticity within 1.5° of the poles is equal to 0.57 times the local planetary vorticity. Based on Cassini ISS, VIMS, and CIRS data, Dyudina et al. (2008) and Dyudina et al. (2009) interpreted the vortex as a hurricane-like eye with eyewall clouds at 88.5° extending 20–70 km above the clouds at the pole. Sromovsky and Fry (2019) argued that an abrupt change of optical thickness could mimic the apparent eyewalls. The region has a 4–7 K warm core extending from the upper troposphere into the stratosphere (Achterberg et al. 2018). The warm core and stable stratification imply downwelling, which is consistent with the observed low phosphine abundance in the core (Fletcher et al. 2008). Downwelling is also consistent with the near absence of high- and medium-level clouds in the eye (Sromovsky et al. 2020), although isolated convective clouds are present (Baines et al. 2018). Outside the eyewall are numerous anticyclonic vortices suggesting a convective origin (Dyudina et al. 2009). Sayanagi et al. (2017) compared the north and south polar cyclones and attributed the differences to seasonal effects. Polar phenomena are extensively reviewed by Sayanagi et al. (2018).

5.2 Eddy Mean-Flow Interaction

Giant planet atmospheres are a superb laboratory for studying the dynamics of rotating fluids. Cloud tracking provides estimates of the winds, and the lack of continents and oceans provides a simpler setting than on Earth. The Cassini mission advanced this field, not only by providing 13 years of observations of Saturn but also by providing a 3-month

flyby of Jupiter with an upgraded suite of instruments compared with those on the Voyager flybys. The Jupiter observations are discussed in Sect. 8 of this paper. Here we focus on observations and models of the jets and vortices in Saturn's atmosphere. Saturn's atmospheric dynamics is extensively reviewed by Showman et al. (2018).

The eddy momentum flux is a fundamental quantity. Eddies are the residuals after the time- and longitude-dependent mean winds $\bar{u}$ and $\bar{v}$ have been subtracted off. The eddy eastward wind is u' and the eddy northward wind is v'. By definition the means of u' and v' are zero, but the mean of their product $\overline{u'v'}$ may be non-zero. Multiplied by the gas density, $\overline{u'v'}$ is the eddy momentum flux—the northward flux of eastward momentum. Using ISS data, Del Genio et al. (2007) and Del Genio and Barbara (2012) measured $\overline{u'v'}$ as a function of latitude (Fig. 13). The middle panel of Fig. 13 shows negative values of $\overline{u'v'}$ at 8–18° north latitude, indicating southward transport of eastward momentum by the eddies. The positive values at 8–18° south latitude indicate northward transport of eastward momentum. In other words, the eddies are subtracting eastward momentum from the westward winds beyond ±8–18° and adding it to the eastward winds within 8° of the equator. This seems counterintuitive, but it also occurs on Earth and Jupiter. The basic requirement is that the eddies have a source of energy that is distinct from the kinetic energy of the zonal jets.

If the eddy momentum flux were the only process acting, the jets could not be in equilibrium. To balance the eddies, there has to be an equatorward meridional flow ($\bar{v} < 0$ in the north, $\bar{v} > 0$ in the south), which carries low-angular momentum air to the equator. Thus air is approaching the equator from both sides. The net result is downwelling at the equator and upwelling where the meridional flows originate, i.e., in the ±8–18° latitude range. This picture applies in the troposphere and is consistent with the inferences drawn from the distributions of PH_3 and AsH_3 in Fig. 2.

Higher up, in the upper troposphere and stratosphere, other processes dominate. In the last paragraph of Sect. 3 we discussed the decay of zonal winds with height. Such decay requires a braking process—a force to the west acting on the eastward winds within ±8° of the equator (Fig. 5), and a force to the east acting on the westward jets farther from the equator. This force has not been identified, but it acts from the cloud tops up into the stratosphere. To balance it, there must be meridional flow, but that meridional flow must be diverging at the equator and converging between the eastward jet at the equator and the westward jets on either side of the equator. This leads to upwelling at the equator and downwelling on either side of the equator. This picture is qualitatively consistent with the inferences drawn from the NH_3 distribution shown in Fig. 2 but is opposite to those drawn from PH_3 and AsH_3. Although the braking force has not been identified, it is based on the decay of zonal jets with height and is consistent with the stacked, oppositely-directed Hadley cells suggested by the tracer distributions. Zuchowski et al. (2009) show that a simple analytic model forced by Newtonian relaxation of heat and momentum, properly aligned, could give rise to the two-cell system.

Zonal jet stability is another important observation. Stability depends on the potential vorticity gradient (Antunano et al. 2019), which depends on vertical structure, both of temperature and wind, but a simple but relevant criterion is that the flow is stable if the

curvature of the zonal wind profile with respect to latitude does not exceed β, which is twice the planet's angular velocity times the cosine of latitude divided by the planetary radius. Interestingly, this stability criterion is violated on Saturn near the peaks of the westward jets, especially at high latitudes, indicating that the zonal jets could be unstable (Antunano et al. 2015; Read et al. 2009a). That does not mean the flow is unstable, however, as there are other stability criteria that involve vertical structure (Dowling 1995). Liao et al. (2007) argue that a statistical equilibrium occurs as the growing wave saturates. In their global vortex analysis, Trammell et al. (2014) find a correlation between the number of vortices and the westward jet peaks, implying at least some degree of instability at those latitudes.

Waves and vortices are another important feature of giant planet atmospheres. Saturn currently has nothing like the Great Red Spot, which has endured for over 100 years, but it has similar structures. Generally, anticyclones last longer than cyclones, but del Rio-Gaztelurrutia et al. (2010, 2018) document a cyclone that lasted for four years. For a comprehensive review of spots and vortices during the Cassini mission, see Hueso et al. (2020). Convective storms can generate waves that transport westward momentum away from their source regions, helping to accelerate eastward jets at the latitudes of the convection (Gunnarson et al. 2018; Liu and Schneider 2015; Sayanagi and Showman 2007). This acceleration must be balanced somewhere, and (Schneider and Liu 2009) argue that the balance occurs through magneto-hydrodynamic drag at 0.3 to 1.4 Mbar where the atmosphere becomes electrically conducting (Liu et al. 2014; Liu and Schneider 2015).

5.3 Modeling Studies

Saturn's north polar hexagon at 75° latitude has inspired several modeling studies, both in the laboratory (Aguiar et al. 2010) and on the computer (Morales-Juberias et al. 2011, 2015; Rostami et al. 2017). Morales-Juberias et al. (2011, 2015) use the EPIC general circulation model with 20 vertical layers, and Rostami et al. (2017) use a shallow water model, which has only one layer. Both models start with an unstable zonal jet at the latitude of the hexagon, and with the right parameter settings the growing wave saturates as a hexagonal pattern that resembles the observed one. Morales-Juberias et al. (2015) get the best fit when the strength of the jet decreases with depth, and Rostami et al. (2017) get the best fit when they include a central cyclone within 2° of the pole. Central cyclones exist at both poles, and the main observable difference between north and south is that the southern jet is at a lower latitude than the northern one, 70.4°S vs. 75.8°N planetocentric (Antunano et al. 2015). The main unknown is the radius of deformation, which is related to the mean stratification within the weather layer—from the tops of the ammonia clouds to the base of the water cloud. Why there is only one hexagon is still uncertain.

Saturn's ribbon at 47° latitude is a less dramatic relative of the hexagon (Sayanagi et al. 2010), since both seem to represent a steady meandering pattern on an eastward jet stream. The models do not explain why the conditions necessary for a long-lived meandering jet stream exist only at certain latitudes on Saturn or why there are no such jet streams on Jupiter. O'Neill et al. (2015, 2016) propose a model of Saturn's polar cyclones in which convection at mid latitudes produces a vortex that is cyclonic at the bottom and anticyclonic at the top. The two halves separate, and the cyclonic vortex drifts to the pole and merges

with other cyclonic vortices to make a single polar vortex. Brueshaber et al. (2019) report on one-layer shallow-water simulations of poleward drifting cyclonic vortices that merge to form polar vortices, and also reveal a mechanism that separateS the polar dynamical regimes of Jupiter, Saturn, and Uranus/Neptune. On the other hand, Antunano et al. (2018) report no meridional migration in the region north of the hexagon, and suggest that mergers do not contribute to the maintenance of the polar vortex. Sanz-Requena et al. (2018, 2019) describe the haze and cloud structure in the north pole and hexagon region.

Saturn's great storm has also inspired modeling studies. One model uses an imposed heat pulse and studies its interaction with the ambient zonal flow (Garcia-Melendo and Sanchez-Lavega 2017). Another model studies how precipitation of water, because of its high molecular mass relative to hydrogen, can stabilize the atmosphere and inhibit convection for decades due to the long radiative time constant of Saturn's atmosphere (Li and Ingersoll 2015). A third model uses a long-term numerical integration of moist convection in a giant planet atmosphere (Sugiyama et al. 2014). The simulations are conducted using a two-dimensional cloud-resolving model that explicitly represents the convective motions and microphysics of NH_3, NH_4SH, and H_2O. It produces intermittent cumulonimbus activity. The time scale is ~60 days, although it is proportional to the water abundance and is therefore likely to be greater for Saturn than for Jupiter.

Numerical models of Saturn's jets and vortices fall into two categories. One is the conventional general circulation model (GCM), which uses hydrostatic balance in the vertical and is valid for large horizontal scales and small vertical scales (Friedson and Moses 2012; Garcia-Melendo et al. 2007; Trammell et al. 2016; Spiga et al. 2020). The other is the fluid sphere model in which the vertical and horizontal scales are comparable and the flow takes place in thick spherical shells (Aurnou et al. 2008; Heimpel and Aurnou 2007; Liu et al. 2014). Computational limitations make it difficult to develop a single model that includes both small and large vertical scales, although the effort to do that is being made (Heimpel et al. 2016; Cuff and Heimpel 2018). One model (Yadav and Bloxham 2020) suggests that Saturn's hexagon could extend down to where the magnetic field limits the flow speed by interacting with the electrically conducting fluid. More often, the practitioners divide into separate camps and work with different theoretical tools. The goal of these studies is to account for the observations—the number of belts and zones, their associated wind speeds, the stability and other properties of large vortices, and the direction of winds at the equator—prograde for Jupiter and Saturn and retrograde for Uranus and Neptune. The global distribution of temperature and outgoing longwave radiation with respect to latitude (Fig. 3), as well as the temperature gradients with respect to the zonal jets (Fig. 4) are another observable that the models could simulate. See the discussion at the end of Sect. 3.

5.4 Lightning

The Cassini RPWS detects the radio waves from lightning at frequencies starting at 1.3 MHz and ranging up to 40 MHz (Fischer et al. 2006a; Fischer et al. 2006b; Fischer et al. 2007; Fischer et al. 2008). A single flash is called a Saturn Electrostatic Discharge (SED), and it lasts for less than the 35.2 ms integration time of the RPWS instrument (Fig. 14). Fundamentally, the duration of an SED is unknown (Farrell et al. 2007). An SED is not

a whistler; it is a freely-propagating radio wave that follows a straight-line path from the source. Although the RPWS is listening virtually all the time, sometimes it detects nothing for months. SED activity is often from a single storm, with SEDs every few seconds for a 5-hour ON period followed by a 5-hour OFF period, when the storm is hidden behind Saturn. Often the storm itself is visible, both in ISS images (Dyudina et al. 2007) and in the images gathered by amateur astronomers at Earth. Criteria used to identify the storm are that it appeared within a day or two after the onset of SED activity and it was always on the side of the planet facing the spacecraft when the RPWS was detecting signals. Thus the number of lightning storms at any one time is likely to be either 0 or 1. In contrast, Earth has ~2000 lightning storms over the globe at all times, and Jupiter has dozens of storms at all times (Little et al. 1999).

Cassini ISS eventually detected the lightning flashes themselves (Dyudina et al. 2010), even on the day side despite the bright background of clouds in sunlight. The secret was to take many short exposures, since a short exposure reduces the background but not the lightning; it does reduce the probability of capturing a flash, so one needs to take many exposures. The diameter of the illuminated spot is about 200 km, indicating that the lightning is 125–250 km below cloud tops. This depth is above the liquid H_2O–NH_3 cloud and may be either in the NH_4SH cloud or the H_2O ice cloud.

The great northern storm of 2010–2011 was a copious lightning emitter (Dyudina et al. 2013; Fischer et al. 2011). The RPWS recorded flashes every 0.2 s. The optical energy per flash was about equal to that of the radio energy (Dyudina et al. 2013), although there is considerable uncertainty in both. The optical energy in single flashes ranged up to 8×10^9 J. The flash rate and total power were hundreds of times greater than those of the smaller southern storms that had been appearing intermittently since the start of Cassini observations. Fischer et al. (2014) proposed that the northern storm could account for a change in the Saturn kilometric radiation (SKR) frequency through its effect on thermospheric winds.

The Saturn lightning results stimulated two reviews of planetary lightning (Yair et al. 2008; Yair 2012). Lightning is an agent of chemical change. Based on VIMS observations, Baines et al. (2009a) proposed that the dark and spectrally featureless clouds associated with giant planet thunderstorms represent small particles of elemental carbon. The particles are postulated to arise from atmospheric methane exposed to high temperatures during the lightning discharge, but Sromovsky et al. (2018) argue that the dark features are more likely regions of reduced optical depth. Dubrovin et al. (2014) study the effect of lightning on the lower ionosphere of Saturn. They find that H_3^+ ions are rapidly produced from the parent H_2^+ ion. On the other hand (Hurley et al. 2012a) searched for but found no correlation between acetylene and thunderstorm activity on Saturn. The Saturn results also stimulated lightning searches throughout the solar system and on exoplanets from Earth-based radio telescopes and from spacecraft (Hodosan et al. 2016; Zarka et al. 2008).

6 Interior Structure and Rotation

6.1 Magnetic and Atmospheric Periodicities

The periodic variation of the dynamo field has been used to estimate the interior rotation rates of Jupiter, Uranus, and Neptune. However, Saturn's dynamo field axis is so closely aligned with its rotation axis that it has no measurable variation. Taking the misalignment of the other three giant planets, 10° for Jupiter, 60° for Uranus, and 47° for Neptune, the 0.007° upper bound for Saturn is highly improbable (1 chance in 10^6 or 10^7), given that the probability of the magnetic axis aligning with the rotation axis goes as the square of the angle between them (Dougherty 2017; Cao et al. 2020). The close alignment means that there is no detectable wobble in the field as the planet rotates and therefore no periodic signal with which to estimate the rotation period of the planet's interior. The SKR radio emissions are tied to currents in the magnetosphere and ionosphere, and the period is variable from year to year (Fischer et al. 2014), which rules out a direct tie to the interior of Saturn.

There have been various attempts to use the atmospheric periods to estimate the interior rotation rate. They use the data in different ways, but they all derive a period that is near the midpoint of the atmospheric periods. Smith et al. (1982) use cloud tracking and choose a reference frame that minimizes the variance of the cloud-tracked zonal wind with respect to latitude, with 10:31:30 ±30 s as the result. Anderson and Schubert (2007) chose the reference frame that minimizes the measured shape of the 100 mbar surface from an equipotential, with 10:32:35 ±13 s as the result. Read et al. (2009b) use the reference frame in which the atmosphere is marginally stable with respect to Arnol'd's second stability criterion, with 10:34:13 ±20 s as the result. Their method uses ISS and CIRS wind and temperature data to estimate potential vorticity in the range 2–270 mbar. The problem with these approaches is that they ignore the thermal wind equation, which allows vertical shear in the zonal winds. Thus the speed at depth might not match the average speed at the tops of the clouds where the winds and temperatures are measured. Read et al. (2009b) argue that the stability criterion depends on the speed of the longest Rossby waves, which are deeply rooted, perhaps extending to the base of the water cloud, but still the problem remains. For instance, the midpoint of the wind distribution at Earth's upper troposphere would give a period between 22 hours and 23 hours for the rotation of the planet, because the average wind at the top of the troposphere is to the east.

The gravity field (Jacobson et al. 2006) also has information about the rotation rate of the interior (Hubbard et al. 2009). As with all planets, Saturn's gravitational potential can be expanded into spherical harmonics, the leading term of which is the spherically symmetric potential −GM/R, followed by the zonal harmonics and the tesseral harmonics. The zonal harmonics are axially symmetric, and each term is proportional to a Legendre polynomial of degree n and a dimensionless amplitude factor J_n. The tesseral harmonics are the longitudinally-varying part of the gravitational potential. Saturn is a fluid planet, and if it were in equilibrium only the zonal harmonics with even n would be present. The J_n reflect the response of the planet to its own rotation, so one could use them to infer the interior rotation rate if the interior structure were known. Conversely, one could infer the interior

structure, e.g., core mass, metallic hydrogen, degree of helium separation, heavy elements in the molecular envelope, etc. if the rotation rate were known (Helled and Guillot 2013; Helled et al. 2015; Hubbard et al. 2009). Further information about the interior could come from the tidal Love number—the magnitude of the planet's response to tidal forces (Lainey et al. 2017). The tidal observations are astrometric data on the orbits of Saturn's moons spanning more than a century and include a large set of Cassini data. The study indicates significant tidal dissipation inside the planet. In all cases, an independent measure of the rotation rate is important for probing the internal structure.

6.2   Normal Modes and Gravity

The tesseral harmonics have an effect on the rings, which are a sensitive seismometer for detecting the non-zonal gravity field (Hedman and Nicholson 2013, 2014). The harmonics are of two types. One type has pattern speeds ranging from 807 to 834 degrees per day, for which the corresponding periods are 10:42 m to 10:22 m, respectively (Fig. 15). These nearly bracket the periods derived from tracking the clouds at various latitudes in Saturn's atmosphere, and could be due to non-zonal structures rotating with the planet. The large range of periods prevents improving on cloud tracking estimates alone.

The other types of tesseral harmonics have pattern speeds near five hours and are thought to be due to normal mode oscillations inside the planet. The precise frequencies of these normal modes depend both on the interior structure and the rotation rate. Parameters of the interior structure include the mass of the core, the helium mass fraction, the heavy-element mass fraction in the metallic and molecular envelopes, and the pressure at the metallic-molecular transition (Mankovich et al. 2019). For a given rotation rate, the interior parameters are adjusted to give the observed values of J_2 and J_4. The rotation rate is varied to give the best fit to the observed frequencies of the ~20 normal modes whose resonant effect on the ring orbits makes them detectable. The planet's rotation affects the frequencies through the Coriolis and centrifugal forces and the ellipticity of level surfaces. The distribution of rotation periods resulting from a broad sample of interior models can be summarized as $10^h 33^m$ (Mankovich et al. 2019). The residuals of the fit do not exhibit any strong evidence of differential rotation inside the planet, but differential rotation cannot be ruled out. The rotation period is consistent with predictions by Militzer et al. (2019) who combined interior models, which were constrained by Cassini's gravity measurements, with observations of the planet's oblateness by the Voyager spacecraft. Based on this analysis, a rotation period of 10:33:34 ± 55 s is predicted for the planet's deep interior.

The even zonal harmonics, especially $n = 6$ and above, can be used to detect differential rotation inside the planet (Galanti and Kaspi 2017; Kaspi 2013). This method is being used both with Cassini at Saturn and with Juno at Jupiter. The odd harmonics have been used only at Jupiter. The software to analyze these data was developed to be used on both planets (Galanti and Kaspi 2016; Galanti et al. 2017; Kaspi et al. 2016). Cassini produced its best gravity data during six dives between the planet and the innermost ring during the final five months of the mission (Iess et al. 2019). On these dives the spacecraft skimmed 2600–3900 km above the cloud tops while the radio link to Earth was monitored to determine the gravitational field of the planet and the mass of the rings. The gravity measurements yielded

unexpectedly large values of the even zonal harmonics J_6, J_8 and J_{10}. These values do not match any interior model that assumes uniform rotation and makes reasonable assumptions about the equation of state and helium rain (Iess et al. 2019). Galanti et al. 2019 confirmed that an acceptable solution can only be found for J_2 and J_4.

One can fit all the even harmonics J_2-J_{10} with a model where unknown winds extend through the planet on cylinders. The best fit is where the atmosphere at the equator rotates 4% faster than the deep interior, but the models also require a region that rotates more slowly than the deep interior, which is surprising because it is not seen in the cloud tracking data. One can also fit the harmonics by assuming the observed cloud-top winds extend to a finite depth. The best fit is with a finite depth of 9000 km. Qualitatively the two results are the same, since the cloud-top winds are fastest at the equator. The depth of the winds for Saturn is 2–3 times deeper than that for Jupiter, but the difference is explained by the more rapid increase of electrical conductivity with depth on Jupiter. A comparison of the deep dynamics of Jupiter and Saturn in light of Juno and Cassini gravity measurements is presented by Kaspi et al. (2020). Whether magnetic drag suppresses differential rotation directly (Guillot et al. 2018) or indirectly through its effect on the stratification (Christensen et al. 2020) is an open question. Another open question is whether the measured odd zonal harmonics of the gravity field could be due to an extension of the cloud-level zonal winds, as seen on Jupiter by Juno (Kaspi et al. 2018). Kong et al. (2018) and Qin et al. (2020) claim that such an extension does not fit the data, and that the cloud-level winds are confined to a thin layer.

Once the gravity signal of the deep winds is adequately incorporated into models for Saturn's interior, reasonable structures are obtained (Iess et al. 2019; Galanti et al. 2019; Movshovitz et al. 2020). The conditions of helium rain are compatible with predictions from ab initio computer simulations. Cores of heavy elements with 15–18 Earth masses are compatible with the core-accretion hypothesis, which requires an 8-Earth mass core to trigger run-away gas accretion. The enrichment of heavy elements in the planet's molecular envelope of 1–3 times solar is lower than expected but still reasonable. This agreement with other sources of information contrasts with the persistent conundrum for Jupiter, for which the inferred heavy abundances are near or subsolar.

A puzzling feature of this analysis is that the same model of the gravitational field cannot fit all of the six passes in a combined, multi-arc orbital solution (Iess et al. 2019). The residuals represent unmodeled accelerations acting on Cassini over time scales of 20–60 min and could be due to time-varying tesseral harmonics. Convection in Saturn's interior is one possible source. Normal modes varying in amplitude and frequency is another. The data were eventually fit by assuming random accelerations of 10 minute duration acting within ±1 hour from pericenter (Iess et al. 2019). The hope is that these high-frequency accelerations do not significantly affect the determination of the even harmonics J_2-J_{10}.

The amplitudes of the normal modes are a separate issue than the normal mode frequencies. Ordinary turbulent convection as on the Sun (Goldreich and Keeley 1977) falls short by at least six orders of magnitude (Markham and Stevenson 2018) because the kinetic energy is so low. Moist convection apparently has enough thermal energy to drive the modes, should it be available to drive them, but the available kinetic energy falls short by two orders of

magnitude (Dederick et al. 2018). Rock storms are an intriguing candidate because their expected energy is greater than for conventional water storms (Markham and Stevenson 2018).

7   Upper Atmosphere Physics and Chemistry

7.1   Chemical Tracers and Ring Rain

The stratosphere entered in the discussion in the sections entitled composition and chemistry, seasonal variations, and zonal jets and temperatures. To reduce the overlap between those sections and this one, we focus here on theoretical models and on the parts of the atmosphere above the stratosphere. The entire subject, upper atmosphere and ionosphere, is reviewed in the book chapter by Nagy et al. (2009). Species like C_2H_2 and C_2H_6 have chemical lifetimes in the stratosphere that are comparable to a season on Saturn, so they can be used as tracers of the meridional circulation and its annual reversal from north to south. At the equator the zonal winds in the stratosphere exhibit a 15-year oscillation that is accompanied by an oscillation of the temperature distribution symmetric about the equator to maintain thermal wind balance.

The simplest chemical model is a diurnally averaged 1-D photochemical model with eddy diffusion chosen to represent dynamical processes. Moses et al. (2000a) developed a model that couples hydrocarbon and oxygen photochemistry, molecular and eddy diffusion, radiative transfer, and condensation to better constrain the chemical species and to identify the important physical processes that control the abundances. Moses et al. (2000b) consider the role of oxygen by comparing their model results with the observed abundances of H_2O and CO_2. They find that an external source of oxygen is necessary, and they estimate its magnitude. Ring particle diffusion and interplanetary dust are mentioned as likely sources (Moses and Poppe 2017).

During Cassini's final orbits, the spacecraft flew between Saturn's upper atmosphere and its innermost ring, the D ring. The Ion Neutral Mass Spectrometer (INMS) identified CH_4, CO_2, CO, N_2, H_2O, NH_3, and organics in the ring material. The INMS estimate of >70% non-icy material exceeded remote sensing estimates and is still an open question (Miller et al. 2020). One source of nanograin particles is Saturn's extended atmosphere extending into the innermost ring (Perry et al. 2018). Another source is electrostatic charging, which could lead to ejection of nanograins out of the ring plane and into the atmosphere by the electromagnetic force (Ip et al. 2016). Further evidence of ring rain is seen in enhanced emissions at latitudes tied to magnetic field lines that cross the equatorial plane at the locations of the inner edges of the A-ring and B-ring and at the orbit of Enceladus (O'Donoghue et al. 2013, 2017).

Spatial and temporal variations in the mixing ratios of chemically reactive species hold clues to the circulation. Figure 16 shows the mixing ratios of C_2H_6 and C_2H_2 in the stratosphere just before and just after northern spring equinox (blue and red points, respectively). These hydrocarbons are produced as a result of methane photolysis at 0.1 Pa pressure levels, and they revert to much lower values by photochemical reactions at deeper levels, including 1 hPa where the mixing ratios are shown. Departures from photochemical equilibrium are

thought to be due to a meridional circulation. The photochemical loss time of C_2H_2 is 3 years and that of C_2H_2 is 600 years, and the turnover time of the stratosphere at the 1 hPa level is between the two loss times (Guerlet et al. 2009; Sylvestre et al. 2015).

Hesman et al. (2009) compare the output of the static photochemical model with observations of C_2H_2 and C_2H_6, and they too find evidence of a meridional circulation. Guerlet et al. (2014) compare the temperatures computed from a radiative equilibrium model with temperatures observed by Cassini CIRS, and they find evidence that other processes, presumably related to dynamics, control Saturn's stratospheric thermal structure. Teanby et al. (2006) place new upper limits on halides in Saturn's stratosphere, but they advise that the abundances in the troposphere could be much larger.

Above the stratosphere, diffusive separation takes over and each gas's density falls off with altitude at its own individual scale height, which depends on its molecular weight. The altitude of the transition is called the homopause. Below the homopause, one finds gaseous hydrocarbons ranging in molecular weight at least up to benzene (Guerlet et al. 2015; Koskinen et al. 2016; Vervack and Moses 2015). These hydrocarbons are the source of stratospheric haze particles at non-auroral latitudes (Moses et al. 2000a; Kim et al. 2012). Above the homopause the major constituent is H_2, which continues into the exosphere where the molecules don't collide with each other except at the exobase (Koskinen et al. 2013). Atomic hydrogen H is also present (Koskinen et al. 2020). Its abundance is generally consistent with models based on photochemistry and transport. The relatively high (380 K to 590 K) exospheric temperature at low to mid latitudes is a long-standing mystery (Shemansky and Liu 2012; Stallard et al. 2012b). Despite the changing seasons, the high temperatures have persisted from the period of the Voyager flybys through the Cassini era (Koskinen et al. 2015). High temperatures do occur in the auroral zones, but dynamical models strongly suggest that the upper atmosphere is geostrophically balanced and cannot convey the high-temperature air to lower latitudes (Fig. 17). One possibility is that atmospheric gravity waves, which are often overlooked in models, could supply enough torque to overcome the Coriolis force and allow enough meridional overturning to warm the equatorial thermosphere (Mueller-Wodarg et al. 2019; Brown et al. 2020).

The first in situ measurements of the equatorial thermosphere occurred during the final month of the Cassini mission, when the spacecraft skimmed through the upper atmosphere on four periapses and also during the final plunge. The Ion Neutral Mass Spectrometer (INMS) measured the profiles of temperature and composition (Yelle et al. 2018). The best fit to the exospheric temperature is in the range 340 to 370 K, with a value during the final plunge of 354 K. The helium profiles are consistent with diffusive equilibrium, but the methane profiles are not. Even well above the homopause, the CH_4/H_2 ratio is nearly constant with height. This points to an external source, the most likely being Saturn's rings (Yelle et al. 2018).

The aurora is caused by precipitating electrons striking the upper atmosphere. The source of the electrons is in the magnetosphere, and the subject is covered mainly in the section entitled Magnetospheres and Plasma Science (MAPS) Discipline Science Results. Some of the questions involve the energy and source of the electrons, how deep they penetrate

into the atmosphere, and what effects they have on the temperatures, chemistry, and electromagnetic emissions associated with the aurora.

The aurora is observed in the ultraviolet (Gerard et al. 2013; Gustin et al. 2009, 2010, 2017), visible (Dyudina et al. 2016), infrared (Melin et al. 2011, 2016; O'Donoghue et al. 2014; Stallard et al. 2012a), and radio wavelengths (Lamy et al. 2009, 2013; Ye et al. 2016). The currents associated with the electrons can be observed when the spacecraft flies through an auroral flux tube (Bunce et al. 2014). And although the magnetosphere of Saturn is much less energetic than that of Jupiter, the footprint of the Enceladus flux tube has detectable emissions (Pryor et al. 2011), though not so bright as those of the Jovian moons: The geysers of Enceladus are weaker than the volcanoes of Io, and the magnetic field of Saturn is weaker than the magnetic field of Jupiter.

For a short, broad-brush summary of the magnetosphere, ionosphere, and atmosphere, we recommend Gombosi and Ingersoll (2010). This science objective is captured in detail in the Magnetospheres and Plasma Science (MAPS) Discipline Science Results under the following Cassini science objectives: Conduct in situ studies of Saturn's ionosphere and inner radiation belt, investigate magnetospheric periodicities, their coupling to the ionosphere and how the SKR periods are imposed from close to the planet (3–5 R_S) out to the deep tail, determine the coupling between Saturn's rings and ionosphere, determine the temporal variability of Enceladus' plume (relevant to the Enceladus auroral footprint).

8   Jupiter Science Results

8.1   Winds, Eddies and Long-Lived Ovals

As it approached and flew past Jupiter in late 2000, Cassini provided three months of valuable data about the atmosphere. It is a photogenic planet; the colorful clouds provide ideal tracers of the winds (Fig. 18). The light and dark bands—the zones and belts—and their associated jet streams have been observed from Earth for more than 100 years. The Great Red Spot (GRS) and its smaller cousins have been observed for just as long. Thus Jupiter is an atmospheric dynamics laboratory, where dynamical phenomena like waves, jets, eddies, and vortices can be studied without the complications of continents, oceans, and large seasonal swings. A 70-day movie shows the clouds in motion at all longitudes and latitudes up to within ~10 degrees of the poles. That movie in cylindrical and polar projections is PIA03452, PIA03453, and PIA03454, and is available at https://photojournal.jpl.nasa.gov/.

The GRS is at least 150 years old, although it could be much older. The three white ovals to the south of the GRS formed in the late 1930s and merged into one oval named BA in the late 1990s. All of these features are anticyclones with circumferential winds greater than 100 ms^{-1}. They drift slowly in longitude but stay fixed in latitude. Combined with Hubble Space Telescope and Galileo data, Cassini data were used to show that the GRS shrank by 15% from 1996 to 2006, both in terms of its visible appearance and its ring of circumferential winds (Asay-Davis et al. 2009; Shetty and Marcus 2010).

The white ovals occupied a single latitude band with anticyclonic vorticity. They avoided each other for 60 years because they were separated by cyclonic regions encroaching into the band from the equatorward side (Youssef and Marcus 2003). When the cyclonic regions got pushed out, the ovals merged. Peak velocities around oval BA remained steady while the color changed from white to red several years later. Using different techniques to measure winds and different definitions of the oval's edge, different groups have documented small changes in the properties of BA over similar time periods (Hueso et al. 2009; Choi et al. 2010; Sussman et al. 2010). The combination of Cassini ISS data and Hubble methane band data was used to understand the changes in vertical cloud structure as BA changed from white to red (Wong et al. 2011). Using ISS data from the Cassini flyby (Li et al. 2004; Choi et al. 2013) and amateur telescopic data (Rogers et al. 2006), several authors have documented the life cycles—formation, shape, lifetime, mergers—of the more numerous smaller spots on Jupiter.

Jupiter's zonal jets are remarkably steady in comparison with Earth's jet streams, which change on time scales of 1 or 2 weeks (Fig. 19). Cassini ISS documented only one latitude outside the equator, near $21°$ planetocentric, where the jet speed had changed by a modest amount from Voyager in 1979 to Cassini in 2000 (Porco et al. 2003; Asay-Davis et al. 2011). Most of the observed variability is in the stratosphere at the equator (Garcia-Melendo et al. 2011a) and is part of a regular ~4 year oscillation similar to the quasi-biennial oscillation on Earth (Flasar et al. 2004; Simon-Miller et al. 2007; Simon-Miller and Gierasch 2010). Meridional transport is inferred indirectly from Cassini CIRS data that give the latitudinal distribution of C_2H_2 and C_2H_6, which have known chemical lifetimes and thereby track the age of air masses in the stratosphere (Liang et al. 2005; Zhang et al. 2013b). Vertical wind shear of the zonal winds is studied by tracking features at different wavelengths that probe different altitudes (Li et al. 2006c). Cassini data.

The alternating white and grey bands in Fig. 19 are the zones and belts, respectively. The zones are defined as having anticyclonic vorticity (clockwise in the northern hemisphere) and the belts as having cyclonic vorticity (counterclockwise in the northern hemisphere). The vertical strip on the right shows the latitudes where bright white storm clouds associated with lightning occurred (Dyudina et al. 2004), and that was usually in the belts. Lighting in the belts has been a puzzle since the Galileo days (Little et al. 1999; Gierasch et al. 2000) because except for the lightning storms, the belts are generally clear and the zones are cloudy. Thus clouds and chemical tracers imply upwelling in the zones (Gierasch et al. 1986), but lightning and the eddy momentum transport imply the opposite. Figure 20 shows that the eddy momentum transport is into the jets (Salyk et al. 2006). To balance the angular momentum, there must be a mean north-south flow that is converging in the zones and diverging in the belts (Ingersoll et al. 2000), implying upwelling in the belts, consistent with lightning. So there is conflicting evidence of upwelling and downwelling. The Cassini data shown in Figs. 19 and 20 have not solved this contradiction, but they have at least focused attention on it (Fletcher et al. 2020). The double Hadley cell suggested for Saturn in Fig. 2 may be the key for Jupiter as well.

Waves in a planetary atmosphere provide information about the medium in which they propagate and also about the sources that excite them. Mesoscale waves—wavelengths ~100

km—are visible from space if the crests and troughs are marked by clouds. The thunder following a lightning strike and the sonic boom following a meteor impact are examples of intense sound waves. Cassini could not detect sound waves, but it did detect thunderstorms and lightning (Dyudina et al. 2004; Porco et al. 2003; Baines et al. 2007). Voyager, Galileo, and New Horizons detected mesoscale wave trains with crests and troughs aligned north-south and wavelengths of ~300 km. Cassini apparently did not detect mesoscale waves (Arregi et al. 2009). They may have been absent at the time of the Cassini flyby or perhaps the waves were unobservable due to lack of cloud tracers. One theory says the mesoscale waves are propagating gravity waves (Flasar and Gierasch 1986), and another theory says they are shear instabilities (Bosak and Ingersoll 2002). The first theory requires an obstacle to the flow. The second theory requires strong shear and weak stratification. The measured phase velocities seem inconsistent with both models (Simon et al. 2015) given reasonable assumptions about the vertical wind shears, so the nature of the mesoscale waves is uncertain.

Cassini also detected large scale periodic patterns with wavelengths ranging up to 20,000 km. Circumpolar waves have wavelengths and phase speeds that suggest they are Rossby waves (Barrado-Izagirre et al. 2008, 2009). Simultaneous observations by ISS, UVIS, and CIRS allow one to probe the vertical structure and opacity sources of the waves (Li et al. 2006b). Radio observations allow one to study how the passage of a wave affects the distribution of ammonia (Cosentino et al. 2017). Cassini observations have been used to support various theories of wave-like features in the South Equatorial Belt—that they are either inertia-gravity waves or Rossby waves (Simon-Miller et al. 2012) or a pattern associated with baroclinic instability at that latitude (Rogers et al. 2016).

Wave mean-flow interactions and cascades of energy from one scale to another are fundamental processes in the dynamics of planetary atmospheres. One theory says that the zonal mean flow forms into a potential vorticity (PV) staircase. PV is a conserved dynamical tracer and the staircase consists of latitude bands with constant PV and sharp boundaries in between. However, quantitative analysis of the Cassini 70-day movie shows that the PV gradient reverses sign and is not zero as the staircase model predicts (Li et al. 2004; Read et al. 2006; Shetty and Marcus 2010). The 70-day movie was also used to show that the eddy momentum transport is into the jets from neighboring latitudes, meaning that the eddies are supplying energy to the jets and not the reverse (Fig. 20) (Salyk et al. 2006). The eddies could be getting their energy from convection (Li et al. 2006a) or the latitudinal gradient of radiative heating, or both (Schneider and Liu 2009). Fourier spectra of the 70-day movie data generally reveal an inverse energy cascade, where kinetic energy flows from intermediate scales to large scales (Choi and Showman 2011; Galperin et al. 2014; Hadjighasem and Haller 2016), but there is evidence of a forward cascade from intermediate scales down to small scales, which has been interpreted as energy input at the intermediate scales, perhaps associated with the radius of deformation through baroclinic instability (Young and Read 2017). Others have compared visible features in the 70-day movie with fine-scale features in their 3-dimensional numerical models to test the models' treatment of unknown processes and parameters (Heimpel et al. 2005, 2016; Morales-Juberias and Dowling 2013).

8.2   Atmospheric Structure and Composition

Reactive gases can serve as tracers that reveal regions of upwelling, downwelling, and meridional motion (Fig. 21). During the Jupiter flyby, Cassini CIRS measured the latitude distributions of C_2H_2 and C_2H_6, which are produced in the upper stratosphere by photodissociation of methane. The rate of production is greatest at the equator where the solar ultraviolet (UV) is greatest. C_2H_2 has a chemical time constant that is short compared to the meridional overturning time, so it decreases toward the poles in response to the reduced solar UV. C_2H_6 has a much longer chemical time constant than C_2H_2 – many hundreds vs. tens of years depending on altitude. One might expect it to have a flat distribution if it were carried poleward faster than the chemical reaction rate. But its abundance increases toward the poles (Nixon et al. 2007, 2010), and that is more difficult to explain (Hue et al. 2018). It is possible to fit the C_2H_6 distribution by adjusting parameters of the meridional circulation, but then the C_2H_2 distribution doesn't fit. Independent estimates of the meridional circulation come from the distributions of HCN and CO_2, which were measured by CIRS (Lellouch et al. 2006), but the problem remains.

Cassini CIRS also measured the latitude distributions of phosphine (Irwin et al. 2004; Fletcher et al. 2009a) and ammonia (Achterberg et al. 2006). The measurements refer to the upper troposphere, at the 100–500 mbar level, and they tell a consistent story. Both gases are removed from the atmosphere at upper levels, phosphine by photodissociation and ammonia by condensation, and both have maximum abundance at the equator and reduced abundance in the cyclonic belts on either side of the equator. This indicates rapid uplift or strong vertical mixing in the equatorial zone and descent in the neighboring belts. Probing still deeper into the troposphere, Cassini VIMS detected a 3 μm absorption that could be a mixture of NH_4SH and NH_3 (Brown et al. 2003; Sromovsky and Fry 2010) and provided new insights into the composition of fresh ammonia clouds (Sromovsky and Fry 2018).

Since the stratosphere is stably stratified, to maintain steady state the updrafts must be heated and the downdrafts must be cooled. The decrease of sunlight toward the poles is consistent with updrafts at the equator and downdrafts at the poles. CIRS measurements of stratospheric temperatures and abundances of radiatively active gases are used to model the radiative forcing (Zhang et al. 2013a, 2013b), which includes the effects of stratospheric aerosols (Zhang et al. 2013c, 2015).

Gaseous abundances can provide clues to planet formation. CIRS measured the nitrogen isotopic ratio in ammonia (Abbas et al. 2004; Fouchet et al. 2004a). The ratio is similar to that on the Sun but different from that on Earth, suggesting that the Earth was somehow isolated from the main reservoir of nitrogen during solar system formation. The hydrogen halides, on the other hand, are depleted relative to solar composition and support the halogens' condensation in ammonium salts (Fouchet et al. 2004b).

The Cassini flyby provided insights into aurora-related phenomena on Jupiter as well. UVIS observations of the He 584 Å line were used to infer enhanced eddy mixing in the polar regions, which may account for the enhancement of heavy hydrocarbons there (Parkinson et al. 2006). Alternately, the enhancement of C_2H_2 and C_2H_6 in the polar regions could be explained by a combination of auroral-driven chemistry and advection by the meridional

circulation (Sinclair et al. 2017, 2019). CIRS observations have also been used to study the sources of heating in the polar stratosphere from 1–10 mbar (Sinclair et al. 2018). The result is that heating by auroral soot particles dominates at 1 mbar altitude, and that heating by charged particles dominates at 10 μbar. Cassini VIMS observations have been used to produce the first maps of H_3^+ emission, temperature, and column density on Jupiter's nightside (Stallard et al. 2015). The enhanced emission in the polar regions is produced by enhanced H_3^+ density rather than higher temperatures, which further points to the importance of auroral chemistry in that region.

Because of its high spatial and spectral resolution and full angular coverage during the flyby, Cassini obtained useful information about the clouds of Jupiter. Cloud color is a long-standing uncertainty: What chemical gives the Red Spot its redness? How many coloring agents are there? Comparison of laboratory experiments and visible spectra from Cassini VIMS suggests that the red chromophore is the product of photolyzed ammonia reacting with acetylene (Carlson et al. 2016; Baines et al. 2019). The chromophore occurs in an optically thin layer above the main cloud deck, and may require upward displacement of the air mass to form. A principal component analysis of Cassini ISS data indicates that the red chromophore explains most of the variance across the planet, but a second coloring agent is required to explain the brownish color of the cyclones in Jupiter's North Equatorial Belt (Ordonez-Etxeberria et al. 2016; Teifel' et al. 2018).

The vertical structure of the cloud layers is another long-standing unknown. Cassini CIRS thermal spectra were used to probe into the clouds at a wavelength of 7.18 μm, where the ammonia gas is relatively transparent (Matcheva et al. 2005). The result is that cloud base is at 0.9–1.1 bar, which is deeper than the nominal ammonia cloud base and might imply another, deeper cloud, possibly NH_4SH. Cassini VIMS covers 4.5–5.1 μm, another wavelength range where the gas is relatively transparent. Holes in the cloud allow thermal radiation to space, so the holes appear as hot spots. The cloud is found to be spectrally flat and at a pressure of 1.2 bar or deeper (Giles et al. 2015). Pure NH_3 cloud and pure NH_4SH cloud do not match the spectra, and some kind of coating is implied. Despite the possibility of coatings, CIRS has detected the spectral signature of NH_3 ice particles in the upper tropospheric clouds (Wong et al. 2004).

The planet's global energy budget is a key to its evolution and internal processes, including the separation of helium from hydrogen in the metallic interior. To determine the energy budget accurately, one has to measure the thermal emission and scattered sunlight at all seasons, latitudes, longitudes, wavelengths, emission angles, incident angles, and phase angles. In practice, one samples these quantities and uses models to fill the gaps. Cassini CIRS, VIMS, and ISS all contribute to this estimate (Simon-Miller et al. 2006; Li et al. 2012; Sato et al. 2013; Mayorga et al. 2016). A comprehensive recent study (Li et al. 2018) reveals that Jupiter's Bond albedo and internal heat, 0.503 ± 0.012 and $7.4785 \pm 0.16 \, Wm^{-2}$ are both $\sim 40\%$ larger than the previous best estimates. The higher luminosity might come from greater helium differentiation, such that Saturn has formed a deep helium-rich shell or core (Mankovich and Fortney 2020).

9   Venus Atmosphere

The Venus flybys yielded useful data at a variety of wavelengths. The VIMS instrument detected thermal emission from the hot surface at wavelengths of 0.85 and 0.90 μm, and thereby provided a new technique for exploring the surface mineralogy (Baines et al. 2000). In an attempt to image the surface, the RADAR instrument was operated at 2.2 cm in both scatterometric and radiometric modes during the encounters, but only the thermal emission from the thick absorbing atmosphere was detected (Lorenz et al. 2001). The UVIS instrument studied the airglow of Venus, focusing on N_2, C, O, and CO as clues to the excitation mechanisms and abundances (Hubert et al. 2010, 2012; Gerard et al. 2011). Lightning on Venus is a long-standing controversial subject. The RPWS instrument on Cassini searched for lightning signals in the frequency range 0.125 to 16 MHz and found none, even though they easily detected lightning at rates of 70 s^{-1} during the Earth flyby several months later (Gurnett et al. 2001).

10   Open Science Questions After Cassini

For an object as complex as Saturn, there will always be unanswered questions following a successful mission, and Cassini is no exception. Here is a list, by no means complete, of objectives that seem possible with future missions and expanded technologies.

Water

Measure the global water abundance and determine its role in bringing heat to the surface. Determine the role of moist convection in maintaining the large-scale motions. A Saturn probe to the base of the water cloud is a challenging but possible objective. Juno-type microwave remote sensing, in addition, is possible and has the advantage of global coverage.

Ammonia

Determine the global ammonia abundance, and map its distribution with depth over the planet. Currently available data are good down to only about 3 bars, which do not necessarily represent the deep well mixed abundance of ammonia. A Saturn probe to 10 bars could make this measurement, and microwave remote sensing is potentially valuable.

Noble Gases

Determine Saturn's noble gas abundances including helium, and their isotopic ratios, as done for Jupiter by the Galileo probe. A Saturn probe could measure noble gases to exquisite precision.

Weather Layer

Determine the vertical profiles of temperature, winds, clouds, condensable gases, longwave and shortwave radiation, and turbulence levels. Again, a Saturn probe is needed. A cloud-resolving model like those used in tropical meteorology, but tailored to the giant planets, is both timely and valuable.

Interior Motions

Determine Saturn's rotation period if such a number exists, or determine the spread of periods if differential motions persist into the interior. Document the time dependence of motions in Saturn's interior.

Interior Structure

Using the power of ring seismology and gravity sounding, improve the understanding of Saturn's internal equation of state, mass distribution, composition, and temperature distribution. Develop a fully coupled interior/weather-layer model as done for Earth's ocean/atmosphere system.

11   Scientific Objectives

This section gives the Saturn portion of the scientific objectives for the prime mission and for the Cassini Solstice Mission, which was a mission extension. The former are listed either as S_AOn or J_AOn, with S for Saturn, J for Jupiter, AO for announcement of opportunity and n as a counter in the list. The latter are listed as SNnx and SCny, with S for Saturn, N for new phenomena to pursue, and C for change, both intrinsic and seasonally driven. Again nx and ny are counters. The list below is reproduced from Volume 1 of the Cassini Mission final report to NASA; Sect. 3, Science mission results; Saturn discipline science results. The full document is available at https://pds-rings.seti.org/cassini/.

- **Saturn Temperature, Clouds, Composition (S_AO1)**

    – **Temperature and clouds (S_AO1)** – Determine temperature field, cloud properties, and composition of the atmosphere of Saturn.

    – **Composition and chemistry (SN1c)** – Measure the spatial and temporal variability of trace gases and isotopes.

- **Saturn Winds and Weather (S_AO2)**

    – **Seasonal Variations (SC1a)** – Observe seasonal variations in temperature, clouds, and composition in three spatial dimensions.

    – **Saturn's Winds (SC1b)** – Observe seasonal changes in the winds at all accessible altitudes coupled with simultaneous observations of clouds, temperatures, composition, and lightning.

    – **Storms (SN1b, SN2a)** – Observe the aftermath of the 2010–2011 storm. Study the life cycles of Saturn's newly discovered atmospheric waves, south polar hurricane, and rediscovered north polar hexagon. Monitor the planet for new storms and respond with observations when they occur.

    – **Atmospheric dynamical processes (S_AO2)** – Measure the global wind field, including wave and eddy components; observe synoptic cloud features and processes.

- **Saturn Lightning Sources and Morphology (S_AO6, SN2a)** – Investigate the sources and the morphology of Saturn lightning—Saturn Electrostatic Discharges (SED)—lightning whistlers.

- **Saturn Interior Structure and Rotation (S_AO3)**

  - **Saturn's Rotation Rate (SN1a)** – Determine Saturn's rotation rate and internal structure despite the planet's unexpected high degree of axisymmetry.

  - **Saturn Formation and Evolution (S_AO5)** – Provide observational constraints (gas composition, isotope ratios, heat flux, ...) on scenarios for the formation and the evolution of Saturn.

- **Aurora, Chemistry, and Upper Atmosphere (SC2a)** – Observe the upper atmosphere and the aurora as it changes on all time scales—minutes to years—and is affected by seasonal and solar cycle forcing.

- **Jupiter atmospheric dynamics (J_AO1)** – Extend the time for studies of atmospheric dynamics beyond the period accessible to the Galileo nominal mission.

- **Jupiter Global Atmospheric Structure and Composition (J_AO2)** – Infer global atmospheric thermal structure and composition with instrumentation not carried by the Galileo Orbiter, complementing the local in situ measurements of the Galileo Probe.

- **Venus atmosphere observations** – No specific objectives were called out.

- **Cruise Planetary and Stellar Internal Oscillations (C_AO5)** – Attempt to detect internal oscillations of Saturn, Jupiter, and some stars.

- **Saturn Ionosphere-Magnetospheric Interaction (S_AO4)** – Study the diurnal variations and magnetic control of the ionosphere of Saturn.

Acknowledgements

Data availability

Cassini data can be accessed on the Planetary Data System (PDS) at https://pds.nasa.gov.

Acronyms

AO	Announcement of Opportunity
CIRS	Composite Infrared Spectrometer

GCM	general circulation model
GRS	Great Red Spot
HST	Hubble Space Telescope
IR	infrared
ISS	Imaging Science Subsystem
MAPS	Magnetospheres and Plasma Science
PV	potential vorticity
QBO	quasi-biennial oscillation
RPWS	Radio and Plasma Wave Science
SAO	Semiannual Oscillation
SED	Saturn Electrostatic Discharges
SKR	Saturn kilometric radiation
UVIS	Ultraviolet Imaging Spectrograph
VIMS	Visual and Infrared Mapping Spectrometer

References

Abbas MM, LeClair A, Owen T, Conrath BJ, Flasar FM, Kunde VG et al. , The nitrogen isotopic ratio in Jupiter's atmosphere from observations by the Composite Infrared Spectrometer on the Cassini spacecraft. Astrophys. J. 602, 1063–1074 (2004). 10.1086/381084

Abbas MM et al. , Distribution of CO_2 in Saturn's atmosphere from Cassini/CIRS infrared observations. Astrophys. J. 776(2), 73 (2013). 10.1088/0004-637x/776/2/73

Achterberg RK, Conrath BJ, Gierasch PJ, Cassini CIRS retrievals of ammonia in Jupiter's upper troposphere. Icarus 182, 169–180 (2006). 10.1016/j.icarus.2005.12.020

Achterberg RK, Gierasch PJ, Conrath BJ, Fletcher LN, Hesman BE, Bjoraker GL, Flasar FM, Changes to Saturn's zonal-mean tropospheric thermal structure after the 2010–2011 northern hemisphere storm. Astrophys. J. 786(2), 92 (2014). 10.1088/0004-637x/786/2/92

Achterberg RK, Flasar FM, Bjoraker GL, Hesman BE, Gorius NJP, Mamoutkine AA et al. , Thermal emission from Saturn's polar cyclones. Geophys. Res. Lett. 45(11), 5312–5319 (2018). 10.1029/2018GL078157

Adriani A, Moriconi ML, D'Aversa E, Oliva F, Filacchione G, Faint luminescent ring over Saturn's polar hexagon. Astrophys. J. 808, L16 (2015). 10.1088/2041-8205/808/1/l16

Aguiar ACB, Read PL, Wordsworth RD, Salter T, Yamazaki YH, A laboratory model of Saturn's north polar hexagon. Icarus 206(2), 755–763 (2010). 10.1016/j.icarus.2009.10.022

Anderson JD, Schubert G, Saturn's gravitational field, internal rotation, and interior structure. Science 317, 1384–1387 (2007). 10.1126/science.1144835 [PubMed: 17823351]

Antunano A, del Rio-Gaztelurrutia T, Sanchez-Lavega A, Hueso R, Dynamics of Saturn's polar regions. J. Geophys. Res., Planets 120(2), 155–176 (2015). 10.1002/2014je004709

Antunano A, del Rio-Gaztelurrutia T, Sanchez-Lavega A, Rodriguez-Aseguinolaza J, Cloud morphology and dynamics in Saturn's northern polar region. Icarus 299, 117–132 (2018). 10.1016/j.icarus.2017.07.017

Antunano A, del Río-Gaztelurrutia T, Sánchez-Lavega A, Read PL, Fletcher LN, Potential vorticity of Saturn's polar regions. J. Geophys. Res. 124, 186–201 (2019). 10.1029/2018JE005764

Arregi J, Rojas JF, Hueso R, Sanchez-Lavega A, Gravity waves in Jupiter's equatorial clouds observed by the Galileo orbiter. Icarus 202, 358–360 (2009). 10.1016/j.icarus.2009.03.028

Asay-Davis XS, Marcus PS, Wong MH, de Pater I, Jupiter's shrinking Great Red Spot and steady Oval BA: Velocity measurements with the "Advection Corrected Correlation Image Velocimetry" automated cloud-tracking method. Icarus 203, 164–188 (2009). 10.1016/j.icarus.2009.05.001

Asay-Davis XS, Marcus PS, Wong MH, de Pater I, Changes in Jupiter's zonal velocity between 1979 and 2008. Icarus 211, 1215–1232 (2011). 10.1016/j.icarus.2010.11.018

Atreya SK, Wong MH, Owen TC, Mahaffy PR, Niemann HB, de Pater I, Drossart P, Encrenaz T, A comparison of the atmospheres of Jupiter and Saturn: deep atmospheric composition, cloud structure, vertical mixing, and origin. Planet. Space Sci. 47(10–11), 1243–1262 (1999). 10.1016/s0032-0633(99)00047-1. [PubMed: 11543193]

Atreya SK, Mahaffy PR, Niemann HB, Wong MH, Owen TC, Composition and origin of the atmosphere of Jupiter - an update, and implications for the extrasolar giant planets. Planet. Space Sci. 51(2), 105–112 (2003). 10.1016/s0032-0633(02)00144-7

Atreya SK, Crida A, Guillot T, Lunine JI, Madhusudhan N, Mousis M, The origin and evolution of Saturn, with exoplanet perspective, in Saturn in the 21st Century, ed. by Baines K, Flasar M, Krupp N, Stallard T (Cambridge University Press, Cambridge, 2019), pp. 5–43

Aurnou J, Heimpel M, Allen L, King E, Wicht J, Convective heat transfer and the pattern of thermal emission on the gas giants. Geophys. J. Int. 173(3), 793–801 (2008). 10.1111/j.1365-246X.2008.03764.x

Auwera JV, Moazzen-Ahmadi N, Flaud JM, Toward an accurate database for the 12 μm region of the ethane spectrum. Astrophys. J. 662(1), 750–757 (2007)

Baines KH, Bellucci G, Bibring JP, Brown RH, Buratti BJ, Bussoletti E et al. , Detection of sub-micron radiation from the surface of Venus by Cassini/VIMS. Icarus 148, 307–311 (2000). 10.1006/icar.2000.6519

Baines KH et al. , The atmospheres of Saturn and Titan in the near-infrared: first results of Cassini/VIMS. Earth Moon Planets 96, 3–4, 119–147 (2005). 10.1007/s11038-005-9058-2

Baines KH, Simon-Miller AA, Orton GS, Weaver HA, Lunsford A, Momary TW et al. , Polar lightning and decadal-scale cloud variability on Jupiter. Science 318, 226–229 (2007). 10.1126/science.1147912 [PubMed: 17932285]

Baines KH, Delitsky ML, Momary TW, Brown RH, Buratti BJ, Clark RN, Nicholson PD, Storm clouds on Saturn: lightning-induced chemistry and associated materials consistent with Cassini/VIMS spectra. Planet. Space Sci. 57(14–15), 1650–1658 (2009a). 10.1016/j.pss.2009.06.025

Baines KH, Momary TW, Fletcher LN, Showman AP, Roos-Serote M, Brown RH, Buratti BJ, Clark RN, Nicholson PD, Saturn's north polar cyclone and hexagon at depth revealed by Cassini/VIMS. Planet. Space Sci. 57(14–15), 1671–1681 (2009b). 10.1016/j.pss.2009.06.026

Baines KH, Sromovsky LA, Fry PM, Momary TW, Brown RH, Buratti BJ, Clark RN, Nicholson PD, Sotin C, The eye of Saturn's north polar vortex: unexpected cloud structures observed at high spatial resolution by Cassini/VIMS. Geophys. Res. Lett. 45, 5867–5875 (2018)

Baines KH, Sromovsky LA, Carlson RW, Momary TW, Fry PM, The visual spectrum of Jupiter's Great Red Spot accurately modeled with aerosols produced by photolyzed ammonia reacting with acetylene. Icarus 330, 217–229 (2019)

Banfield D, Conrath BJ, Gierasch PJ, Nicholson PD, Matthews K, Near-IR spectrophotometry of Jovian aerosols - meridional and vertical distributions. Icarus 134(1), 11–23 (1998). 10.1006/icar.1998.5942

Barrado-Izagirre N, Sanchez-Lavega A, Perez-Hoyos S, Hueso R, Jupiter's polar clouds and waves from Cassini and HST images: 1993–2006. Icarus 194, 173–185 (2008). 10.1016/j.icarus.2007.08.025

Barrado-Izagirre N, Perez-Hoyos S, Sanchez-Lavega A, Brightness power spectral distribution and waves in Jupiter's upper cloud and hazes. Icarus 202, 181–196 (2009). 10.1016/j.icarus.2009.02.015

Barstow JK, Irwin PGJ, Fletcher LN, Giles RS, Merlet C, Probing Saturn's tropospheric cloud with Cassini/VIMS. Icarus 271, 400–417 (2016). 10.1016/j.icarus.2016.01.013

Beebe RF, Comparative study of the dynamics of the outer planets. Space Sci. Rev. 116(1–2), 137–154 (2005). 10.1007/s11214-005-1952-4

Bosak T, Ingersoll AP, Shear instabilities as a probe of Jupiter's atmosphere. Icarus 158(2), 401–409 (2002). 10.1006/icar.2002.6886

Brown RH, Baines KH, Bellucci G, Bibring JP, Buratti BJ, Capaccioni F et al. , Observations with the Visual and Infrared Mapping Spectrometer (VIMS) during Cassini's flyby of Jupiter. Icarus 164, 461–470 (2003). 10.1016/s0019-1035(03)00134-9

Brown Z, Koskinen T, Muller-Wodarg I, West R, Jouchoux A, Esposito L, A pole-to-pole pressure-temperature map of Saturn's thermosphere from Cassini Grand Finale data. Nat. Astron. 4, 872–879 (2020). 10.1038/s41550-020-1060-0

Brueshaber SB, Sayanagi KM, Dowling TE, Dynamical regimes of giant planet polar vortices. Icarus 323, 46–61 (2019)

Bunce EJ et al. , Cassini nightside observations of the oscillatory motion of Saturn's northern auroral oval. J. Geophys. Res. Space Phys. 119(5), 3528–3543 (2014). 10.1002/2013ja019527

Cao H, Dougherty MK, Hunt GJ, Provan G, Cowley SWH, Bunce EJ, Kellock S, Stevenson DJ, The landscape of Saturn's internal magnetic field from the Cassini Grand Finale. Icarus 344, UNSP 113541 (2020)

Carlson RW, Baines KH, Anderson MS, Filacchione G, Simon AA, Chromophores from photolyzed ammonia reacting with acetylene: application to Jupiter's Great Red Spot. Icarus 274, 106–115 (2016). 10.1016/j.icarus.2016.03.008

Cavalie T, Dobrijevic M, Fletcher LN, Loison JC, Hickson KM, Hue V, Hartogh P, Photochemical response to the variation of temperature in the 2011–2012 stratospheric vortex of Saturn. Astron. Astrophys. 580, A55 (2015). 10.1051/0004-6361/201425444

Cavalie T, Hue V, Hartogh P, Moreno R, Lellouch E, Feuchtgruber H, Jarchow C, Cassidy T, Fletcher LN, Billebaud F, Dobrijevic M, Rezac L, Orton GS, Rengel M, Fouchet T, Guerlet S, Herschel map of Saturn's stratospheric water, delivered by the plumes of Enceladus. Astron. Astrophys. 630, A87 (2019)

Choi DS, Showman AP, Power spectral analysis of Jupiter's clouds and kinetic energy from Cassini. Icarus 216, 597–609 (2011). 10.1016/j.icarus.2011.10.001

Choi DS, Showman AP, Brown RH, Cloud features and zonal wind measurements of Saturn's atmosphere as observed by Cassini/VIMS. J. Geophys. Res., Planets 114, E04007 (2009). 10.1029/2008je003254

Choi DS, Showman AP, Vasavada AR, The evolving flow of Jupiter's White Ovals and adjacent cyclones. Icarus 207, 359–372 (2010). 10.1016/j.icarus.2009.10.013

Choi DS, Showman AP, Vasavada AR, Simon-Miller AA, Meteorology of Jupiter's equatorial hot spots and plumes from Cassini. Icarus 223, 832–843 (2013). 10.1016/j.icarus.2013.02.001

Christensen UR, Wicht J, Dietrich W, Mechanisms for limiting the depth of zonal winds in the gas giant planets. Astrophys. J. 890, 61 (2020)

Conrath BJ, Gautier D, Saturn helium abundance: a reanalysis of Voyager measurements. Icarus 144(1), 124–134 (2000). 10.1006/icar.1999.6265

Conrath BJ, Gautier D, Hanel RA, Hornstein JS, The helium abundance of Saturn from Voyager measurements. Astrophys. J. 282(2), 807–815 (1984). 10.1086/162267

Cosentino RG, Butler B, Sault B, Morales-Juberias R, Simon A, de Pater I, Atmospheric waves and dynamics beneath Jupiter's clouds from radio wavelength observations. Icarus 292, 168–181 (2017). 10.1016/j.icarus.2017.01.006

Cuff K, Heimpel M, Effects of neutral buoyancy outer boundary condition in models of deep convection in giant planets. Phys. Earth Planet. Inter. 282, 89–99 (2018)

Dederick E, Jackiewicz J, Guillot T, An analysis of stochastic Jovian oscillation excitation by moist convection. Astrophys. J. 856, 50 (2018)

Del Genio AD, Barbara JM, Constraints on Saturn's tropospheric general circulation from Cassini ISS images. Icarus 219(2), 689–700 (2012). 10.1016/j.icarus.2012.03.035

Del Genio AD, Barbara JM, An objective classification of Saturn cloud features from Cassini ISS images. Icarus 271, 222–236 (2016). 10.1016/j.icarus.2016.02.011

Del Genio AD, Barbara JM, Ferrier J, Ingersoll AP, West RA, Vasavada AR, Spitale J, Porco CC, Saturn eddy momentum fluxes and convection: first estimates from Cassini images. Icarus 189(2), 479–492 (2007). 10.1016/j.icarus.2007.02.013

Del Genio AD, Achterberg RK, Baines KH, Flasar FM, Read PL, Sanchez-Lavega A, Showman AP, Saturn atmospheric structure and dynamics, in Saturn from Cassini-Huygens, ed. by Doughterty MK, Esposito LW, Krimigis SM(Springer, Dordrecht, 2009), pp. 113–159

del Rio-Gaztelurrutia T, Legarreta J, Hueso R, Perez-Hoyos S, Sanchez-Lavega A, A long-lived cyclone in Saturn's atmosphere: observations and models. Icarus 209(2), 665–681 (2010). 10.1016/j.icarus.2010.04.002

del Rio-Gaztelurrutia T, Sanchez-Lavega A, Antunano A, Legarreta J, Garcia-Melendo E, Sayanagi KM et al. , A planetary-scale disturbance in a long living three vortex coupled system in Saturn's atmosphere. Icarus 302, 499–513 (2018). 10.1016/j.icarus.2017.11.029

Desch MD, Kaiser ML, Voyager measurement of the rotation period of Saturn's magnetic field. Geophys. Res. Lett. 8(3), 253–256 (1981). 10.1029/GL008i003p00253

Devi VM, Kleiner I, Sams RL, Brown LR, Benner DC, Fletcher LN, Line positions and intensities of the phosphine (PH3) pentad near 4.5 μm. J. Mol. Spectrosc. 298, 11–23 (2014). 10.1016/j.jms.2014.01.0130022-2852

Dobrijevic M, Cavalie T, Billebaud F, A methodology to construct a reduced chemical scheme for 2D-3D photochemical models: application to Saturn. Icarus 214(1), 275–285 (2011). 10.1016/j.icarus.2011.04.027

Dougherty M (Cassini magnetometer team), Cassini's magnetometer at Saturn. Astron. Geophys. 58(4), 36–42 (2017). 10.1093/astrogeo/atx140

Dowling TE, Dynamics of Jovian atmospheres. Annu. Rev. Fluid Mech. 27, 293–334 (1995). 10.1146/annurev.fl.27.010195.001453

Dubrovin D, Luque A, Gordillo-Vazquez FJ, Yair Y, Parra-Rojas FC, Ebert U, Price C, Impact of lightning on the lower ionosphere of Saturn and possible generation of halos and sprites. Icarus 241, 313–328 (2014). 10.1016/j.icarus.2014.06.025

Dyudina UA, Del Genio AD, Ingersoll AP, Porco CC, West RA, Vasavada AR, Barbara JM, Lightning on Jupiter observed in the H-alpha line by the Cassini imaging science subsystem. Icarus 172, 24–36 (2004). 10.1016/j.icarus.2004.07.014

Dyudina UA, Ingersoll AP, Ewald SP, Porco CC, Fischer G, Kurth W, Desch M, Del Genio A, Barbara J, Ferrier J, Lightning storms on Saturn observed by Cassini ISS and RPWS during 2004–2006. Icarus 190(2), 545–555 (2007). 10.1016/j.icarus.2007.03.035

Dyudina UA et al. , Dynamics of Saturn's south polar vortex. Science 319(5871), 1801 (2008). 10.1126/science.1153633 [PubMed: 18369142]

Dyudina UA et al. , Saturn's south polar vortex compared to other large vortices in the Solar System. Icarus 202(1), 240–248 (2009). 10.1016/j.icarus.2009.02.014

Dyudina UA, Ingersoll AP, Ewald SP, Porco CC, Fischer G, Kurth WS, West RA, Detection of visible lightning on Saturn. Geophys. Res. Lett. 37, L09205 (2010). 10.1029/2010gl043188

Dyudina UA, Ingersoll AP, Ewald SP, Porco CC, Fischer G, Yair Y, Saturn's visible lightning, its radio emissions, and the structure of the 2009–2011 lightning storms. Icarus 226(1), 1020–1037 (2013). 10.1016/j.icarus.2013.07.013

Dyudina UA, Zhang X, Li L, Kopparla P, Ingersoll AP, Dones L, Verbiscer A, Yung YL, Reflected light curves, spherical and bond albedos of Jupiter- and Saturn-like exoplanets. Astrophys. J. 822(2), 76 (2016). 10.3847/0004-637x/822/2/76

Farrell WM, Kaiser ML, Fischer G, Zarka P, Kurth WS, Gurnett DA, Are Saturn electrostatic discharges really superbolts? A temporal dilemma. Geophys. Res. Lett. 34, 6 (2007). 10.1029/2006gl028841

Fegley B, Lodders K, Chemical models of the deep atmospheres of Jupiter and Saturn. Icarus 110(1), 117–154 (1994). 10.1006/icar.1994.1111

Fischer G et al. , Saturn lightning recorded by Cassini/RPWS in 2004. Icarus 183(1), 135–152 (2006a). 10.1016/j.icarus.2006.02.010

Fischer G, Macher W, Gurnett DA, Desch MD, Lecacheux A, Zarka P, Kurth WS, Kaiser ML, Discrimination between Jovian radio emissions and Saturn electrostatic discharges. Geophys. Res. Lett. 33, 21 (2006b). 10.1029/2006gl026766

Fischer G, Kurth WS, Dyudina UA, Kalser ML, Zarka P, Lecacheux A, Ingersoll AP, Gurnett DA, Analysis of a giant lightning storm on Saturn. Icarus 190(2), 528–544 (2007). 10.1016/j.icarus.2007.04.002

Fischer G, Gurnett DA, Kurth WS, Akalin F, Zarka P, Dyudina UA, Farrell WM, Kaiser ML, Atmospheric electricity at Saturn. Space Sci. Rev. 137(1–4), 271–285 (2008). 10.1007/s11214-008-9370-z

Fischer G et al. , A giant thunderstorm on Saturn. Nature 475(7354), 75–77 (2011). 10.1038/nature10205 [PubMed: 21734705]

Fischer G, Ye SY, Groene JB, Ingersoll AP, Sayanagi KM, Menietti JD, Kurth WS, Gurnett DA, A possible influence of the Great White Spot on Saturn kilometric radiation periodicity. Ann. Geophys. 32(12), 1463–1476 (2014). 10.5194/angeo-32-1463-2014

Flasar FM, Temperatures, winds, and composition in the Saturnian system. Science 307(5713), 1247–1251 (2005). 10.1126/science.1105806 [PubMed: 15618486]

Flasar F, Gierasch P, Mesoscale waves as a probe of Jupiter's deep atmosphere. J. Atmos. Sci. 43(22), 2683–2707 (1986). 10.1175/1520-0469(1986)043<2683:MWAAPO>2.0.CO;2

Flasar FM, Kunde VG, Achterberg RK, Conrath BJ, Simon-Miller AA, Nixon CA, Gierasch PJ, Romani PN, Bezard B, Irwin P, Bjoraker GL, Brasunas JC, Jennings DE, Pearl JC, Smith MD, Orton GS, Spilker LJ, Carlson R, Calcutt SB, Read PL, Taylor FW, Parrish P, Barucci A, Courtin R, Coustenis A, Gautier D, Lellouch E, Marten A, Prange R, Biraud Y, Fouchet T, Ferrari C, Owen TC, Abbas MM, Samuelson RE, Raulin F, Ade P, Cesarsky CJ, Grossman KU, Coradini A, An intense stratospheric jet on Jupiter. Nature 427, 132–135 (2004) [PubMed: 14712270]

Fletcher LN, Irwin PGJ, Teanby NA, Orton GS, Parrish PD, Calcutt SB, Bowles N, de Kok R, Howett C, Taylor FW, The meridional phosphine distribution in Saturn's upper troposphere from Cassini/CIRS observations. Icarus 188(1), 72–88 (2007a). 10.1016/j.icarus.2006.10.029

Fletcher LN, Irwin PGJ, Teanby NA, Orton GS, Parrish PD, de Kok R, Howett C, Calcutt SB, Bowles N, Taylor FW, Characterizing Saturn's vertical temperature structure from Cassini/CIRS. Icarus 189(2), 457–478 (2007b). 10.1016/j.icarus.2007.02.006

Fletcher LN, Irwin PGJ, Orton GS, Teanby NA, Achterberg RK, Bjoraker GL, Read PL, Simon-Miller AA, Howett C, de Kok R, Bowles N, Calcutt SB, Hesman B, Flasar FM, Temperature and composition of Saturn's polar hot spots and hexagon. Science 319(5859), 79–81 (2008) [PubMed: 18174438]

Fletcher LN, Orton GS, Teanby NA, Irwin PGJ, Phosphine on Jupiter and Saturn from Cassini/CIRS. Icarus 202, 543–564 (2009a). 10.1016/j.icarus.2009.03.023

Fletcher LN, Orton GS, Teanby NA, Irwin PGJ, Bjoraker GL, Methane and its isotopologues on Saturn from Cassini/CIRS observations. Icarus 199(2), 351–367 (2009b). 10.1016/j.icarus.2008.09.019

Fletcher LN, Achterberg RK, Greathouse TK, Orton GS, Conrath BJ, Simon-Miller AA, Teanby N, Guerlet S, Irwin PGJ, Flasar FM, Seasonal change on Saturn from Cassini/CIRS observations, 2004–2009. Icarus 208(1), 337–352 (2010). 10.1016/j.icarus.2010.01.022

Fletcher LN, Baines KH, Momary TW, Showman AP, Irwin PGJ, Orton GS, Roos-Serote M, Merlet C, Saturn's tropospheric composition and clouds from Cassini/VIMS 4.6–5.1 μm nightside spectroscopy. Icarus 214(2), 510–533 (2011a). 10.1016/j.icarus.2011.06.006

Fletcher LN, Hesman BE, Irwin PGJ, Baines KH, Momary TW, Sanchez-Lavega A, Flasar FM, Read PL, Orton GS, Simon-Miller A, Hueso R, Bjoraker GL, Mamoutkine A, del Rio-Gaztelurrutia T, Gomez JM, Buratti B, Clark RN, Nicholson PD, Sotin C, Thermal structure and dynamics of Saturn's northern springtime disturbance. Science 332(6036), 1413–1417 (2011b). 10.1126/science.1204774 [PubMed: 21596955]

Fletcher LN et al. , The origin and evolution of Saturn's 2011–2012 stratospheric vortex. Icarus 221(2), 560–586 (2012). 10.1016/j.icarus.2012.08.024

Fletcher LN, Greathouse TK, Orton GS, Irwin PGJ, Mousis O, Sinclair JA, Giles RS, The origin of nitrogen on Jupiter and Saturn from the 15N/14N ratio. Icarus 238, 170–190 (2014). 10.1016/j.icarus.2014.05.007

Fletcher LN, Irwin PGJ, Sinclair JA, Orton GS, Giles RS, Hurley J, Gorius N, Achterberg RK, Hesman BE, Bjoraker GL, Seasonal evolution of Saturn's polar temperatures and composition. Icarus 250, 131–153 (2015). 10.1016/j.icarus.2014.11.022

Fletcher LN, Irwin PGJ, Achterberg RK, Orton GS, Flasar FM, Seasonal variability of Saturn's tropospheric temperatures, winds and para-H_2 from Cassini far-IR spectroscopy. Icarus 264, 137–159 (2016). 10.1016/j.icarus.2015.09.009

Fletcher LN, Guerlet S, Orton GS, Cosentino RG, Fouchet T, Irwin PGJ, Li LM, Flasar FM, Gorius N, Morales-Juberias R, Disruption of Saturn's quasi-periodic equatorial oscillation by the great northern storm. Nat. Astron. 1(11), 765–770 (2017). 10.1038/s41550-017-0271-5

Fletcher LN, Gustafsson M, Orton GS, Hydrogen dimers in giant-planet infrared spectra. Astrophys. J. Suppl. Ser. 235, 24 (2018a)

Fletcher LN, Orton GS, Sinclair JA, Guerlet S, Read PL, Antunano A, Achterberg RK, Flasar FM, Irwin PGJ, Bjoraker GL, Hurley J, Hesman BE, Segura M, Gorius N, Mamoutkine A, Calcutt SB, A hexagon in Saturn's northern stratosphere surrounding the emerging summertime polar vortex. Nat. Commun. 9, 3564 (2018b) [PubMed: 30177694]

Fletcher LN, Greathouse TK, Guerlet S, Moses JI, West RA, Saturn's seasonally changing atmosphere: thermal structure, composition and aerosols, in Saturn in the 21st Century, ed. by Baines KH, Flasar FM, Krupp N, Stallard T(Cambridge University Press, Cambridge, 2018c), pp. 251–294. 10.1017/9781316227220.010

Fletcher LN, Kaspi Y, Guillot T, Showman AP, How well do we understand the belt/zone circulation of giant planet atmospheres? Space Sci. Rev. 216(2), 30 (2020). 10.1007/s11214-019-0631-9 [PubMed: 32214508]

Fouchet T, Irwin PGJ, Parrish P, Calcutt SB, Taylor FW, Nixon CA, Owen T, Search for spatial variation in the Jovian 15N/14N ratio from Cassini/CIRS observations. Icarus 172(1), 50–58 (2004a). 10.1016/j.icarus.2003.11.011

Fouchet T, Orton G, Irwin PGJ, Calcutt SB, Nixon CA, Upper limits on hydrogen halides in Jupiter from Cassini/CIRS observations. Icarus 170, 237–241 (2004b). 10.1016/j.icarus.2004.03.013

Fouchet T, Guerlet S, Strobel DF, Simon-Miller AA, Bézard B, Flasar FM, An equatorial oscillation in Saturn's middle atmosphere. Nature 453(7192), 200–202 (2008). 10.1038/nature06912 [PubMed: 18464737]

Fouchet T, Moses JI, Conrath BJ, Saturn: composition and chemistry, in Saturn from Cassini-Huygens, ed. by Doughterty MK, Esposito LW, Krimigis SM(Springer, Dordrecht, 2009), pp. 83–112

Fouchet T, Greathouse TK, Spiga A, Fletcher LN, Guerlet S, Leconte J, Orton GS, Stratospheric aftermath of the 2010 storm on Saturn as observed by the TEXES instrument. I. Temperature structure. Icarus 277, 196–214 (2016). 10.1016/j.icarus.2016.04.030

Friedson AJ, Moses JI, General circulation and transport in Saturn's upper troposphere and stratosphere. Icarus 218(2), 861–875 (2012). 10.1016/j.icarus.2012.02.004

Galanti E, Kaspi Y, An adjoint-based method for the inversion of the Juno and Cassini gravity measurements into wind fields. Astrophys. J. 820(2), 91 (2016). 10.3847/0004-637x/820/2/91

Galanti E, Kaspi Y, Prediction for the flow-induced gravity field of Saturn: implications for Cassini's Grand Finale. Astrophys. J. Lett. 843, 2 (2017). 10.3847/2041-8213/aa7aec

Galanti E, Kaspi Y, Tziperman E, A full, self-consistent treatment of thermal wind balance on oblate fluid planets. J. Fluid Mech. 810, 175–195 (2017). 10.1017/jfm.2016.687

Galanti E, Kaspi Y, Miguel Y, Guillot T, Durante D, Racioppa P, Iess L, Saturn's deep atmospheric flows revealed by the Cassini Grand Finale gravity measurements. Geophys. Res. Lett. 46(2), 616–624 (2019). 10.1029/2018GL078087

Galperin B, Young RMB, Sukoriansky S, Dikovskaya N, Read PL, Lancaster AJ, Armstrong D, Cassini observations reveal a regime of zonostrophic macroturbulence on Jupiter. Icarus 229, 295–320 (2014). 10.1016/j.icarus.2013.08.030

Garcia-Melendo E, Sanchez-Lavega A, Shallow water simulations of Saturn's giant storms at different latitudes. Icarus 286, 241–260 (2017). 10.1016/j.icarus.2016.10.006

Garcia-Melendo E, Sanchez-Lavega A, Hueso R, Numerical models of Saturn's long-lived anticyclones. Icarus 191(2), 665–677 (2007). 10.1016/j.icarus.2007.05.020

Garcia-Melendo E, Sanchez-Lavega A, Rojas JF, Perez-Hoyos S, Hueso R, Vertical shears in Saturn's eastward jets at cloud level. Icarus 201(2), 818–820 (2009). 10.1016/j.icarus.2009.02.022

Garcia-Melendo E, Sanchez-Lavega A, Legarreta J, Perez-Hoyos S, Hueso R, A strong high altitude narrow jet detected at Saturn's equator. Geophys. Res. Lett. 37, L22204 (2010). 10.1029/2010gl045434

Garcia-Melendo E, Arregi J, Rojas JF, Hueso R, Barrado-Izagirre N, Gomez-Forrellad JM et al. , Dynamics of Jupiter's equatorial region at cloud top level from Cassini and HST images. Icarus 211, 1242–1257 (2011a). 10.1016/j.icarus.2010.11.020

Garcia-Melendo E, Perez-Hoyos S, Sanchez-Lavega A, Hueso R, Saturn's zonal wind profile in 2004–2009 from Cassini ISS images and its long-term variability. Icarus 215(1), 62–74 (2011b). 10.1016/j.icarus.2011.07.005

Garcia-Melendo E, Hueso R, Sanchez-Lavega A, Legarreta J, del Rio-Gaztelurrutia T, Perez-Hoyos S, Sanz-Requena JF, Atmospheric dynamics of Saturn's 2010 giant storm. Nat. Geosci. 6(7), 525–529 (2013). 10.1038/ngeo1860

Gerard JC, Hubert B, Gustin J, Shematovich VI, Bisikalo D, Gladstone GR, Esposito LW, EUV spectroscopy of the Venus dayglow with UVIS on Cassini. Icarus 211, 70–80 (2011). 10.1016/j.icarus.2010.09.020

Gerard JC, Gustin J, Pryor WR, Grodent D, Bonfond B, Radioti A, Gladstone GR, Clarke JT, Nichols JD, Remote sensing of the energy of auroral electrons in Saturn's atmosphere: Hubble and Cassini spectral observations. Icarus 223(1), 211–221 (2013). 10.1016/j.icarus.2012.11.033

Gierasch P, Conrath B, Magalhaes J, Zonal mean properties of Jupiter's upper troposphere from Voyager infrared observations. Icarus 67, 456–483 (1986)

Gierasch PJ, Ingersoll AP, Banfield D, Ewald SP, Helfenstein P, Simon-Miller A, Vasavada A, Breneman HH, Senske DA (Galileo Imaging Team), Observation of moist convection in Jupiter's atmosphere. Nature 403(6770), 628–630 (2000). 10.1038/35001017 [PubMed: 10688191]

Giles RS, Fletcher LN, Irwin PGJ, Cloud structure and composition of Jupiter's troposphere from 5 μm Cassini VIMS spectroscopy. Icarus 257, 457–470 (2015). 10.1016/j.icarus.2015.05.030

Goldreich P, Keeley D, Solar seismology 1. Stability of solar P-modes. Astrophys. J. 211, 934–942 (1977)

Gombosi TI, Ingersoll AP, Saturn: atmosphere, ionosphere, and magnetosphere. Science 327(5972), 1476–1479 (2010). 10.1126/science.1179119 [PubMed: 20299587]

Guerlet S, Fouchet T, Bezard B, Simon-Miller AA, Flasar FM, Vertical and meridional distribution of ethane, acetylene and propane in Saturn's stratosphere from CIRS/Cassini limb observations. Icarus 203, 214–232 (2009). 10.1016/j.icarus.2009.04.002

Guerlet S, Fouchet T, Bezard B, Moses JI, Fletcher LN, Simon-Miller AA, Flasar FM, Meridional distribution of CH3C2H and C4H2 in Saturn's stratosphere from CIRS/Cassini limb and nadir observations. Icarus 209(2), 682–695 (2010). 10.1016/j.icarus.2010.03.033

Guerlet S, Fouchet T, Bezard B, Flasar FM, Simon-Miller AA, Evolution of the equatorial oscillation in Saturn's stratosphere between 2005 and 2010 from Cassini/CIRS limb data analysis. Geophys. Res. Lett. 38, L09201 (2011). 10.1029/2011gl047192

Guerlet S et al. , Global climate modeling of Saturn's atmosphere. Part I: evaluation of the radiative transfer model. Icarus 238, 110–124 (2014). 10.1016/j.icarus.2014.05.010

Guerlet S, Fouchet T, Vinatier S, Simon AA, Dartois E, Spiga A, Stratospheric benzene and hydrocarbon aerosols detected in Saturn's auroral regions. Astron. Astrophys. 580, A89 (2015)

Guerlet S, Fouchet T, Spiga A, Flasar FM, Fletcher LN, Hesman BE, Gorius N, Equatorial oscillation and planetary wave activity in Saturn's stratosphere through the Cassini epoch. J. Geophys. Res., Planets 123(1), 246–261 (2018). 10.1002/2017JE005419

Guillot T, A comparison of the interiors of Jupiter and Saturn. Planet. Space Sci. 47(10–11), 1183–1200 (1999). 10.1016/s0032-0633(99)00043-4.

Guillot T, Miguel Y, Militzer B, Hubbard WB, Kaspi Y, Galanti E et al. , A suppression of differential rotation in Jupiter's deep interior. Nature 555(7695), 227 (2018). 10.1038/nature25775 [PubMed: 29517000]

Gunnarson JL, Sayanagi KM, Blalock JJ, Fletcher LN, Ingersoll AP, Dyudina UA et al. , Saturn's new ribbons: Cassini observations of planetary waves in Saturn's 42N atmospheric jet. Geophys. Res. Lett. 45(15), 7399–7408 (2018). 10.1029/2018GL078156

Gurnett DA, Zarka P, Manning R, Kurth WS, Hospodarsky GB, Averkamp TF et al. , Non-detection at Venus of high-frequency radio signals characteristic of terrestrial lightning. Nature 409, 313–315 (2001). 10.1038/35053009 [PubMed: 11201733]

Gustin J, Gerard JC, Pryor W, Feldman PD, Grodent D, Holsclaw G, Characteristics of Saturn's polar atmosphere and auroral electrons derived from HST/STIS, FUSE and Cassini/UVIS spectra. Icarus 200(1), 176–187 (2009). 10.1016/j.icarus.2008.11.013

Gustin J, Stewart I, Gerard JC, Esposito L, Characteristics of Saturn's FUV airglow from limb-viewing spectra obtained with Cassini-UVIS. Icarus 210(1), 270–283 (2010). 10.1016/j.icarus.2010.06.031

Gustin J, Grodent D, Radioti A, Pryor W, Lamy L, Ajello J, Statistical study of Saturn's auroral electron properties with Cassini/UVIS FUV spectral images. Icarus 284, 264–283 (2017). 10.1016/j.icarus.2016.11.017

Hadjighasem A, Haller G, Geodesic transport barriers in Jupiter's atmosphere: a video-based analysis. SIAM Rev. 58, 69–89 (2016). 10.1137/140983665

Hanel RA, Conrath BJ, Kunde VG, Pearl JC, Pirraglia JA, Albedo, internal heat flux, and energy balance of Saturn. Icarus 53(2), 262–285 (1983). 10.1016/0019-1035(83)90147-1

Hanley TR, Steffes PG, Karpowicz BM, A new model of the hydrogen and helium-broadened microwave opacity of ammonia based on extensive laboratory measurements. Icarus 202(1), 316–335 (2009). 10.1016/j.icarus.2009.02.002

Hedman MM, Nicholson PD, Kronoseismology: using density waves in Saturn's C ring to probe the planet's interior. Astron. J. 146, 1 (2013). 10.1088/0004-6256/146/1/12

Hedman MM, Nicholson PD, More kronoseismology with Saturn's rings. Mon. Not. R. Astron. Soc. 444(2), 1369–1388 (2014). 10.1093/mnras/stu1503

Heimpel M, Aurnou J, Turbulent convection in rapidly rotating spherical shells: a model for equatorial and high latitude jets on Jupiter and Saturn. Icarus 187(2), 540–557 (2007). 10.1016/j.icarus.2006.10.023

Heimpel M, Aurnou J, Wicht J, Simulation of equatorial and high-latitude jets on Jupiter in a deep convection model. Nature 438, 193–196 (2005). 10.1038/nature04208 [PubMed: 16281029]

Heimpel M, Gastine T, Wicht J, Simulation of deep-seated zonal jets and shallow vortices in gas giant atmospheres. Nat. Geosci. 9, 19 (2016). 10.1038/ngeo2601

Helled R, Guillot T, Interior models of Saturn: including the uncertainties in shape and rotation. Astrophys. J. 767(2), 113 (2013). 10.1088/0004-637x/767/2/113

Helled R, Galanti E, Kaspi Y, Saturn's fast spin determined from its gravitational field and oblateness. Nature 520, 202–U140 (2015). 10.1038/nature14278 [PubMed: 25807487]

Hersant F, Gautier D, Tobie G, Lunine JI, Interpretation of the carbon abundance in Saturn measured by Cassini. Planet. Space Sci. 56(8), 1103–1111 (2008). 10.1016/j.pss.2008.02.007

Hesman BE et al. , Saturn's latitudinal C2H2 and C2H6 abundance profiles from Cassini/CIRS and ground-based observations. Icarus 202(1), 249–259 (2009). 10.1016/j.icarus.2009.02.013

Hesman BE et al. , Elusive ethylene detected in Saturn's northern storm region. Astrophys. J. 760(1), 24 (2012). 10.1088/0004-637x/760/1/24

Hodosan G, Helling C, Asensio-Torres R, Vorgul I, Rimmer PB, Lightning climatology of exoplanets and brown dwarfs guided by solar system data. Mon. Not. R. Astron. Soc. 461(4), 3927–3947 (2016). 10.1093/mnras/stw1571

Howett CJA, Irwin PGJ, Teanby NA, Simon-Miller A, Calcutt SB, Fletcher LN, de Kok R, Meridional variations in stratospheric acetylene and ethane in the southern hemisphere of the Saturnian atmosphere as determined from Cassini/CIRS measurements. Icarus 190(2), 556–572 (2007). 10.1016/j.icarus.2007.03.009

Hubbard WB, Dougherty MK, Gautier D, Jacobson R, The interior of Saturn, in Saturn from Cassini-Huygens, ed. by Doughterty MK, Esposito LW, Krimigis SM (Springer, Dordrecht, 2009), pp. 75–81

Hubert B, Gerard JC, Gustin J, Shematovich VI, Bisikalo DV, Stewart AI, Gladstone GR, UVIS observations of the FUV OI and CO 4P Venus dayglow during the Cassini flyby. Icarus 207, 549–557 (2010). 10.1016/j.icarus.2009.12.029

Hubert B, Gerard JC, Gustin J, Bisikalo DV, Shematovich VI, Gladstone GR, Cassini-UVIS observation of dayglow FUV emissions of carbon in the thermosphere of Venus. Icarus 220, 635–646 (2012). 10.1016/j.icarus.2012.06.002

Hue V, Cavalie T, Dobrijevic M, Hersant F, Greathouse TK, 2D photochemical modeling of Saturn's stratosphere. Part I: seasonal variation of atmospheric composition without meridional transport. Icarus 257, 163–184 (2015). 10.1016/j.icarus.2015.04.001

Hue V, Greathouse TK, Cavalie T, Dobrijevic M, Hersant F, 2D photochemical modeling of Saturn's stratosphere. Part II: feedback between composition and temperature. Icarus 267, 334–343 (2016). 10.1016/j.icarus.2015.12.007

Hue V, Hersant E, Cavalie T, Dobrijevic M, Sinclair JA, Photochemistry, mixing and transport in Jupiter's stratosphere constrained by Cassini. Icarus 307, 106–123 (2018)

Hueso R, Legarreta J, Garcia-Melendo E, Sanchez-Lavega A, Perez-Hoyos S, The Jovian anticyclone BA II. Circulation and interaction with the zonal jets. Icarus 203, 499–515 (2009). 10.1016/j.icarus.2009.05.004

Hueso R, Legarreta J, Perez-Hoyos S, Rojas JF, Sanchez-Lavega A, Morgado A, The international outer planets watch atmospheres node database of giant-planet images. Planet. Space Sci. 58(10), 1152–1159 (2010). 10.1016/j.pss.2010.04.006

Hueso R, Sanchez-Lavega A, Rojas JF, Simon AA, Barry T, del Rio-Gaztelurrutia T, Antunano A, Sayanagi KM, Delcroix M, Fletcher LN, Garcia-Melendo E, Perez-Hoyos S, Blalock J, Colas F, Gomez-Forrellad JM, Gunnarson JL, Peach D, Wong MH, Saturn atmospheric dynamics one year after Cassini: long-lived features and time variations in the drift of the hexagon. Icarus 336, UNSP 113429 (2020)

Hurley J, Irwin PGJ, Fletcher LN, Moses JI, Hesman B, Sinclair J, Merlet C, Observations of upper tropospheric acetylene on Saturn: no apparent correlation with 2000 km-sized thunderstorms. Planet. Space Sci. 65, 21–37 (2012a). 10.1016/j.pss.2011.12.026

Hurley J, Fletcher LN, Irwin PGJ, Calcutt SB, Sinclair JA, Merlet C, Latitudinal variation of upper tropospheric NH_3 on Saturn derived from Cassini/CIRS far-infrared measurements. Planet. Space Sci. 73(1), 347–363 (2012b). 10.1016/j.pss.2012.08.003

Iess L, Militzer B, Kaspi Y, Nicholson P, Durante D, Pacioppa P, Anabtawi A, Galanti E, Hubbard W, Mariani MJ, Tortora P, Wahl S, Zannoni M, Measurement and implications of Saturn's gravity field and ring mass. Science (2019). 10.1125/science.aat2965

Ingersoll AP, Gierasch PJ, Banfield D, Vasavada AR (Galileo Imaging Team), Moist convection as an energy source for the large-scale motions in Jupiter's atmosphere. Nature 403(6770), 630–632 (2000). 10.1038/35001021 [PubMed: 10688192]

Ingersoll AP, Ewald SP, Sayanagi KM, Blalock JJ, Saturn's atmosphere at 1–10 kilometer resolution. Geophys. Res. Lett. 45(15), 7851–7856 (2018). 10.1029/2018GL079255

Ip WH, Liu CM, Pan KC, Transport and electrodynamical coupling of nano-grains ejected from the Saturnian rings and their possible ionospheric signatures. Icarus 276, 163–169 (2016). 10.1016/j.icarus.2016.04.004

Irwin PGJ, Parrish P, Fouchet T, Calcutt SB, Taylor FW, Simon-Miller AA, Nixon CA, Retrievals of Jovian tropospheric phosphine from Cassini/CIRS. Icarus 172, 37–49 (2004). 10.1016/j.icarus.2003.09.027

Jacobson RA et al. , The gravity field of the Saturnian system from satellite observations and spacecraft tracking data. Astron. J. 132(6), 2520–2526 (2006). 10.1086/508812

Janssen MA, Ingersoll AP, Allison MD, Gulkis S, Laraia AL, Baines KH, Edgington SG, Anderson YZ, Kelleher K, Oyafuso FA, Saturn's thermal emission at 2.2-cm wavelength as imaged by the Cassini RADAR radiometer. Icarus 226(1), 522–535 (2013). 10.1016/j.icarus.2013.06.008

Jennings DE et al. , Composite infrared spectrometer (CIRS) on Cassini. Appl. Opt. 56(18), 5274–5294 (2017). 10.1364/ao.56.005274 [PubMed: 29047582]

Kaspi Y, Inferring the depth of the zonal jets on Jupiter and Saturn from odd gravity harmonics. Geophys. Res. Lett. 40(4), 676–680 (2013). 10.1029/2012gl053873

Kaspi Y, Davighi JE, Galanti E, Hubbard WB, The gravitational signature of internal flows in giant planets: comparing the thermal wind approach with barotropic potential-surface methods. Icarus 276, 170–181 (2016). 10.1016/j.icarus.2016.04.001

Kaspi Y, Galanti E, Hubbard WB, Stevenson DJ, Bolton SJ, Iess L et al. , Jupiter's atmospheric jet streams extend thousands of kilometres deep. Nature 555(7695), 223 (2018). 10.1038/nature25793 [PubMed: 29516995]

Kaspi Y, Galanti E, Showman AP, Stevenson DJ, Guillot T, Iess L, Bolton SJ, Comparison of the deep atmospheric dynamics of Jupiter and Saturn in light of the Juno and Cassini gravity measurements. Space Sci. Rev. 216, 84 (2020)

Kim SJ, Geballe TR, The 2.9–4.2 micron spectrum of Saturn: clouds and CH4, PH3, and NH3. Icarus 179(2), 449–458 (2005). 10.1016/j.icarus.2005.06.015

Kim SJ, Sim CK, Lee DW, Courtin R, Moses JI, Minh YC, The three-micron spectral feature of the Saturnian haze: implications for the haze composition and formation process. Planet. Space Sci. 65, 122–129 (2012). 10.1016/j.pss.2012.02.013

Kong D, Zhang K, Schubert G, Anderson JD, Origin of Jupiter's cloud-level zonal winds remains a puzzle even after Juno. Proc. Natl. Acad. Sci. USA 115(34), 8499–8504 (2018). 10.1073/pnas.1805927115 [PubMed: 30087183]

Koskinen TT, Guerlet S, Atmospheric structure and helium abundance on Saturn from Cassini/UVIS and CIRS observations. Icarus 307, 161–171 (2018). 10.1016/j.icarus.2018.02.020

Koskinen TT, Sandel BR, Yelle RV, Capalbo FJ, Holsclaw GM, McClintock WE, Edgington S, The density and temperature structure near the exobase of Saturn from Cassini UVIS solar occultations. Icarus 226(2), 1318–1330 (2013). 10.1016/j.icarus.2013.07.037

Koskinen TT, Sandel BR, Yelle RV, Strobel DF, Muller-Wodarg ICF, Erwin JT, Saturn's variable thermosphere from Cassini/UVIS occultations. Icarus 260, 174–189 (2015). 10.1016/j.icarus.2015.07.008

Koskinen TT, Moses JI, West RA, Guerlet S, Jouchoux A, The detection of benzene in Saturn's upper atmosphere. Geophys. Res. Lett. 43(15), 7895–7901 (2016). 10.1002/2016gl070000

Koskinen TT, Sandel BR, Yelle R, Holsclaw GM, Quemerais E, Saturn in Lyman alpha: a comparison of Cassini and Voyager observations. Icarus 339, UNSP 113594 (2020)

Lainey V, Jacobson RA, Tajeddine R, Cooper NJ, Murray C, Robert V et al. , New constraints on Saturn's interior from Cassini astrometric data. Icarus 281, 286–296 (2017). 10.1016/j.icarus.2016.07.014

Lamy L, Cecconi B, Prange R, Zarka P, Nichols JD, Clarke JT, An auroral oval at the footprint of Saturn's kilometric radio sources, colocated with the UV aurorae. J. Geophys. Res. Space Phys. 114, A10212 (2009). 10.1029/2009ja014401

Lamy L, Prange R, Pryor W, Gustin J, Badman SV, Melin H, Stallard T, Mitchell DG, Brandt PC, Multispectral simultaneous diagnosis of Saturn's aurorae throughout a planetary rotation. J. Geophys. Res. Space Phys. 118(8), 4817–4843 (2013). 10.1002/jgra.50404

Laraia AL, Ingersoll AP, Janssen MA, Gulkis S, Oyafuso F, Allison M, Analysis of Saturn's thermal emission at 2.2-cm wavelength: spatial distribution of ammonia vapor. Icarus 226(1), 641–654 (2013). 10.1016/j.icarus.2013.06.017

Lellouch E, Bezard B, Strobel DF, Bjoraker GL, Flasar FM, Romani PN, On the HCN and CO2 abundance and distribution in Jupiter's stratosphere. Icarus 184, 478–497 (2006). 10.1016/j.icarus.2006.05.018

Li C, Ingersoll AP, Moist convection in hydrogen atmospheres and the frequency of Saturn's giant storms. Nat. Geosci. 8(5), 398–403 (2015). 10.1038/ngeo2405

Li LM, Ingersoll AP, Vasavada AR, Porco CC, Del Genio AD, Ewald SP, Life cycles of spots on Jupiter from Cassini images. Icarus 172, 9–23 (2004). 10.1016/j.icarus.2003.10.015

Li LM, Ingersoll AP, Huang XL, Interaction of moist convection with zonal jets on Jupiter and Saturn. Icarus 180, 113–123 (2006a). 10.1016/j.icarus.2005.08.016

Li LM, Ingersoll AP, Vasavada AR, Simon-Miller AA, Achterberg RK, Ewald SP et al. , Waves in Jupiter's atmosphere observed by the Cassini ISS and CIRS instruments. Icarus 185, 416–429 (2006b). 10.1016/j.icarus.2006.08.005

Li LM, Ingersoll AP, Vasavada AR, Simon-Miller AA, Del Genio AD, Ewald SP et al. , Vertical wind shear on Jupiter from Cassini images. J. Geophys. Res., Planets 111, E04004 (2006c). 10.1029/2005je002556

Li LM, Gierasch PJ, Achterberg RK, Conrath BJ, Flasar FM, Vasavada AR, Ingersoll AP, Banfield D, Simon-Miller AA, Fletcher LN, Strong jet and a new thermal wave in Saturn's equatorial stratosphere. Geophys. Res. Lett. 35, 23 (2008). 10.1029/2008gl035515

Li LM et al. , Saturn's emitted power. J. Geophys. Res., Planets 115, E11002 (2010). 10.1029/2010je003631

Li LM et al. , Equatorial winds on Saturn and the stratospheric oscillation. Nat. Geosci. 4(11), 750–752 (2011). 10.1038/ngeo1292

Li LM, Baines KH, Smith MA, West RA, Perez-Hoyos S, Trammell HJ et al. , Emitted power of Jupiter based on Cassini CIRS and VIMS observations. J. Geophys. Res., Planets 117, E11002 (2012). 10.1029/2012je004191

Li LM et al. , Strong temporal variation over one Saturnian year: from Voyager to Cassini. Sci. Rep. 3, 2410 (2013). 10.1038/srep02410 [PubMed: 23934437]

Li LM, Jiang X, Trammell HJ, Pan YF, Hernandez J, Conrath BJ et al. , Saturn's giant storm and global radiant energy. Geophys. Res. Lett. 42, 2144–2148 (2015). 10.1002/2015gl063763

Li L, Jiang X, West RA, Gierasch PJ, Perez-Hoyos S, Sanchez-Lavega A, Fletcher LN, Fortney JJ, Knowles B, Porco CC, Baines KH, Fry PM, Mallama A, Achterberg RK, Simon AA, Nixon CA, Orton GS, Dyudina UA, Ewald SP, Schmude RW, Less absorbed solar energy and more internal heat for Jupiter. Nat. Commun. 9, 3709 (2018) [PubMed: 30213944]

Liang MC, Shia RL, Lee AYT, Allen M, Friedson AJ, Yung YL, Meridional transport in the stratosphere of Jupiter. Astrophys. J. 635, L177–L180 (2005). 10.1086/499624

Liao XH, Feng TH, Zhang KK, On the saturation and temporal variation of mean zonal flows: an implication for equatorial jets on giant planets. Astrophys. J. 666(1), L41–L44 (2007). 10.1086/521526

Little B, Anger CD, Ingersoll AP, Vasavada AR, Senske DA, Breneman HH, Borucki WJ, Galileo SSIT, Galileo images of lightning on Jupiter. Icarus 142(2), 306–323 (1999). 10.1006/icar.1999.6195

Liu JJ, Schneider T, Scaling of off-equatorial jets in giant planet atmospheres. J. Atmos. Sci. 72(1), 389–408 (2015). 10.1175/jas-d-13-0391.1

Liu JJ, Schneider T, Fletcher LN, Constraining the depth of Saturn's zonal winds by measuring thermal and gravitational signals. Icarus 239, 260–272 (2014). 10.1016/j.icarus.2014.05.036

Liu T, Sayanagi KM, Brueshaber SR, Blalock JJ, Ingersoll AP, Dyudina UA, Ewald SP, Saturn's north polar vortex structure extracted from cloud images by the optical flow method. J. Geophys. Res., Planets 124, 3041–3062 (2019)

Lorenz RD, Elachi C, West RD, Johnson WTK, Janssen MA, Moghaddam M et al. , Cassini Radio Detection and Ranging (RADAR): Earth and Venus observations. J. Geophys. Res. Space Phys. 106, 30271–30279 (2001). 10.1029/2001ja900035

Lunine J, Chemistry of the solar system revealed in the interiors of the giant planets. Proc. Int. Astron. Union 7(S280), 249–260 (2011). 10.1017/S1743921311025026. The Molecular Universe

Mankovich CR, Fortney JJ, Evidence for a dichotomy in the interior structures of Jupiter and Saturn from helium phase separation. Astrophys. J. 889, 51 (2020)

Mankovich C, Marley MS, Fortney JJ, Movshovitz N, Cassini ring seismology as a probe of Saturn's interior. I. Rigid rotation. Astrophys. J. 871(1), 1 (2019). 10.3847/1538-4357/aaf798

Markham S, Stevenson D, Excitation mechanisms for Jovian seismic modes. Icarus 306, 200–213 (2018)

Matcheva KI, Conrath BJ, Gierasch PJ, Flasar FM, The cloud structure of the Jovian atmosphere as seen by the Cassini/CIRS experiment. Icarus 179, 432–448 (2005). 10.1016/j.icarus.2005.06.020

Mayorga LC, Jackiewicz J, Rages K, West RA, Knowles B, Lewis N, Marley MS, Jupiter's phase variations from Cassini: a testbed for future direct-imaging missions. Astron. J. 152, 209 (2016). 10.3847/0004-6256/152/6/209

Melin H, Stallard T, Miller S, Gustin J, Galand M, Badman SV, Pryor WR, O'Donoghue J, Brown RH, Baines KH, Simultaneous Cassini VIMS and UVIS observations of Saturn's southern aurora:

comparing emissions from H, H$_2$ and H3+ at a high spatial resolution. Geophys. Res. Lett. 38, L15203 (2011). 10.1029/2011gl048457

Melin H et al. , Simultaneous multi-scale and multi-instrument observations of Saturn's aurorae during the 2013 observing campaign. Icarus 263, 56–74 (2016). 10.1016/j.icarus.2015.08.021

Militzer B, Wahl S, Hubbard WB, Models of Saturn's interior constructed with an accelerated concentric Maclaurin spheroid method. Astrophys. J. 879, 78 (2019)

Miller KE, Waite JH, Perryman RS, Perry ME, Bouquet A, Magee BA, Bolton B, Brockwell T, Hedman MM, Glein CR, Cassini INMS constraints on the composition and latitudinal fractionation of Saturn ring rain material. Icarus 339, UNSP 113595 (2020)

Morales-Juberias R, Dowling TE, Jupiter's Great Red Spot: fine-scale matches of model vorticity patterns to prevailing cloud patterns. Icarus 225, 216–227 (2013). 10.1016/j.icarus.2013.03.026

Morales-Juberias R, Sayanagi KM, Dowling TE, Ingersoll AP, Emergence of polar-jet polygons from jet instabilities in a Saturn model. Icarus 211(2), 1284–1293 (2011). 10.1016/j.icarus.2010.11.006

Morales-Juberias R, Sayanagi KM, Simon AA, Fletcher LN, Cosentino RG, Meandering shallow atmospheric jet as a model of Saturn's north-polar hexagon. Astrophys. J. Lett. 806, 1 (2015). 10.1088/2041-8205/806/1/l18

Moses JI, Greathouse TK, Latitudinal and seasonal models of stratospheric photochemistry on Saturn: comparison with infrared data from IRTF/TEXES. J. Geophys. Res., Planets 110, E09007 (2005)

Moses JI, Poppe AR, Dust ablation on the giant planets: consequences for stratospheric photochemistry. Icarus 297, 33–58 (2017) [PubMed: 30842686]

Moses JI, Bezard B, Lellouch E, Gladstone GR, Feuchtgruber H, Allen M, Photochemistry of Saturn's atmosphere - I. Hydrocarbon chemistry and comparisons with ISO observations. Icarus 143, 244–298 (2000a). 10.1006/icar.1999.6270

Moses JI, Lellouch E, Bezard B, Gladstone GR, Feuchtgruber H, Allen M, Photochemistry of Saturn's atmosphere II. Effects of an influx of external oxygen. Icarus 145(1), 166–202 (2000b). 10.1006/icar.1999.6320

Moses JI, Armstrong ES, Fletcher LN, Friedson AJ, Irwin PGJ, Sinclair JA, Hesman BE, Evolution of stratospheric chemistry in the Saturn storm beacon region. Icarus 261, 149–168 (2015). 10.1016/j.icarus.2015.08.012 [PubMed: 30842685]

Mousis O, Alibert Y, Benz W, Saturn's internal structure and carbon enrichment. Astron. Astrophys. 449(1), 411–415 (2006). 10.1051/0004-6361:20054224

Movshovitz N, Fortney JJ, Mankovich C, Thorngren D, Helled R, Saturn's probable interior: an exploration of Saturn's potential interior density structures. Astrophys. J. 891, 109 (2020)

Mueller-Wodarg ICF, Koskinen TT, Moore L, Serigano J, Yelle RV, Horst S et al. , Atmospheric waves and their possible effect on the thermal structure of Saturn's thermosphere. Geophys. Res. Lett. 46(5), 2372–2380 (2019). 10.1029/2018GL081124

Nagy AF, Kliore AJ, Mendillo M, Miller S, Moore L, Moses JI, Muller-Wodarg I, Shemansky D, Upper atmosphere and ionosphere of Saturn, in Saturn from Cassini-Huygens, ed. by Doughterty MK, Esposito LW, Krimigis SM(Springer, Dordrecht, 2009), pp. 181–201

Nettelmann N, Pustow R, Redmer R, Saturn layered structure and homogeneous evolution models with different EOSs. Icarus 225(1), 548–557 (2013). 10.1016/j.icarus.2013.04.018

Nixon CA, Achterberg RK, Conrath BJ, Irwin PGJ, Teanby NA, Fouchet T et al. , Meridional variations of C2H2 and C2H6 in Jupiter's atmosphere from Cassini CIRS infrared spectra. Icarus 188, 47–71 (2007). 10.1016/j.icarus.2006.11.016

Nixon CA, Achterberg RK, Romani PN, Allen M, Zhang X, Teanby NA et al. , Abundances of Jupiter's trace hydrocarbons from Voyager and Cassini. Planet. Space Sci. 58, 1667–1680 (2010). 10.1016/j.pss.010.05.008

O'Donoghue J, Stallard TS, Melin H, Jones GH, Cowley SWH, Miller S et al. , The domination of Saturn's low-latitude ionosphere by ring 'rain,'. Nature 496(7444), 193–195 (2013). 10.1038/nature12049 [PubMed: 23579676]

O'Donoghue J, Stallard TS, Melin H, Cowley SWH, Badman SV, Moore L, Miller S, Tao C, Baines KH, Blake JSD, Conjugate observations of Saturn's northern and southern H3+ aurorae. Icarus 229, 214–220 (2014). 10.1016/j.icarus.2013.11.009

O'Donoghue J, Moore L, Connerney JEP, Melin H, Stallard TS, Miller S, Baines KH, Redetection of the ionospheric H3+ signature of Saturn's "ring rain". Geophys. Res. Lett. 44, 11762–11769 (2017). 10.1002/2017gl075932

Oliva F, Adriani A, Moriconi ML, Liberti GL, D'Aversa E, Filacchione G, Clouds and hazes vertical structure of a Saturn's giant vortex from Cassini/VIMS-V data analysis. Icarus 278, 215–237 (2016). 10.1016/j.icarus.2016.06.021

O'Neill ME, Emanuel KA, Flierl GR, Polar vortex formation in giant-planet atmospheres dues to moist convection. Nat. Geosci. 8(7), 523–U118 (2015). 10.1038/ngeo2459

O'Neill ME, Emanuel KA, Flierl GR, Weak jets and strong cyclones: shallow water modeling of giant planet polar caps. J. Atmos. Sci. 73, 1841–1855 (2016). 10.1175/JAS-D-15-0314.1

Ordonez-Etxeberria I, Hueso R, Sanchez-Lavega A, Perez-Hoyos S, Spatial distribution of Jovian clouds, hazes and colors from Cassini ISS multi-spectral images. Icarus 267, 34–50 (2016). 10.1016/j.icarus.2015.12.008

Orton G, Friedson A, Caldwell J, Hammel H, Baines K, Bergstralh J, Martin T, Malcom M, West R, Golisch W, Griep D, Kaminski C, Tokunaga A, Baron R, Shure M, Thermal maps of Jupiter - spatial-organization and time-dependence of stratospheric temperatures, 1980 to 1990. Science 252, 537–542 (1991) [PubMed: 17838486]

Orton GS, Yanamandra-Fisher PA, Fisher BM, Friedson AJ, Parrish PD, Nelson JF, Bauermeister AS, Fletcher L, Gezari DY, Varosi F, Tokunaga AT, Caldwell J, Baines KH, Hora JL, Ressler ME, Fujiyoshi T, Fuse T, Hagopian H, Martin TZ, Bergstralh JT, Howett C, Hoffmann WF, Deutsch LK, Van Cleve JE, Noe E, Adams JD, Kassis M, Tollestrup E, Semi-annual oscillations in Saturn's low-latitude stratospheric temperatures. Nature 453, 196–199 (2008) [PubMed: 18464736]

Owen T, Encrenaz T, Element abundances and isotope ratios in the giant planets and Titan. Space Sci. Rev. 106(1–4), 121–138 (2003). 10.1023/a:1024633603624.

Parkinson CD, Stewart AIF, Wong AS, Yung YL, Ajello JM, Enhanced transport in the polar mesosphere of Jupiter: evidence from Cassini UVIS helium 584 angstrom airglow. J. Geophys. Res., Planets 111, E02002 (2006). 10.1029/2005je002539

Perez-Hoyos S, Sanchez-Lavega A, On the vertical wind shear of Saturn's equatorial jet at cloud level. Icarus 180(1), 161–175 (2006). 10.1016/j.icarus.2005.07.011

Perez-Hoyos S, Sanchez-Lavega A, French RG, Short-term changes in the belt/zone structure of Saturn's southern hemisphere (1996–2004). Astron. Astrophys. 460(2), 641–645 (2006). 10.1051/0004-6361:20065972

Perez-Hoyos S, Sanz-Requena JF, Sanchez-Lavega A, Irwin PGJ, Smith A, Saturn's tropospheric particles phase function and spatial distribution from Cassini ISS 2010–11 observations. Icarus 277, 1–18 (2016). 10.1016/j.icarus.2016.04.022

Perry ME, Waite JH, Mitchell DG, Miller KE, Cravens TE, Perryman RS, Moore L, Yelle RV, Hsu H-W, Hedman MM, Cuzzi JN, Strobel DF, Hamil OQ, Glein CR, Paxton LJ, Teolis BD, McNutt RL, Material flux from the rings of Saturn into its atmosphere. Geophys. Res. Lett. 45, 10093–10100 (2018)

Pierel JDR, Nixon CA, Lellouch E, Fletcher LN, Bjoraker GL, Achterberg RK, Bezard B, Hesman BE, Irwin PGJ, Flasar FM, D/H Ratios on Saturn and Jupiter from Cassini CIRS. Astron. J. 154, 5 (2017). 10.3847/1538-3881/aa899d

Porco CC, West RA, McEwen A, Del Genio AD, Ingersoll AP, Thomas P et al. , Cassini imaging of Jupiter's atmosphere, satellites, and rings. Science 299, 1541–1547 (2003). 10.1126/science.1079462 [PubMed: 12624258]

Porco CC et al. , Cassini imaging science: initial results on Saturn's atmosphere. Science 307(5713), 1243–1247 (2005). 10.1126/science.1107691 [PubMed: 15731441]

Pryor WR et al. , The auroral footprint of Enceladus on Saturn. Nature 472(7343), 331–333 (2011). 10.1038/nature09928 [PubMed: 21512570]

Pryor WR, Esposito LW, Jouchoux A, West RA, Grodent D, Gerard J-C, Radioti A, Lamy L, Koskinen T, Cassini UVIS detection of Saturn's north polar hexagon in the Grand Finale orbits. J. Geophys. Res., Planets 124, 1979–1988 (2019)

Qin S, Kong D, Zhang K, Schubert G, Huang Y, Interpreting the equatorially antisymmetric gravitational field of Saturn measured by the Cassini Grand Finale. Astrophys. J. 890, 26 (2020)

Read PL, A chorus of the winds—on Saturn! J. Geophys. Res., Planets 123, 1007–1011 (2018)

Read PL, Gierasch PJ, Conrath BJ, Simon-Miller A, Fouchet T, Yamazaki YH, Mapping potential-vorticity dynamics on Jupiter. I: zonal-mean circulation from Cassini and Voyager 1 data. Q. J. R. Meteorol. Soc. 132, 1577–1603 (2006). 10.1256/qj.05.34

Read PL, Conrath BJ, Fletcher LN, Gierasch PJ, Simon-Miller AA, Zuchowski LC, Mapping potential vorticity dynamics on Saturn: zonal mean circulation from Cassini and Voyager data. Planet. Space Sci. 57, 1682–1698 (2009a). 10.1016/j.pss.2009.03.004

Read PL, Dowling TE, Schubert G, Saturn's rotation period from its atmospheric planetary-wave configuration. Nature 460(7255), 608–610 (2009b). 10.1038/nature08194

Rogers JH, Mettig HJ, Cidadao A, Sherrod PC, Peach D, Merging circulations on Jupiter: observed differences between cyclonic and anticyclonic mergers. Icarus 185, 244–257 (2006). 10.1016/j.icarus.2006.05.022

Rogers JH, Fletcher LN, Adamoli G, Jacquesson M, Vedovato M, Orton GS, A dispersive wave pattern on Jupiter's fastest retrograde jet at 20°S. Icarus 277, 354–369 (2016). 10.1016/j.icarus.2016.05.028

Roman MT, Banfield D, Gierasch PJ, Saturn's cloud structure inferred from Cassini ISS. Icarus 225(1), 93–110 (2013). 10.1016/j.icarus.2013.03.015

Rostami M, Zeitlin V, Spiga A, On the dynamical nature of Saturn's north polar hexagon. Icarus 297, 59–70 (2017)

Salyk C, Ingersoll AP, Lorre J, Vasavada A, Del Genio AD, Interaction between eddies and mean flow in Jupiter's atmosphere: analysis of Cassini imaging data. Icarus 185, 430–442 (2006). 10.1016/j.icarus.2006.08.007

Sanchez-Lavega A, Saturn's Great White Spots, chaos: an interdisciplinary. J. Nonlinear Sci. 4(2), 341–353 (1994). 10.1063/1.166012

Sanchez-Lavega A, Rojas JF, Sada PV, Sada PV, Saturn's zonal winds at cloud level. Icarus 147(2), 405–420 (2000). 10.1006/icar.2000.6449

Sanchez-Lavega A, Hueso R, Perez-Hoyos S, Rojas JF, French RG, Saturn's cloud morphology and zonal winds before the Cassini encounter. Icarus 170(2), 519–523 (2004). 10.1016/j.icarus.2004.05.002

Sanchez-Lavega A, Hueso R, Perez-Hoyos S, Rojas JF, A strong vortex in Saturn's South Pole. Icarus 184(2), 524–531 (2006). 10.1016/j.icarus.2006.05.020

Sanchez-Lavega A, Hueso R, Perez-Hoyos S, The three-dimensional structure of Saturn's equatorial jet at cloud level. Icarus 187(2), 510–519 (2007). 10.1016/j.icarus.2006.10.022

Sanchez-Lavega A et al. , Deep winds beneath Saturn's upper clouds from a seasonal long-lived planetary-scale storm. Nature 475(7354), 71–74 (2011). 10.1038/nature10203 [PubMed: 21734704]

Sanchez-Lavega A et al. , Ground-based observations of the long-term evolution and death of Saturn's 2010 Great White Spot. Icarus 220(2), 561–576 (2012). 10.1016/j.icarus.2012.05.033

Sanchez-Lavega A et al. , The long- term steady motion of Saturn's hexagon and the stability of its enclosed jet stream under seasonal changes. Geophys. Res. Lett. 41(5), 1425–1431 (2014). 10.1002/2013gl059078

Sanchez-Lavega A et al. , An enduring rapidly moving storm as a guide to Saturn's equatorial jet's complex structure. Nat. Commun. 7, 13262 (2016). 10.1038/ncomms13262 [PubMed: 27824031]

Sánchez-Lavega A, Fischer G, Fletcher L, García-Melendo E, Hesman B, Pérez-Hoyos S, Sromovsky L, The great Saturn storm of 2010–2011, in Saturn in the 21st Century, ed. by Baines K, Flasar F, Krupp N, Stallard T Cambridge Planetary Science (Cambridge University Press, Cambridge, 2018), pp. 377–416. 10.1017/9781316227220.013

Sanchez-Lavega A, Garcia-Munoz A, del Rio-Gaztelurrutia T, Perez-Hoyos S, Sanz-Requena JF, Hueso R, Guerlet S, Peralta J, Multilayer hazes over Saturn's hexagon from Cassini ISS limb images. Nat. Commun. 11, 2281 (2020a) [PubMed: 32385300]

Sanchez-Lavega A, Garcia-Melendo E, Legarreta J, Hueso R, del Rio-Gaztelurrutia T, Sanz-Requena JF, Perez-Hoyos S, Simon AA, Wong MH, Soria M, Gomez-Forrellad JM, Barry T, Delcroix

M, Sayanagi KM, Blalock JJ, Gunnarson JL, Dyudina U, Ewald S, A complex storm system in Saturn's north polar atmosphere in (2018). Nat. Astron. 4, 180–187 (2020b)

Sanz-Requena JF, Pérez-Hoyos S, Sánchez-Lavega A, Antuñano A, Irwin PGJ, Haze and cloud structure of Saturn's north pole and hexagon wave from Cassini/ISS imaging. Icarus 305, 284–300 (2018). 10.1016/j.icarus.2017.12.043

Sanz-Requena JF, Pérez-Hoyos S, Sánchez-Lavega A, del Rio-Gaztelurrutia T, Irwin PGJ, Hazes and clouds in a singular triple vortex in Saturn's atmosphere from HST/WFC3 multispectral imaging. Icarus 333, 22–36 (2019). 10.1016/j.icarus.2019.05.037

Sato TM, Satoh T, Kasaba Y, Retrieval of Jovian cloud structure from the Cassini ISS limb-darkening data I. Continuum scattering phase functions for cloud and haze in the South Tropical Zone. Icarus 222, 100–121 (2013). 10.1016/j.icarus.2012.09.035

Sayanagi KM, Showman AP, Effects of a large convective storm on Saturn's equatorial jet. Icarus 187(2), 520–539 (2007). 10.1016/j.icarus.2006.10.020

Sayanagi KM, Morales-Juberias R, Ingersoll AP, Saturn's northern hemisphere ribbon: simulations and comparison with the meandering Gulf stream. J. Atmos. Sci. 67, 2658–2678 (2010). 10.1175/2010jas3315.1

Sayanagi KM, Dyudina UA, Ewald SP, Fischer G, Ingersoll AP, Kurth WS, Muro GD, Porco CC, West RA, Dynamics of Saturn's great storm of 2010–2011 from Cassini ISS and RPWS. Icarus 223(1), 460–478 (2013). 10.1016/j.icarus.2012.12.013

Sayanagi KM, Dyudina UA, Ewald SP, Muro GD, Ingersoll AP, Cassini ISS observation of Saturn's String of Pearls. Icarus 229, 170–180 (2014). 10.1016/j.icarus.2013.10.032

Sayanagi KM, Blalock JJ, Dyudina UA, Ewald SP, Ingersoll AP, Cassini ISS observation of Saturn's north polar vortex and comparison to the south polar vortex. Icarus 285, 68–82 (2017). 10.1016/j.icarus.2016.12.011

Sayanagi KM, Baines KH, Dyudina U, Fletcher LN, Sánchez-Lavega A, West RA, Saturn's polar atmosphere, in Saturn in the 21st Century, ed. by Baines KH, Flasar FM, Krupp N, Stallard T (Cambridge University Press, Cambridge, 2018), pp. 337–376. 10.1017/9781316227220.012

Schinder PJ, Flasar FM, Marouf EA, French RG, McGhee CA, Kliore AJ, Rappaport NJ, Barbinis E, Fleischman D, Anabtawi A, Saturn's equatorial oscillation: evidence of descending thermal structure from Cassini radio occultations. Geophys. Res. Lett. 38, L08205 (2011). 10.1029/2011gl047191

Schinder PJ, Flasar FM, Marouf EA, French RG, Anabtawi A, Barbinis E, Kliore AJ, A numerical technique for two-way radio occultations by oblate axisymmetric atmospheres with zonal winds. Radio Sci. 50(7), 712–727 (2015). 10.1002/2015rs005690

Schneider T, Liu J, Formation of jets and equatorial superrotation on Jupiter. J. Atmos. Sci. 66(3), 579–601 (2009). 10.1175/2008JAS2798.1

Shemansky DE, Liu X, Saturn upper atmospheric structure from Cassini EUV and FUV occultations. Can. J. Phys. 90(8), 817–831 (2012). 10.1139/p2012-036

Shetty S, Marcus PS, Changes in Jupiter's Great Red Spot (1979–2006) and Oval BA (2000–2006). Icarus 210, 182–201 (2010). 10.1016/j.icarus.2010.06.026

Showman AP, de Pater I, Dynamical implications of Jupiter's tropospheric ammonia abundance. Icarus 174(1), 192–204 (2005). 10.1016/j.icarus.2004.10.004

Showman AP, Ingersoll AP, Achterberg R, Kaspi Y, The global atmospheric circulation of Saturn, in Saturn in the 21st Century, ed. by Baines KH, Flasar FM, Krupp N, Stallard T (Cambridge University Press, Cambridge, 2018), pp. 295–336. 10.1017/9781316227220.011

Simon AA, Li L, Reuter DC, Small-scale waves on Jupiter: a reanalysis of new horizons, Voyager, and Galileo data. Geophys. Res. Lett. 42(8), 2612–2618 (2015). 10.1002/2015GL063433

Simon-Miller AA, Gierasch PJ, On the long-term variability of Jupiter's winds and brightness as observed from Hubble. Icarus 210, 258–269 (2010). 10.1016/j.icarus.2010.06.020

Simon-Miller AA, Conrath BJ, Gierasch PJ, Orton GS, Achterberg RK, Flasar FM, Fisher BM, Jupiter's atmospheric temperatures: from Voyager IRIS to Cassini CIRS. Icarus 180, 98–112 (2006). 10.1016/j.icarus.2005.07.019

Simon-Miller AA, Poston BW, Orton GS, Fisher B, Wind variations in Jupiter's equatorial atmosphere: a QQO counterpart? Icarus 186, 192–203 (2007). 10.1016/j.icarus.2006.08.009

Simon-Miller AA, Rogers JH, Gierasch PJ, Choi D, Allison MD, Adamoli G, Mettig HJ, Longitudinal variation and waves in Jupiter's south equatorial wind jet. Icarus 218, 817–830 (2012). 10.1016/j.icarus.2012.01.022

Sinclair JA, Irwin PGJ, Fletcher LN, Moses JI, Greathouse TK, Friedson AJ, Hesman B, Hurley J, Merlet C, Seasonal variations of temperature, acetylene and ethane in Saturn's atmosphere from 2005 to 2010, as observed by Cassini-CIRS. Icarus 225(1), 257–271 (2013). 10.1016/j.icarus.2013.03.011

Sinclair JA, Irwin PGJ, Fletcher LN, Greathouse T, Guerlet S, Hurley J, Merlet C, From Voyager-IRIS to Cassini-CIRS: interannual variability in Saturn's stratosphere? Icarus 233, 281–292 (2014). 10.1016/j.icarus.2014.02.009

Sinclair JA, Orton GS, Greathouse TK, Fletcher LN, Moses JI, Hue V, Irwin PGJ, Jupiter's auroral-related stratospheric heating and chemistry I: analysis of Voyager-IRIS and Cassini-CIRS spectra. Icarus 292, 182–207 (2017). 10.1016/j.icarus.2016.12.033

Sinclair JA, Orton GS, Greathouse TK, Fletcher LN, Moses JI, Hue V, Irwin PGJ, Jupiter's auroral-related stratospheric heating and chemistry II: analysis of IRTF-TEXES spectra measured in December 2014. Icarus 300, 305–326 (2018). 10.1016/j.icarus.2017.09.016

Sinclair JA, Moses JI, Hue V, Greathouse TK, Orton GS, Fletcher LN, Irwin PGJ, Jupiter's auroral-related stratospheric heating and chemistry III: abundances of C2H4, CH3C2H, C4H2 and C6H6 from Voyager-IRIS and Cassini-CIRS. Icarus 328, 176–193 (2019)

Smith BA, Soderblom L, Batson RM, Bridges PM, Inge JL, Masursky H, Shoemaker E, Beebe RF, Boyce J, Briggs G, Bunker A, Collins SA, Hansen C, Johnson TV, Mitchell JL, Terrile RJ, Cook AF, Cuzzi JN, Pollack JB, Danielson GE, Ingersoll AP, Davies ME, Hunt GE, Morrison D, Owen T, Sagan C, Veverka J, Strom R, Suomi VE, A new look at the Saturn system: the Voyager 2 images. Science 215(4532), 504–537 (1982). 10.1126/science.215.4532.504 [PubMed: 17771273]

Spiga A, Guerlet S, Millour E, Indurain M, Meurdesoif Y, Cabanes S, Dubos T, Leconte J, Boissinot A, Lebonnois S, Sylvestre M, Fouchet T, Global climate modeling of Saturn's atmosphere. Part II: multi-annual high-resolution dynamical simulations. Icarus 335, UNSP 113377 (2020)

Spilker LJ, Cassini's final year at Saturn: science highlights and discoveries. Geophys. Res. Lett. 46, 5754–5758 (2019)

Sromovsky LA, Fry PM, The source of widespread 3 μm absorption in Jupiter's clouds: constraints from 2000 Cassini VIMS observations. Icarus 210, 230–257 (2010). 10.1016/j.icarus.2010.06.039

Sromovsky LA, Fry PM, Composition and structure of fresh ammonia clouds on Jupiter based on quantitative analysis of Galileo/NIMS and New Horizons/LEISA spectra. Icarus 307, 347 (2018)

Sromovsky LA, Fry PM, Interpretation of shadows and antishadows on Saturn and the evidence against south polar eyewalls. Icarus (2019, in press). 10.1016/j.icarus.2019.113399

Sromovsky LA, Baines KH, Fry PM, Saturn's Great Storm of 2010–2011: evidence for ammonia and water ices from analysis of VIMS spectra. Icarus 226(1), 402–418 (2013). 10.1016/j.icarus.2013.05.043

Sromovsky LA, Baines KH, Fry PM, Momary TW, Cloud clearing in the wake of Saturn's Great Storm of 2010–2011 and suggested new constraints on Saturn's He/H2 ratio. Icarus 276, 141–162 (2016). 10.1016/j.icarus.2016.04.031

Sromovsky LA, Baines KH, Fry PM, Carlson RW, A possibly universal red chromophore for modeling color variations on Jupiter. Icarus 291, 232–244 (2017). 10.1016/j.icarus.2016.12.014

Sromovsky LA, Baines KH, Fry PM, Models of bright storm clouds and related dark ovals in Saturn's Storm Alley as constrained by 2008 Cassini/VIMS spectra. Icarus 302, 360 (2018)

Sromovsky LA, Baines KH, Fry PM, Saturn's south polar cloud composition and structure inferred from 2006 Cassini/VIMS spectra and ISS images. Icarus 344, 113398 (2020). 10.1016/j.icarus.2019.113398

Stallard TS, Melin H, Miller S, Badman SV, Brown RH, Baines KH, Peak emission altitude of Saturn's H3+ aurora. Geophys. Res. Lett. 39, L15103 (2012a). 10.1029/2012gl052806

Stallard TS, Melin H, Miller S, O'Donoghue J, Cowley SW, Badman SV, Adriani A, Brown RH, Baines KH, Temperature changes and energy inputs in giant planet atmospheres: what we are

learning from H3+. Philos. Trans. A Math. Phys. Eng. Sci. 370(1978), 5213–5224 (2012b). 10.1098/rsta.2012.0028

Stallard TS, Melin H, Miller S, Badman SV, Baines KH, Brown RH et al. , Cassini VIMS observations of H3+ emission on the nightside of Jupiter. J. Geophys. Res. Space Phys. 120, 6948–6973 (2015). 10.1002/2015ja021097

Studwell A, Li L, Jiang X, Baines KH, Fry PM, Momary TW, Dyudina UA, Saturn's global zonal winds explored by Cassini/VIMS 5-μm images. Geophys. Res. Lett. 45, 6823–6831 (2018)

Sugiyama K, Nakajima K, Odaka M, Kuramoto K, Hayashi YY, Numerical simulations of Jupiter's moist convection layer: structure and dynamics in statistically steady states. Icarus 229, 71–91 (2014). 10.1016/j.icarus.2013.10.016

Sussman MG, Chanover NJ, Simon-Miller AA, Vasavada AR, Beebe RF, Analysis of Jupiter's Oval BA: a streamlined approach. Icarus 210, 202–210 (2010). 10.1016/j.icarus.2010.06.044

Sylvestre M, Guerlet S, Fouchet T, Spiga A, Flasar FM, Hesman B, Bjoraker GL, Seasonal changes in Saturn's stratosphere inferred from Cassini/CIRS limb observations. Icarus 258, 224–238 (2015). 10.1016/j.icarus.2015.05.025

Teanby NA, Fletcher LN, Irwin PGJ, Fouchet T, Orton GS, New upper limits for hydrogen halides on Saturn derived from Cassini-CIRS data. Icarus 185(2), 466–475 (2006). 10.1016/j.icarus.2006.07.011

Teifel VG', Vdovichenko VD, Lysenko PG, Karimov AM, Kirienko GA, Bondarenko NNet al. , Ammonia in Jupiter's atmosphere: spatial and temporal variations of the NH3 absorption bands at 645 and 787 Nm. Sol. Syst. Res. 52(6), 480–494 (2018). 10.1134/S0038094618060072

Tejfel VG, Latitudinal variations of the molecular absorption on Saturn and seasonal changes of the atmospheric state at S- and N-hemispheres. Terr. Atmos. Ocean. Sci. 16(1), 231–240 (2005). 10.3319/tao.2005.16.1.231(aa)

Temma T, Chanover NJ, Simon-Miller AA, Glenar DA, Hillman JJ, Kuehn DM, Vertical structure modeling of Saturn's equatorial region using high spectral resolution imaging. Icarus 175(2), 464–489 (2005). 10.1016/j.icarus.2004.11.006

Trammell HJ, Li LM, Jiang X, Smith M, Horst S, Vasavada A, The global vortex analysis of Jupiter and Saturn based on Cassini imaging science subsystem. Icarus 242, 122–129 (2014). 10.1016/j.icarus.2014.07.019

Trammell HJ et al. , Vortices in Saturn's northern hemisphere (2008–2015) observed by Cassini ISS. J. Geophys. Res., Planets 121(9), 1814–1826 (2016). 10.1002/2016je005122 [PubMed: 29629249]

Vasavada AR, Horst SM, Kennedy MR, Ingersoll AP, Porco CC, Del Genio AD, West RA, Cassini imaging of Saturn: southern hemisphere winds and vortices. J. Geophys. Res., Planets 111, E5 (2006). 10.1029/2005je002563

Vervack RJ, Moses JI, Saturn's upper atmosphere during the Voyager era: reanalysis and modeling of the UVS occultations. Icarus 258, 135–163 (2015). 10.1016/j.icarus.2015.06.007

West RA, Baines KH, Karkoschka E, Sanchez-Lavega A, Clouds and aerosols in Saturn's atmosphere, in Saturn from Cassini-Huygens, ed. by Doughterty MK, Esposito LW, Krimigis SM(Springer, Dordrecht, 2009), pp. 161–179

Wong MH, Bjoraker GL, Smith MD, Flasar FM, Nixon CA, Identification of the 10-μm ammonia ice feature on Jupiter. Planet. Space Sci. 52, 385–395 (2004). 10.1016/j.pss.2003.06.005

Wong MH, de Pater I, Asay-Davis X, Marcus PS, Go CY, Vertical structure of Jupiter's Oval BA before and after it reddened: what changed? Icarus 215, 211–225 (2011). 10.1016/j.icarus.2011.06.032

Yadav RK, Bloxham J, Deep rotating convection generates the polar hexagon on Saturn. Proc. Natl. Acad. Sci. USA 117, 13991–13996 (2020) [PubMed: 32513703]

Yair Y, New results on planetary lightning. Adv. Space Res. 50(3), 293–310 (2012). 10.1016/j.asr.2012.04.013

Yair Y, Fischer G, Simoes F, Renno N, Zarka P, Updated review of planetary atmospheric electricity. Space Sci. Rev. 1371–4, 29–44 (2008). 10.1007/s11214-008-9349-9

Ye SY, Fischer G, Kurth WS, Menietti JD, Gurnett DA, Rotational modulation of Saturn's radio emissions after equinox. J. Geophys. Res. Space Phys. 121(12), 11714–11728 (2016). 10.1002/2016ja023281

Yelle RV, Serigano J, Koskinen TT, Horst SM, Perry ME, Perryman RS, Waite JH, Thermal structure and composition of Saturn's upper atmosphere from Cassini/ion neutral mass spectrometer measurements. Geophys. Res. Lett. 45(20), 10951–10958 (2018). 10.1029/2018GL078454

Young RMB, Read PL, Forward and inverse kinetic energy cascades in Jupiter's turbulent weather layer. Nat. Phys. 13, 1135 (2017). 10.1038/nphys4227

Youssef A, Marcus PS, The dynamics of Jovian white ovals from formation to merger. Icarus 162(1), 74–93 (2003). 10.1016/S0019-1035(02)00060-X

Zarka P, Farrell W, Fischer G, Konovalenko A, Ground-based and space-based radio observations of planetary lightning. Space Sci. Rev. 137(1–4), 257–269 (2008). 10.1007/s11214-008-9366-8

Zhang X, Nixon CA, Shia RL, West RA, Irwin PGJ, Yelle RV et al. , Radiative forcing of the stratosphere of Jupiter, Part I: atmospheric cooling rates from Voyager to Cassini. Planet. Space Sci. 88, 3–25 (2013a). 10.1016/j.pss.2013.07.005

Zhang X, Shia R-L, Yung YL, Jovian stratosphere as a chemical transport system: benchmark analytical solutions. Astrophys. J. 767, 172 (2013b). 10.1088/0004-637x/767/2/172

Zhang X, West RA, Banfield D, Yung YL, Stratospheric aerosols on Jupiter from Cassini observations. Icarus 226, 159–171 (2013c). 10.1016/j.icarus.2013.05.020

Zhang X, West RA, Irwin PGJ, Nixon CA, Yung YL, Aerosol influence on energy balance of the middle atmosphere of Jupiter. Nat. Commun. 6, 10231 (2015). 10.1038/ncomms10231 [PubMed: 26694318]

Zuchowski LC, Yamazaki YH, Read PL, Modeling Jupiter's cloud bands and decks 1, jet scale meridional circulations. Icarus 200, 548–562 (2009). 10.1016/j.icarus.2008.11.024
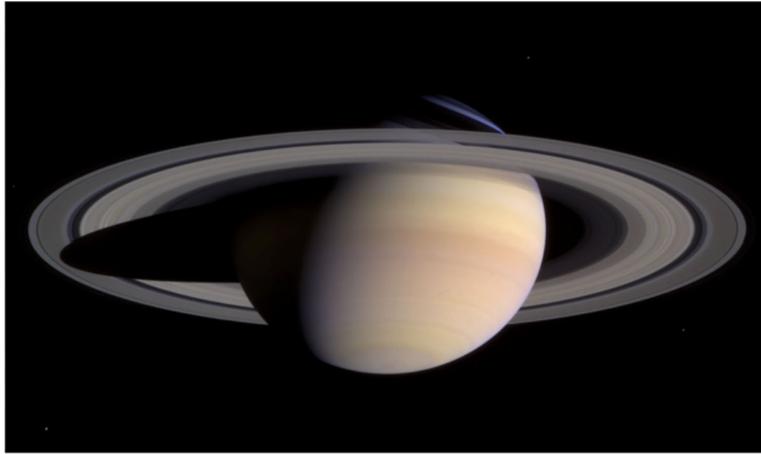
Fig. 1.
Image taken by the ISS in 2004 as Cassini was approaching Saturn. It was summer in the south, and the sunlight was driving a rich hydrocarbon chemistry. Temperatures were 10–20 K warmer in the south. The north was mostly shielded from sunlight, and the skies were blue, as shown by the sliver of atmosphere visible above the ring (PIA05389)
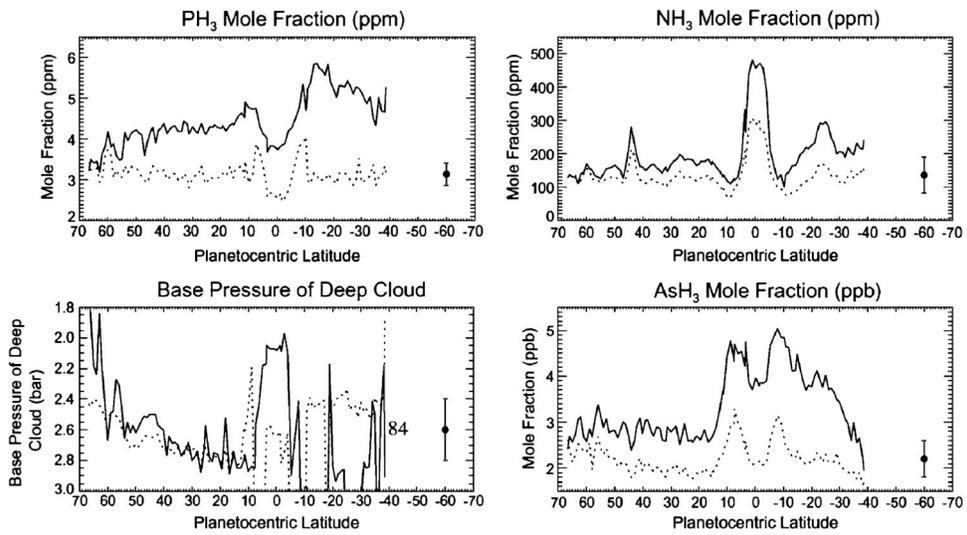
Fig. 2.

Tropospheric chemical abundances from Cassini VIMS. On first look, the profiles do not tell a consistent story. NH_3 shows a high mole fraction at the equator, consistent with upwelling there and downwelling on either side at 10–12° latitude, but PH_3 and AsH_3 show low abundances at the equator, consistent with downwelling. The data may be indicating a double Hadley cell, with rising motion at the higher altitudes at the equator and sinking motion deeper down (Fletcher et al. 2011a)
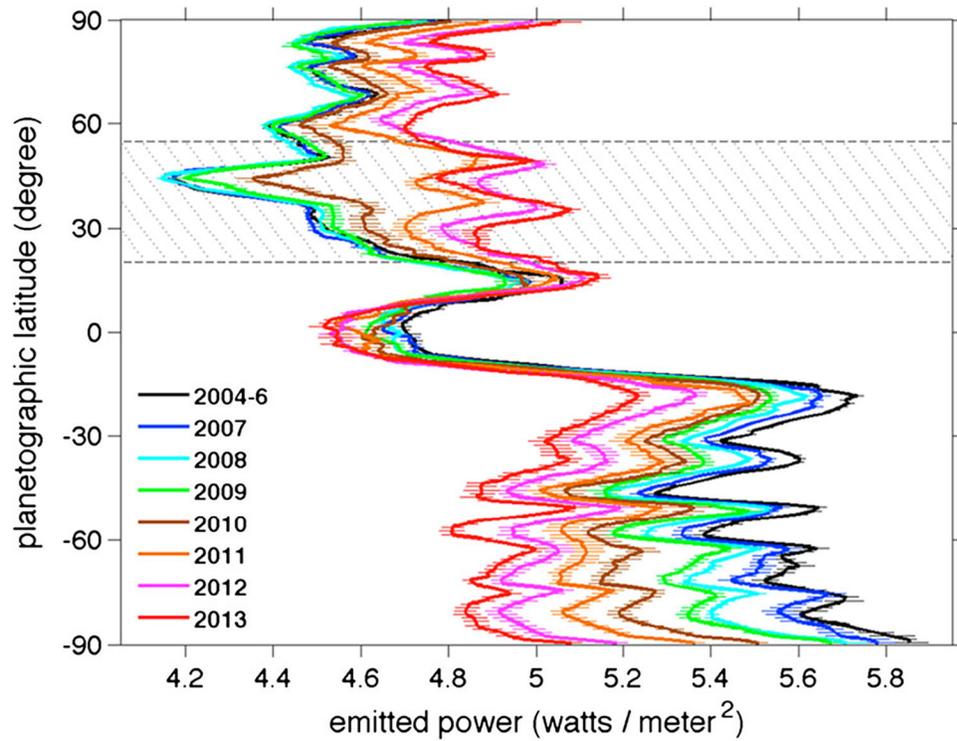
Fig. 3.
Thermal emission of the planet in units of W m^{-2} from Cassini CIRS. In the south the season was early summer in 2004 and mid fall in 2013. The decrease in thermal emission in the south was due to cooling of the atmosphere. Comparing the years before and after 2011, it is clear that the great storm increased the thermal emission by 5–10% in the 30–40° latitude band, and that the anomaly persisted for several years (Li et al. 2015)
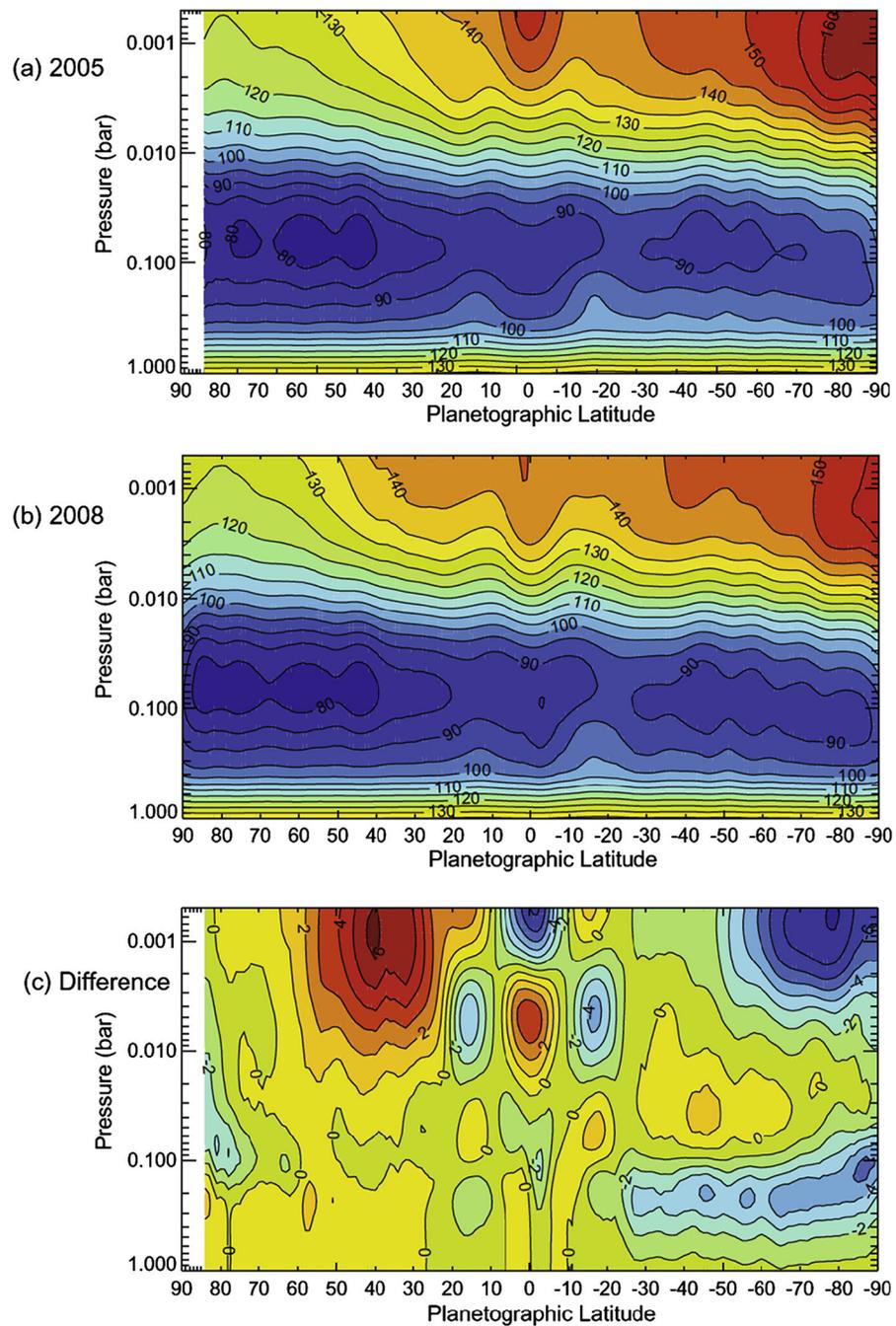
Fig. 4.

Temperature as a function of latitude and altitude from Cassini CIRS. In 2005 the season was mid-winter in the north, and in 2008 the season was late winter. Vernal equinox was August 10, 2009. The south is warmer than the north in both years, although most of the hemispheric contrast and most of the difference between 2005 and 2008 is confined to high altitudes (Fletcher et al. 2010)
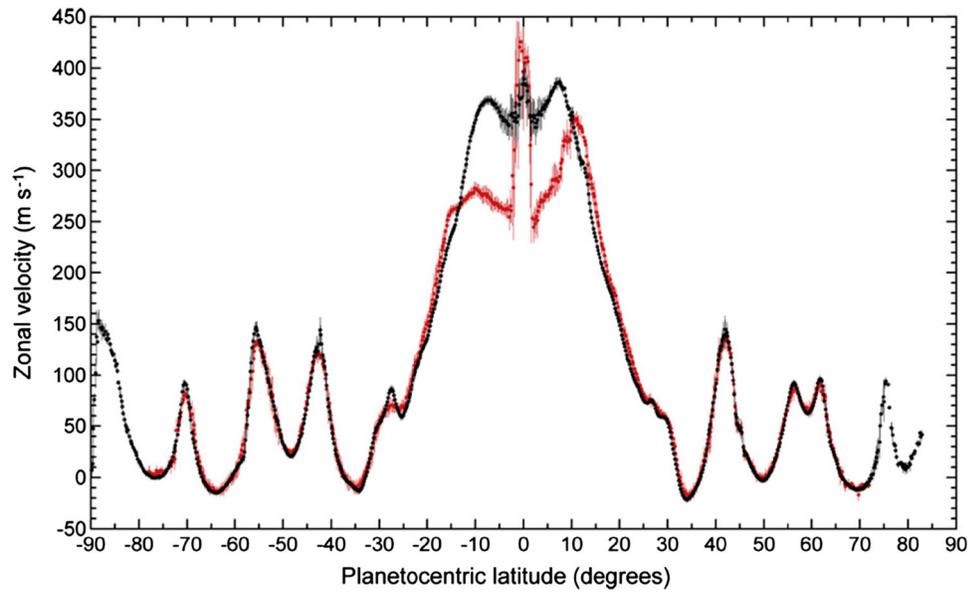
Fig. 5.
Atmospheric zonal velocity for Saturn from Cassini ISS. The black curve is data from the 350 to 700 mbar levels, and the red curve is data from 100 to 200 mbar. The differences are small except for a latitude band ±15° from the equator (Garcia-Melendo et al. 2011b)
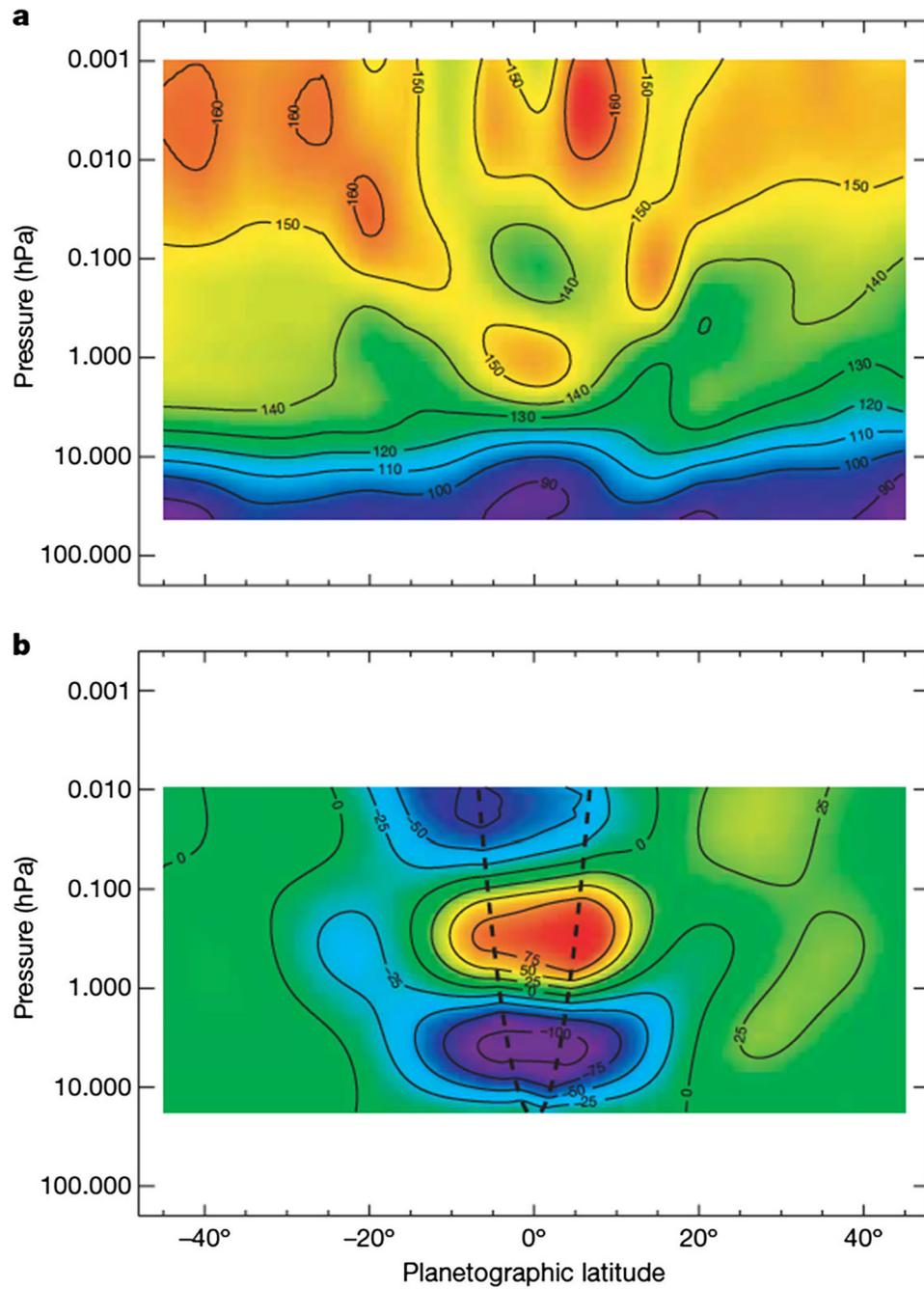
Fig. 6.

Oscillation of temperature (upper panel) and mean zonal wind (lower panel) at the equator from Cassini CIRS. The pattern moves down with time and has a ~15-year period (Orton et al. 2008; Fouchet et al. 2008; Guerlet et al. 2018). A similar pattern on Jupiter has a period of ~4 years (Orton et al. 1991). The Figure is from Fouchet et al. (2008)
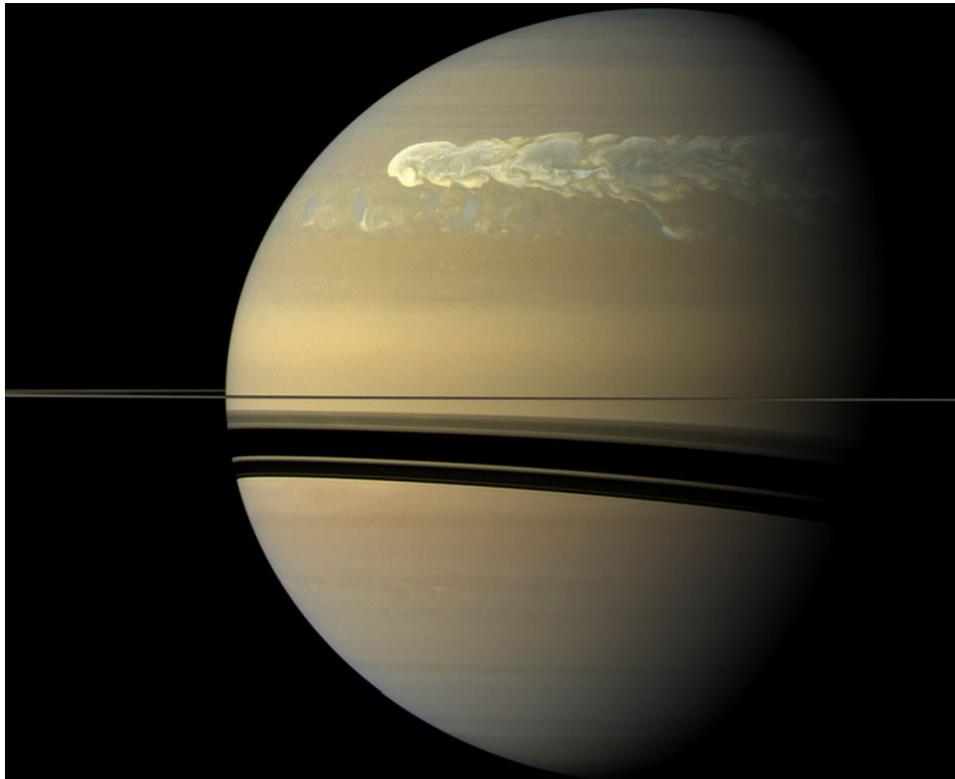
Fig. 7.
Saturn imaged by Cassini ISS on February 25, 2011. The great storm of 2010–2011 is clearly visible in a band centered at 30–40° latitude. Since its appearance on December 5, 2010, the head of the storm had drifted west and overtaken the tail (PIA 12826)
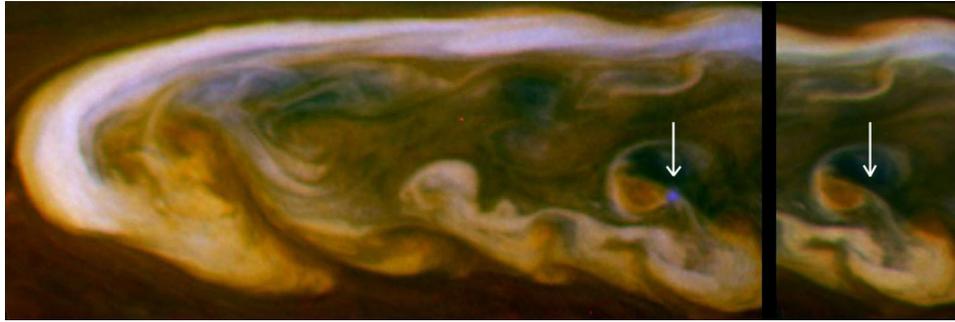
Fig. 8.

Lightning flash in Saturn's great storm of 2010–2011. The color composite consists of three images taken in rapid succession at three different wavelengths. A lightning flash occurred while the blue-filtered image was taken, making a blue spot in the composite image, left. The same region was imaged 30 minutes later and did not see a lightning flash, right (PIA14921)
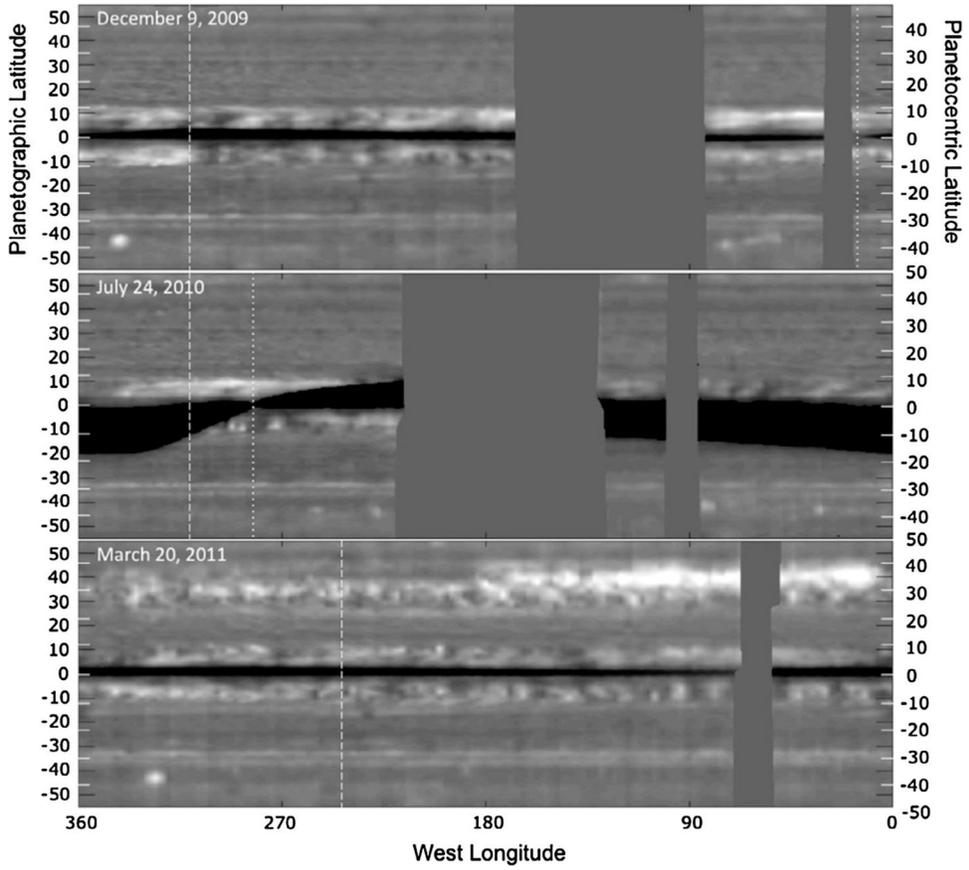
Fig. 9.
Cylindrical projection of Saturn's thermal emission at 2.2 cm wavelength, obtained by the Cassini RADAR in passive (non-transmitting) mode. The dark band at the equator is due to the rings, which are colder than the planet itself. The top two panels show the planet before the great storm. The lower panel shows warm emission at the location of the storm. Ammonia is the principal absorber at 2.2 cm wavelength, so the warm emission is due to ammonia depletion allowing radiation from deeper levels to reach the detector (Janssen et al. 2013)
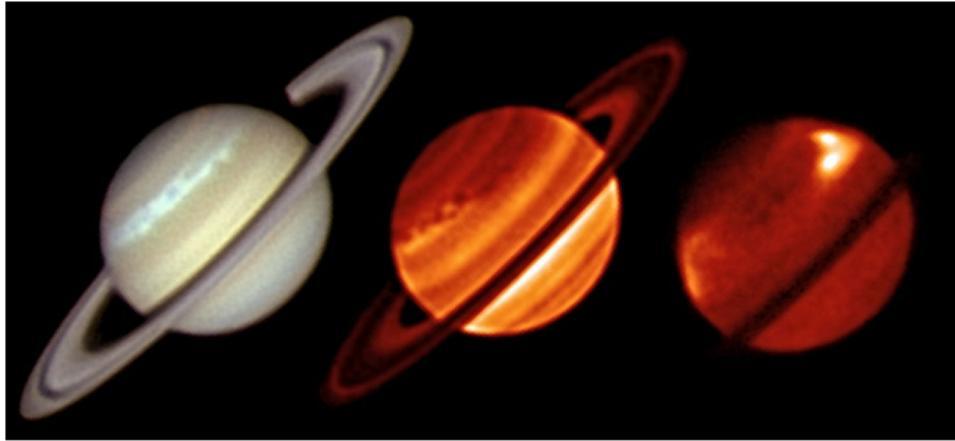
Fig. 10.
Visible light image, left, and infrared images sensitive to temperatures in the 200–500 mbar level, center, and the 1–10 mbar level, right, on January 19, 2011. The stratospheric beacon stands out in the right image. The visible light image was from the International Outer Planet Watch database (Hueso et al. 2010), and the infrared images were from the Very Large Telescope (VLT) in Chile (Fletcher et al. 2011b)
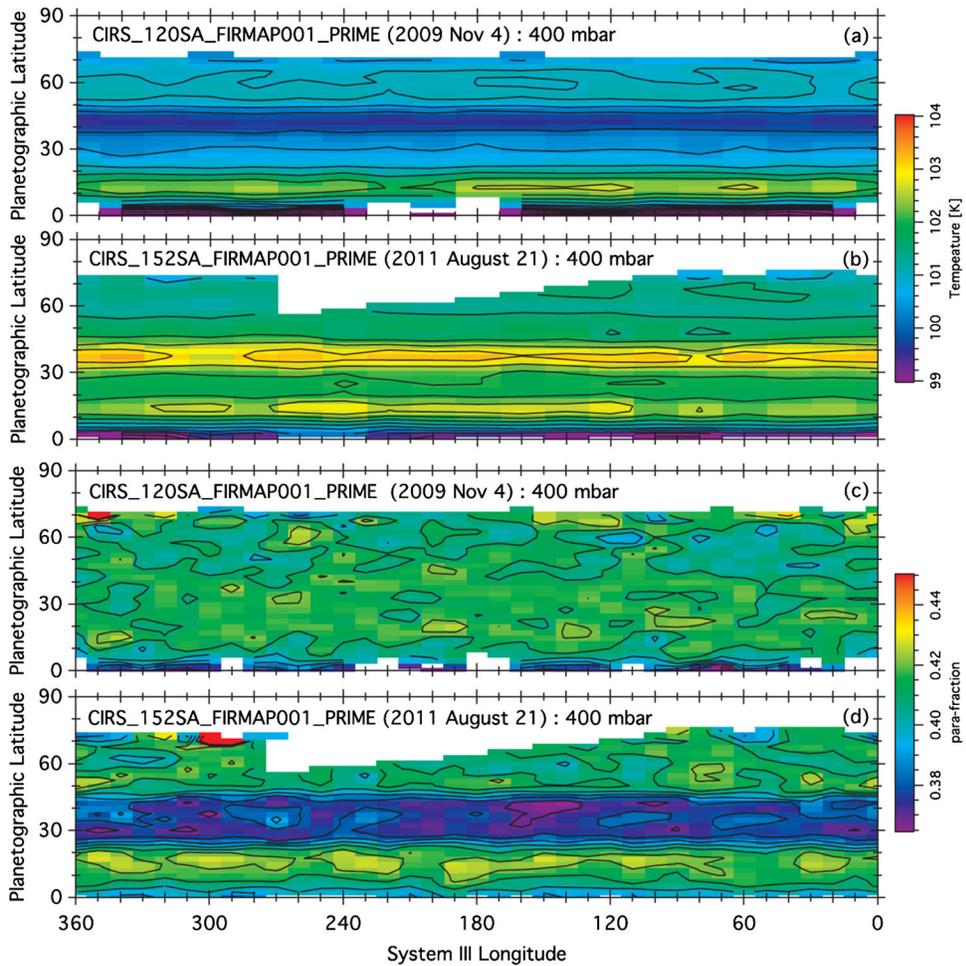
Fig. 11.

Cassini CIRS cylindrical projections showing evidence of air being dredged up from below. The top two panels show tropospheric temperature before and after the storm and the band from 30–40° planetographic has warmed by several degrees. The bottom two panels show the two chemical states (nuclear spins parallel and nuclear spins anti-parallel) of molecular hydrogen H_2 before and after the great storm. The 30–40° band shows a low para fraction, which indicates that the air has risen from below cloud base (Achterberg et al. 2014)
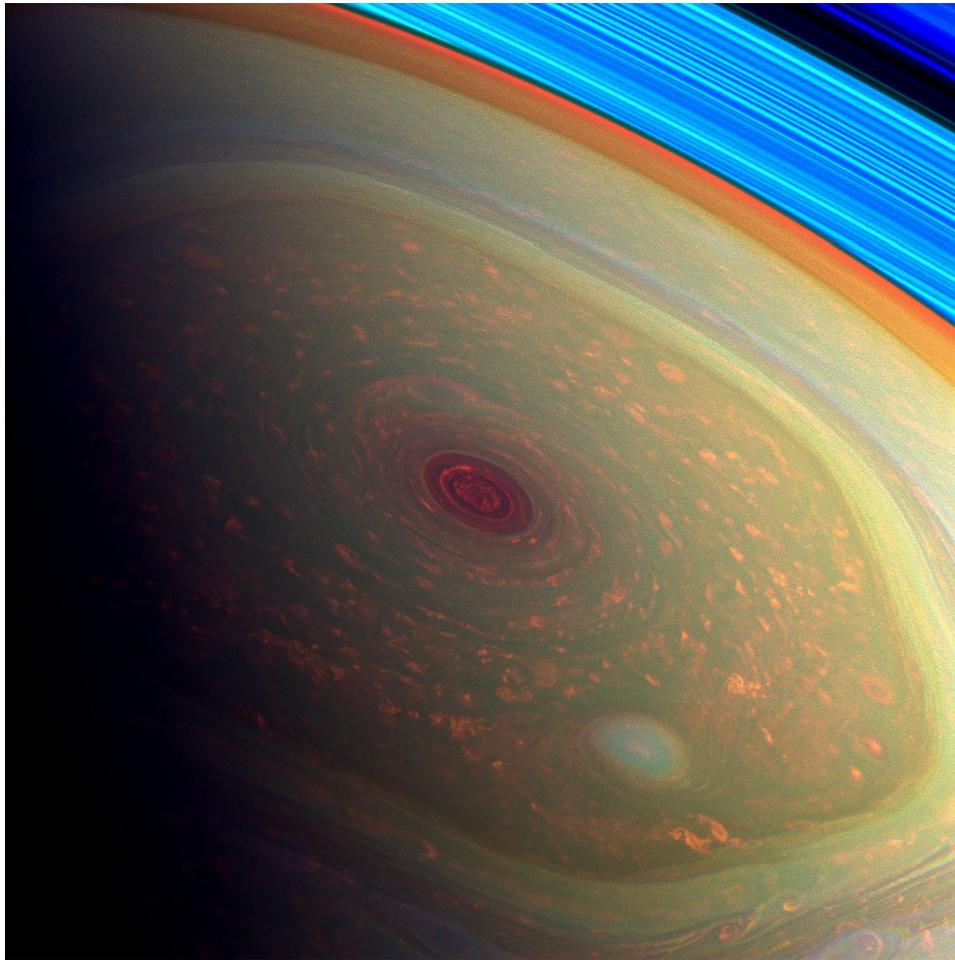
Fig. 12.

Saturn's north polar hexagon and polar cyclone. This false color image was taken on November 27, 2012 by the Cassini ISS. The MT3 and MT2 images, which look dark due to absorption by methane gas in the atmosphere, are projected as blue and green, respectively. The CB2 image, which is not sensitive to methane absorption, is projected as red. The color balance is chosen to make the planet's atmosphere look realistic. The rings look bright blue because there is no methane gas between the rings and the spacecraft. The red spot in the center extends from the pole to a latitude of 88–89°. It looks red in the false-color image because the clouds are deep and methane gas absorbs the sunlight before it can reflect off the clouds and reach the spacecraft. The spot is a cyclone with winds of ~100 ms^{-1} [PIA14946]
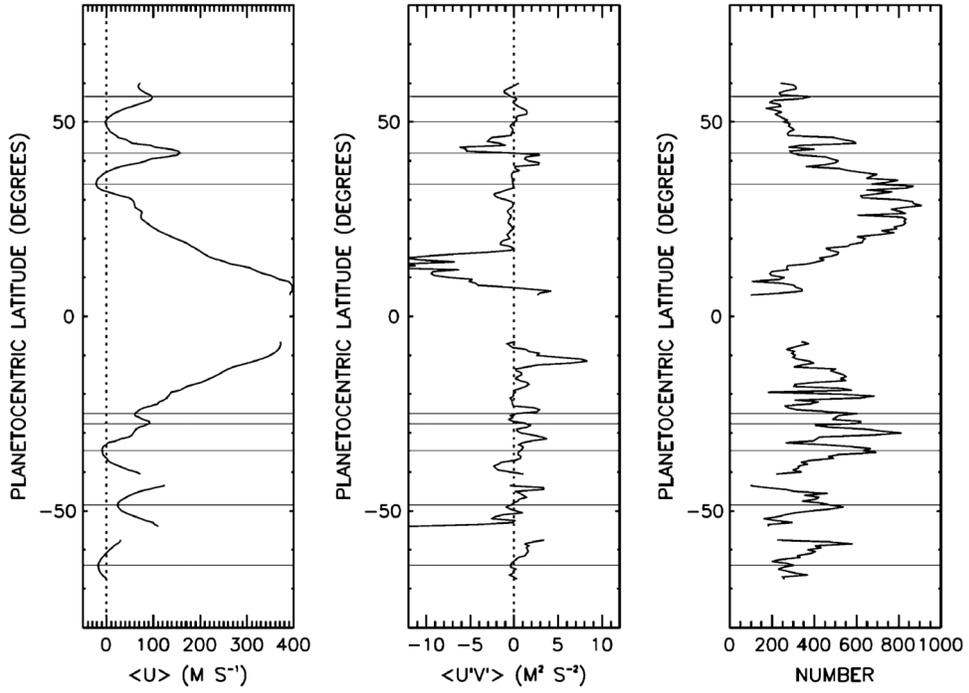
Fig. 13.

Eddy momentum transport for Saturn from Cassini ISS. The eastward and northward eddy winds u′ and v′ are the departures from the zonal means. Their product $\overline{u'v'}$ averaged over longitude and multiplied by density is the northward eddy flux of eastward momentum. The fact that this quantity has the same sign as $\partial \bar{u}/\partial y$, which is the increase of the mean eastward wind with latitude, says that the eddies are putting energy into the jets and not the reverse. The left panel is $\bar{u}$, the middle panel is $\overline{u'v'}$, and the right panel is the number of velocity measurements per 0.5° latitude bin (Del Genio and Barbara 2012)

Saturn electrostatic discharges intensity

ISS image coverage of Saturn at latitudes 34−36 South

ISS coverage (lower panel) or RPWS coverage (upper panel)

Cloud at latitude near 35 S
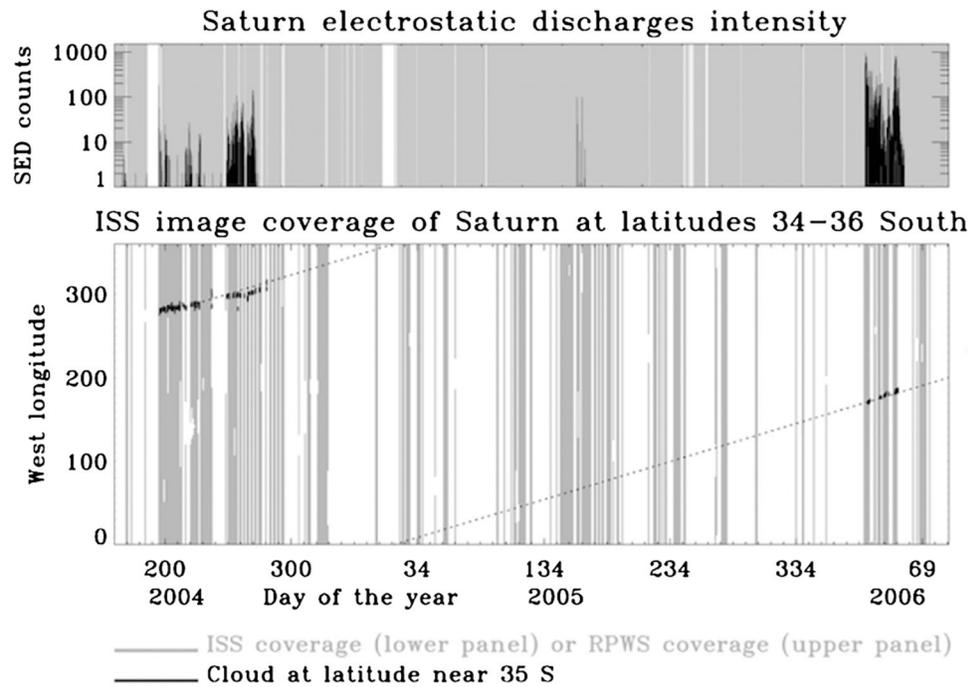
Fig. 14.

Saturn electrostatic discharge counts, SEDs, which are roughly equivalent to lightning strikes, over a 2-year period starting in 2004. The SEDs are detected by the RPWS instrument, which is ON continuously. The lower panel shows ISS coverage of latitudes −34° to −36°, where all the storms were occurring, and it is clear that storms were seen only when the RPWS was detecting SED's (Dyudina et al. 2007)
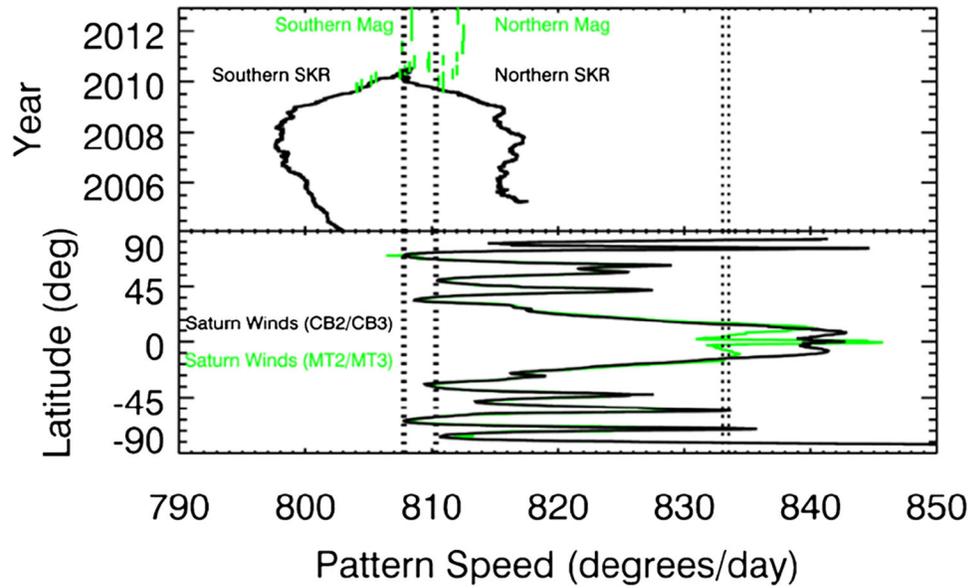
Fig. 15.

Ring seismology. The vertical dotted lines are the speeds of non-axisymmetric patterns in Saturn's rings. Only the patterns that match the planet's rotation are shown. They could be due to floating masses in the interior of Saturn. For comparison, periods of exterior magnetic fields, radio emissions, and clouds in the atmosphere are shown. Other patterns with speeds twice as fast are likely due to normal mode oscillations of the planet (Hedman and Nicholson 2014)
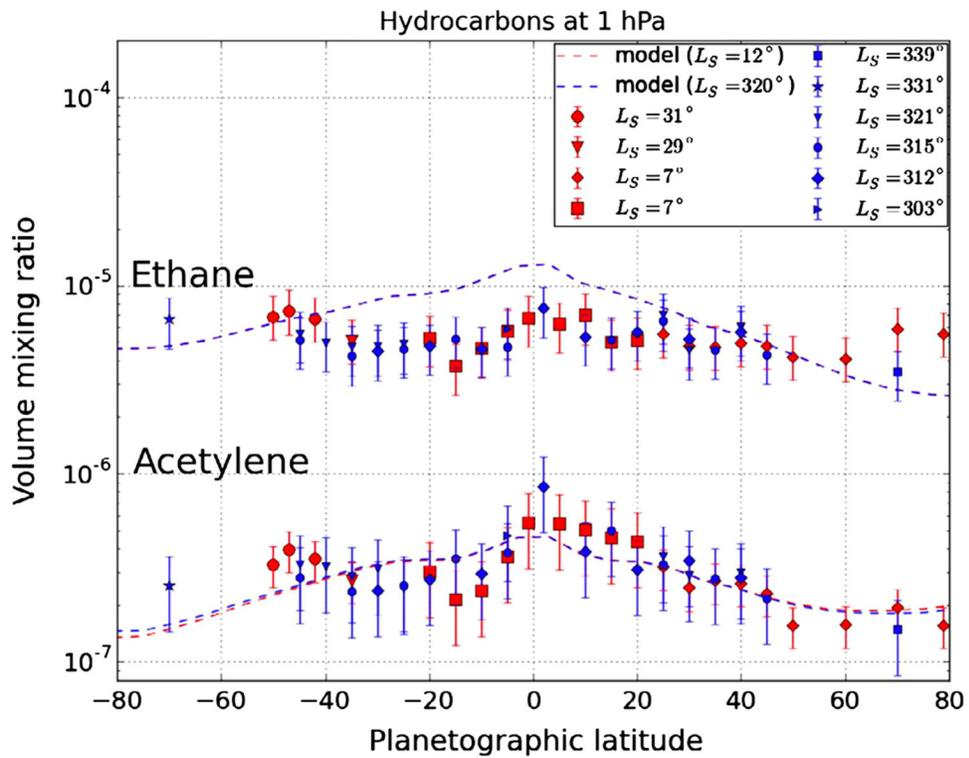
Fig. 16.

Hydrocarbons in the stratosphere at 1 mbar pressure. $L_s = 0°$ and $L_s = 360°$ are the first day of northern spring on successive years. The dashed lines are the results of a 1D photochemical model with seasons (Moses and Greathouse 2005). Ring shadow is included in the model, which has vertical mixing of species but no meridional circulation. The data are from the CIRS instrument on Cassini (Sylvestre et al. 2015)
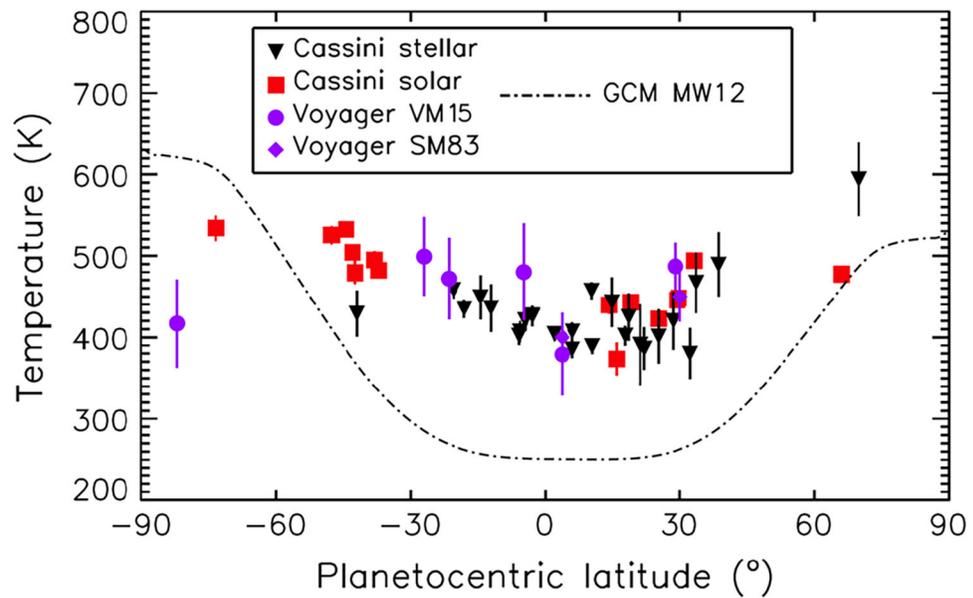
Fig. 17.

Comparison of Cassini UVIS observations with Voyager observations and with a 3-D general circulation model. The model result is represented by the smooth dot-dashed line, and it is significantly low (colder) equatorward of ±60° in both hemispheres. The problem is that the air from the Polar Regions, heated by auroral currents, cools before it reaches the lower latitudes. What keeps it warm is an ongoing mystery (Koskinen et al. 2015)

Fig. 18.
The highest-resolution, full-disk color mosaic of Jupiter ever taken. Jupiter more than filled
the field of view of the ISS, so the mosaic was assembled from over 30 individual images,
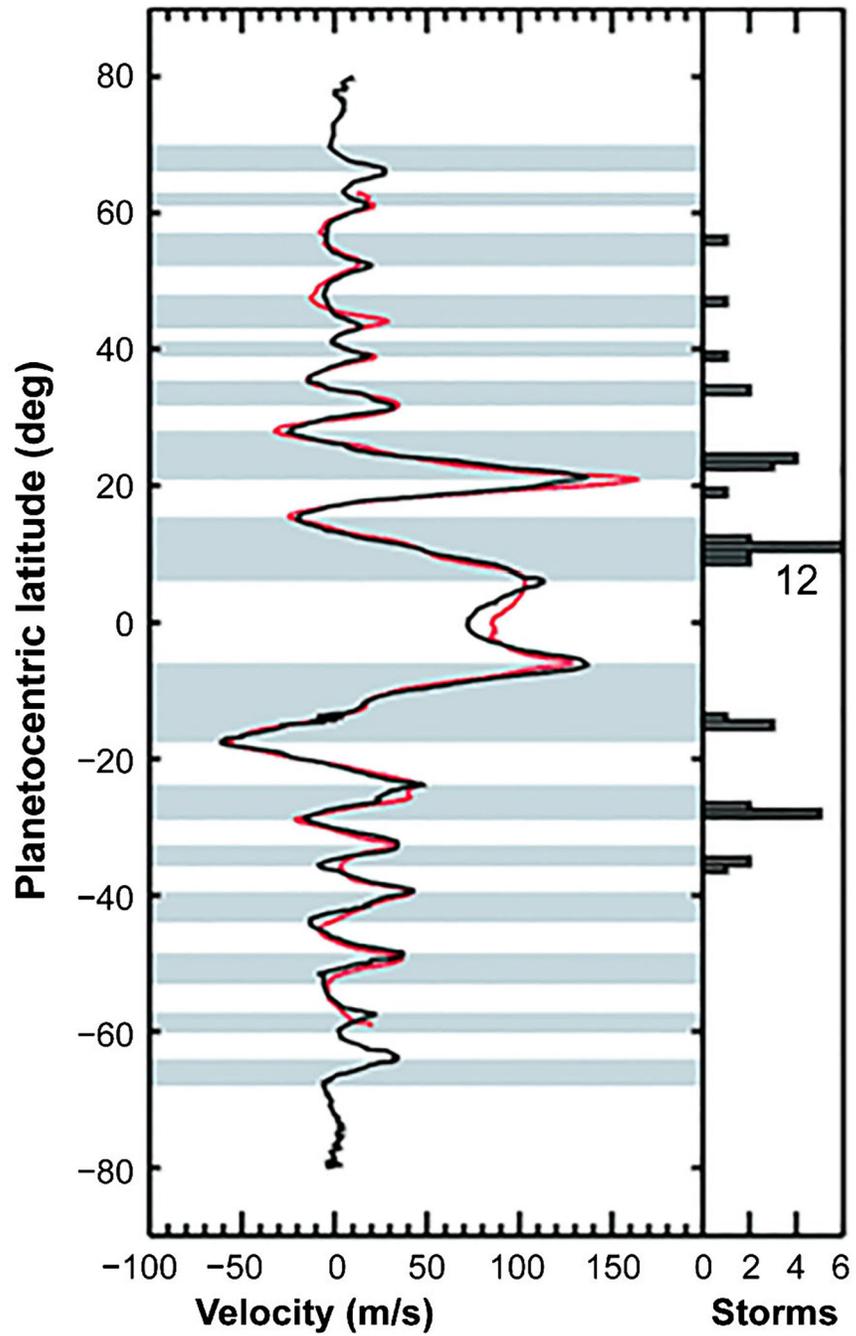allowing for the planet's rotation as the images were taken [PIA04866]

Fig. 19.
Atmospheric zonal velocity for Jupiter. The black curve is from Cassini ISS data in late 2000, and the red curve is from Voyager data in mid-1979. The jets are remarkably steady over this 21-year interval (Porco et al. 2003)
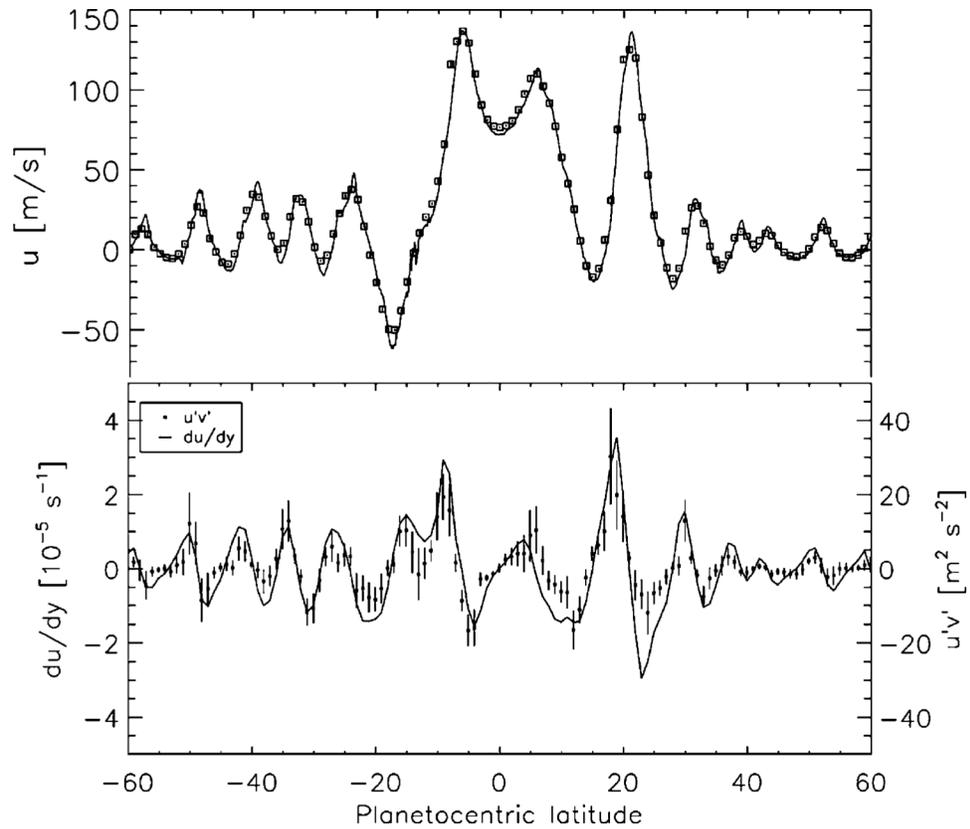
Fig. 20.

Eddy momentum transport for Jupiter from Cassini ISS. The eastward and northward eddy winds u′ and v′ are the departures from the zonal means. Their product $\overline{u'v'}$ averaged over longitude and multiplied by density is the northward eddy flux of eastward momentum. The fact that this quantity has the same sign as $\partial \bar{u}/\partial y$, which is the increase of the mean eastward wind with latitude, says that the eddies are putting energy into the jets and not the reverse (Salyk et al. 2006)
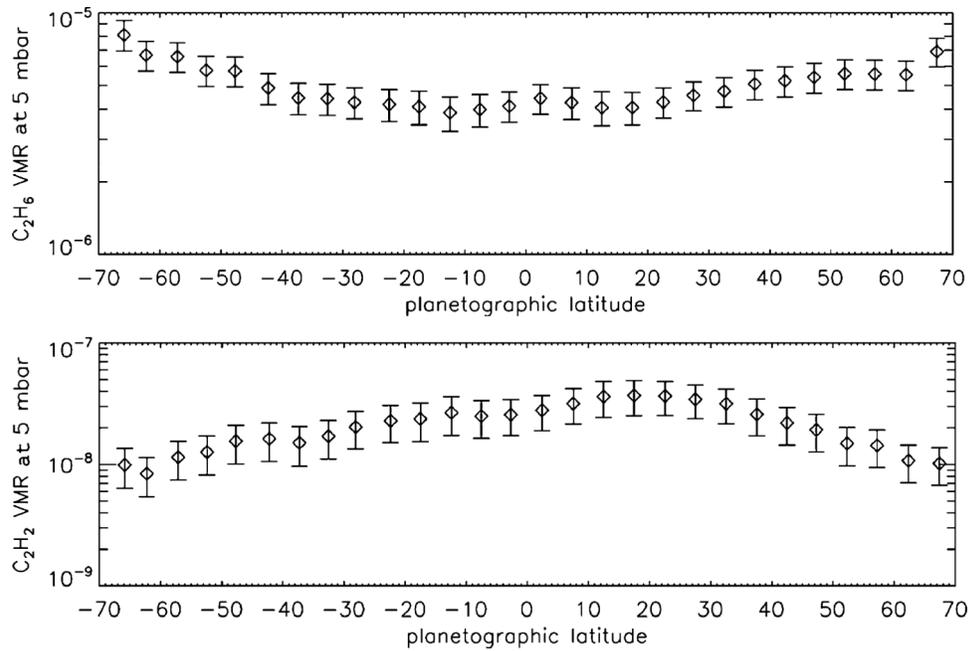
Fig. 21.
Chemical tracers in Jupiter's atmosphere at 5 mbar from Cassini CIRS. Both acetylene and ethane are formed at low latitudes by solar UV. In photochemical equilibrium their abundances would be greatest at pressures less than 0.1 mbar. C_2H_2 has a short chemical time constant, $\sim 3 \times 10^7$ s, so its abundance reflects photochemical equilibrium with lower sunlight toward the poles. C_2H_6 has a long lifetime, $\sim 3 \times 10^{10}$ s, so its abundance at 5 mbar reflects transport by the meridional circulation. The time constant of this circulation is between the lifetimes of the two molecules (Nixon et al. 2007)